Semiclassics beyond the diagonal approximation

Dissertation

zur Erlangung des Doktorgrades

der Naturwissenschaften (Dr. rer. nat.)

der naturwissenschaftlichen Fakultät II – Physik

der Universität Regensburg

vorgelegt von

Marko Turek

aus Halle (Saale)

Februar 2004

Promotionsgesuch eingereicht am 05. Februar 2004
Promotionskolloquium am 21. April 2004

Die Arbeit wurde von Prof. Dr. Klaus Richter angeleitet.
Prüfungsausschuß:

Vorsitzender:	Prof. Dr. Christian Back
1. Gutachter:	Prof. Dr. Klaus Richter
2. Gutachter:	Prof. Dr. Matthias Brack
Weiterer Prüfer:	Prof. Dr. Tilo Wettig

Abstract

The statistical properties of the energy spectrum of classically chaotic closed quantum systems are the central subject of this thesis. It has been conjectured by O. Bohigas, M.-J. Giannoni and C. Schmit that the spectral statistics of chaotic systems is universal and can be described by random-matrix theory. This conjecture has been confirmed in many experiments and numerical studies but a formal proof is still lacking. In this thesis we present a semiclassical evaluation of the spectral form factor which goes beyond M.V. Berry's diagonal approximation. To this end we extend a method developed by M. Sieber and K. Richter for a specific system: the motion of a particle on a two-dimensional surface of constant negative curvature. In particular we prove that these semiclassical methods reproduce the random-matrix theory predictions for the next to leading order correction also for a much wider class of systems, namely non-uniformly hyperbolic systems with $f \geq 2$ degrees of freedom. We achieve this result by extending the configuration-space approach of M. Sieber and K. Richter to a canonically invariant phase-space approach.

Zusammenfassung

Das zentrale Thema dieser Arbeit sind die statistischen Eigenschaften des Energiespektrums geschlossener Quantensysteme deren klassische Analoga durch chaotische Dynamik gekennzeichnet sind. Für diese Systeme stellten O. Bohigas, M.-J. Giannoni und C. Schmit die Vermutung auf, daß die spektrale Statistik universell ist und den Vorhersagen der Zufallsmatrixtheorie folgt. Diese Vermutung wurde bereits durch eine Vielzahl von Experimenten und numerischen Untersuchungen bestätigt, ein formaler Beweis konnte bisher jedoch nicht gefunden werden. In dieser Arbeit wird der spektrale Formfaktor auf der Grundlage semiklassischer Methoden berechnet, die über M.V. Berrys Diagonalnäherung hinaus gehen. Die Grundlage dafür stellt die Erweiterung einer Methode von M. Sieber und K. Richter dar, welche für die Bewegung eines Teilchens auf einer zweidimensionalen Fläche konstanter negativer Krümmung entwickelt wurde. Insbesondere wird in der vorliegenden Arbeit gezeigt, daß die Anwendung dieser semiklassischen Methoden auf die viel größere Klasse nicht-uniformer hyperbolischer Systeme mit beliebiger Anzahl von Freiheitsgraden ebenfalls die Vorhersagen der Zufallsmatrixtheorie reproduziert. Zu diesem Zweck wird eine kanonisch invariante Phasenraummethode entwickelt, welche den Ortsraumzugang von M. Sieber und K. Richter erweitert.

Contents

CHAPTER 1

Introduction

1.1 Chaos in classical and quantum mechanics

The chaotic motion of macroscopic bodies as well as the quantum mechanical properties of microscopic particles have been intensively studied for more or less one hundred years now. Nevertheless it took more than fifty years until the first significant attempts were made to bring the two fields together. The traditional theory for classical mechanics goes back to NEWTON, LAGRANGE and HAMILTON. According to this theory the dynamical state of any macroscopic body is described by its position $\mathbf{q}_t$ and its velocity $\dot{\mathbf{q}}_t$ or momentum $\mathbf{p}_t$ at a given time t. The motion of this macroscopic object can then be described quantitatively by solving the equations of motion. The solution uniquely determines the position and the momentum at any later time t for given initial conditions $(\mathbf{q}_0, \mathbf{p}_0)$ at time $t = 0$. Therefore, the state of a classical body (or a system of many bodies) can be uniquely characterized in terms of a point $\mathbf{x} = (\mathbf{q}, \mathbf{p})$ in the associated phase space and the dynamics of the body is then given by the trajectory $\mathbf{x}_t$ in that phase space. This implies that the motion as described in the framework of classical mechanics is completely *deterministic*. However, this does not mean that the motion represented by the solution $\mathbf{x}_t$ necessarily shows a simple and regular behavior as a function of time. As one can imagine, the motion of many particles interacting with each other, e.g. via their gravitational or electromagnetic forces, can easily become extremely complex. In this case it would be hopeless to look for a specific solution of the equations of motion and one typically employs statistical theories for the characterization of this type of systems. But also systems with only a few degrees of freedom can show

a very complex dynamical behavior. This can be caused by non-linearities in the equations of motion. For example, already the problem of describing the dynamics of three interacting bodies can lead to very complex solutions as first shown by POINCARÉ in 1892 [Poi92]. This complex behavior is related to the fact that the dynamics shows a very sensitive dependence on the initial conditions. By this one means that two trajectories starting at close points $\mathbf{x}_0^{(1)}$ and $\mathbf{x}_0^{(2)}$ in phase space diverge from each other very rapidly, i.e. exponentially. The distance $|\mathbf{x}_t^{(1)} - \mathbf{x}_t^{(2)}|$ between two initially close trajectories grows approximately as $\sim \exp \lambda t$ with time t until it reaches more or less the system size. Here, $\lambda > 0$ is the so-called LYAPUNOV exponent which characterizes the time scale of the exponential growth. If a bounded and energy conserving system is considered this sensitive dependence on the initial conditions leads to a chaotic motion. This especially implies that it is impossible to predict the dynamics of a chaotic system for long times $\lambda t \gg 1$ as the initial conditions can always be measured with a certain accuracy only.

A definition of a classical system with regular motion can be given in terms of the invariants of motion [Arn01]. Assume that there are f degrees of freedom for the dynamics, e.g. $f = 3$ for the motion of a single particle in the three dimensional space. For closed systems without dissipation the total energy E is conserved. If there are further $f - 1$ independent functions $h(\mathbf{q}_t, \mathbf{p}_t)$ that are invariant under the classical dynamics then the system is called integrable and shows regular dynamics. These constants of motion can be chosen to be actions. They restrict the motion in phase space to tori which form an f dimensional hypersurface in the $2f$ dimensional phase space. Hence the time evolution of a state is either periodic or quasi-periodic. If on the other hand there are no further conserved quantities besides the energy then the motion in phase space is only restricted to a $2f-1$ dimensional hypersurface. In this case the dynamics can be either completely chaotic or partially chaotic, which is then called mixed.

After the early work by POINCARÉ on the three body problem several significant contributions were made to the field of chaotic dynamics, e.g. by BIRKHOFF, KOLMOGOROV, SMALE and others, and the original description suitable in the theory of classical mechanics was extended towards the more general mathematical concept of dynamical systems (see e.g. [ASY96], [Rei96] and [GH02]). However, until the mid 1970's these activities were mostly of purely mathematical nature. It was only then when digital computers started to become a common scientific tool that the interest in chaotic dynamical systems began to grow significantly. Extensive numerical studies of dynamical systems and computer experiments stimulated the application of the theory of dynamical systems to a large variety of different fields such as biology (e.g. predator-prey models), hydrodynamics (e.g. RAYLEIGH-BERNARD convection), nonlinear electrical circuits and many others (see e.g. [Sch84], [Ott93] and [LL92]).

As opposed to macroscopic bodies, the dynamics of microscopically small par-

ticles (such as electrons in semiconductor devices) has to be treated within the framework of quantum theory, see e.g. [Mer98]. It is described in terms of a wave function $\Psi(\mathbf{q}, t)$ which is a solution of the SCHRÖDINGER equation. The concept that single points in a phase space represent the state of the system can no longer be applied because of the HEISENBERG uncertainty principle. This principle basically states that a single quantum state occupies a finite phase-space volume $(2\pi\hbar)^f$ determined by PLANCK's constant $\hbar$. Due to the linearity of the SCHRÖDINGER equation with respect to the wave function $\Psi(\mathbf{q}, t)$ one would not expect any simple relation to chaotic behavior, i.e. sensitive dependence on the initial conditions, as described above. The time evolution of an arbitrary state being a superposition of energy eigenstates is quasi-periodic. On the other hand one can always study the classical limit of the quantum dynamics of a given system by 'making' the particle under consideration macroscopically large again. This limit is given when the typical wavelengths appearing in the wave functions are negligible compared to all other length scales of the system. The following question then arises naturally. Consider two different closed quantum systems with one of them showing regular and the other chaotic dynamics in the classical limit. Can one then find a criterion based on the SCHRÖDINGER equation only, i.e. its energy eigenvalues E_n or eigenfunctions $\Psi_n(\mathbf{q}, t)$, to distinguish these two systems? To put it in other words, is the chaotic nature of the underlying classical system observable within its quantum mechanical description? The physical phenomena related to this kind of questions are central to the field of quantum chaos [Ber87]. Numerous experiments and numerical simulations do indeed show different statistical properties of the eigenfunctions and eigenenergies if chaotic quantum systems are compared to integrable systems. This is for example reflected in different nearest neighbor distributions or two-point correlation functions for the energy eigenvalues (for an overview see e.g. [Les89, Stö99, Haa01]).

Of particular interest in this field is the semiclassical regime. Roughly speaking, this regime lies in the middle between classical mechanics and quantum mechanics. Here, one expects that classical objects like trajectories play a role while quantum effects like interference are still present. Semiclassics is comparable to the transition from wave optics to ray optics in the limit of short wavelengths. Formally, the semiclassical limit can be achieved by letting $\hbar \to 0$ as all other parameters in the problem remain unchanged. A very instructive discussion on how the semiclassical limit emerges from quantum mechanics can be found in [Ber89].

Various semiclassical methods have been developed since the early days of quantum mechanics. For integrable systems a semiclassical quantization can be performed using the action variables that define the invariant tori in phase space. One can make a canonical variable transformation so that the HAMILTONian is expressed in terms of these actions [Arn01]. The BOHR-SOMMERFELD quantization scheme is then based on the requirement that each of these actions is an integer multiple

of PLANCK's constant ($2\pi\hbar$). However, as EINSTEIN already pointed out in 1917 [Ein17], this quantization procedure is not applicable to chaotic systems.

It was only in the early 1970's when the first links between classically chaotic HAMILTONian systems and their quantum mechanical counterparts could be made. M. GUTZWILLER derived a formula for the semiclassical limit of the density of states in terms of a sum over classical periodic orbits (see [Gut90] and references therein). This trace formula expresses the density of states (which is directly related to the set of quantum mechanical eigenenergies) in terms of classical quantities like the actions and the stabilities of the periodic orbits. The original theory of GUTZWILLER gives only the leading contributions in $\hbar$ with respect to the analytic parts in the density of states — thus being exact in the semiclassical limit $\hbar \to 0$. Later on it was extended to an expansion in this small parameter [GA93, AG93]. However, there are certain technical problems connected with the trace formula concerning the convergence of the sum over periodic orbits, see e.g. [Ber89] for a discussion of these issues. Despite these subtleties GUTZWILLER's trace formula is a frequently used tool to study the quantum mechanical energy eigenvalues of chaotic systems in the semiclassical limit. Our analysis of the spectral form factor is based on this trace formula.

Not only the energy eigenvalues but also the individual eigenfunctions $\Psi_n(\mathbf{q})$ of the SCHRÖDINGER equation are influenced by the underlying classical dynamics [Hel96]. According to SHNIRELMAN's theorem the probability density $|\Psi_n(\mathbf{q})|^2$ is for almost all energy eigenstates of a classically chaotic system given by the microcanonical distribution [Shn74]. However, there can be exceptions in the form of scarred wave functions [Hel84, Hel89]. These scars are due to a localization of the wave function in the vicinity of a periodic orbit. Statistical properties of energy eigenfunctions belonging to a certain energy interval were studied by BOGOMOLNY [Bog88] who showed that energy averaged wave functions can indeed show an enhanced probability density in the vicinity of classical periodic orbits. However, the first model for wave functions in chaotic systems was developed by BERRY [Ber77]. This so-called random wave model proposes that the wave functions $\Psi_n(\mathbf{q})$ are random superpositions of plane waves and was successfully applied to a variety of physical systems (see e.g. [AL97], [BS02] and references therein). A proof for this model could not yet be found and chaotic wave functions are still subject to ongoing research activities.

Besides the above mentioned interest in fundamental questions concerning the correspondence principle between quantum mechanics and its classical limit there are many practical applications for which a sound understanding of semiclassical methods and issues concerning quantum chaos is essential. Semiclassical methods have successfully been applied to atomic and molecular physics, e.g. photo-absorption spectra of RYDBERG atoms and atoms in magnetic fields [FW89] or the semiclassical treatment of the Helium atom [WRT92]). Another important field where semiclassical methods have been applied with great success is that of mesoscopic electronic devices [Ric00]. Here the idea is that most of the relevant physically quantities,

as for example in electronic transport problems [Jen95], can be expressed in terms of single electron GREEN's functions. Therefore, a semiclassical treatment of these systems can be achieved by employing similar semiclassical approximations for the GREEN's function as GUTZWILLER used when deriving the density of states. For example, in this way it was shown that classical chaotic dynamics of a semiconductor microstructure has experimentally measurable consequences for its quantum conductance [Mai90, BJS93]. A semiclassical analysis of the KUBO formula for the conductance of mesoscopic systems is given in [Arg95, Arg96], a semiclassical description of tunneling is presented in [BR99], chaotic scattering is reviewed in [Ott93] and decoherence phenomena were discussed in [FH03].

Another physically slightly different yet formally very close research field is that of microwave billiards [Stö99, Ric01]. In this case the same semiclassical methods can be applied as the HELMHOLTZ equation, which describes the microwaves, has the same structure as the SCHRÖDINGER equation when two-dimensional systems are considered. Therefore, experiments on microwave billiards can yield many insights into problems related to quantum chaos.

A general introduction into the field of quantum chaos based on a broad selection of experimental results is given in [Stö99]. More fundamental questions and the most widely used techniques are presented in [Rei92, BB97, Haa01]. Collections of many important original results and overviews over central issues concerning quantum chaos can be found in the conference proceedings [Les89] and [Qua00] as well as in [Cas95].

In the remaining sections of this introduction we first give a short overview on how exactly certain statistical properties of the eigenenergies are related to the underlying classical dynamics. In particular, we describe the relation between the so-called random-matrix theory and the quantum mechanical energy levels of a chaotic system. This relation was explicitly stated for the first time in a conjecture by BOHIGAS, GIANNONI and SCHMIT [BGS84]. Then we briefly summarize why certain model systems, namely billiard systems and quantum graphs, are suitable candidates when investigating chaotic systems. Finally we give an outline for this thesis.

1.2 Random-matrix theory and BGS conjecture

A very successful model to describe the quantum properties of various complex systems is given within the framework of the random-matrix theory. This theory has been developed by WIGNER, DYSON and MEHTA in the 1950's and 1960's to deal with the spectra of complex many-body quantum systems like large nuclei [Por65, Meh90]. The basic idea of this approach is that matrices occurring in the quantum mechanical treatment of complex systems, like the HAMILTONian or the scattering matrix, can be modeled by *random* matrices. The only restriction imposed on these

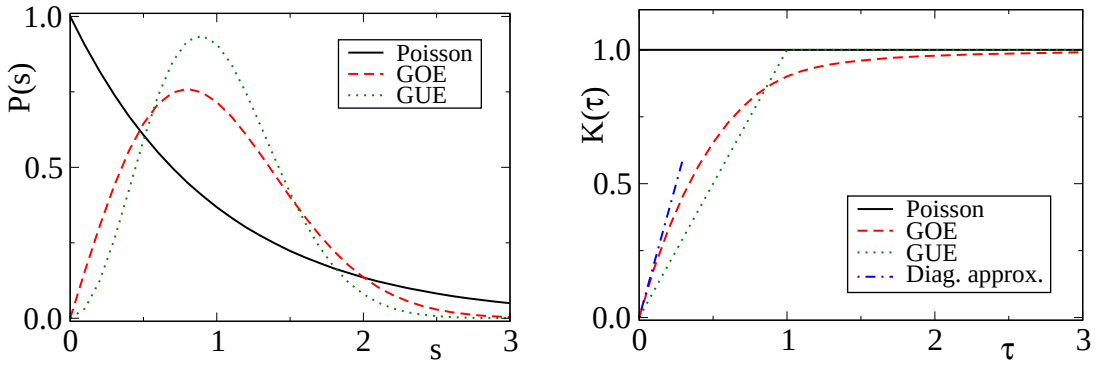

(a) Nearest neighbor distribution

(b) Spectral form factor

Figure 1.1: (a) *Nearest neighbor distribution. The solid line represents a* Poissonian *distribution of the energy levels while the dashed and dotted lines are results of the random-matrix theory. In subfigure* (b) *we present the corresponding results for the spectral form factor* $K(\tau)$*. The additional dashed-dotted line shows the result of the semiclassical evaluation using the diagonal approximation in the GOE case.*

matrices is that they belong to the same symmetry class as the original quantum mechanical operator. For example, the Hamiltonian of a complex quantum system with time-reversal symmetry is described by an ensemble of hermitian matrices being invariant under orthogonal transformations. This ensemble is the so-called Gaussian orthogonal ensemble (GOE). A nice and rather recent review on the theory of random matrices in quantum physics can be found in [GMGW98].

However, as it turns out, random-matrix theories can also be applied to chaotic systems which possess only few degrees of freedom. This has first been conjectured by Bohigas, Giannoni and Schmit [BGS84] in 1984 (BGS-conjecture). They numerically investigated the eigenenergy spectrum of a single particle in a two-dimensional quantum system with the shape of a Sinai billiard. Based on these results they conjectured that the fluctuations in the spectra of all chaotic systems (more specifically, of all so-called K-systems) show the same statistical properties as the eigenvalues of random matrices belonging to the appropriate ensemble. If this conjecture is indeed applicable to *all* chaotic systems then it would provide a system independent and thus universal mean to identify the type of the underlying classical dynamics on a purely quantum mechanical basis.

To illustrate the meaning of the conjecture we briefly discuss the nearest neighbor distribution of energy eigenvalues and the spectral form factor as two examples. In order to extract the fluctuations in the energy spectrum it is first rescaled by the system specific mean density of states. For the nearest neighbor distribution one then considers the probability $P(s)$ that a certain difference s between any two consecutive rescaled energy levels occurs. For the semiclassical limit of a quantum system

with corresponding integrable classical dynamics BERRY and TABOR argued that $P(s)$ is given by the POISSON distribution [BT77] $P(s) = \exp[-s]$, see Fig. 1.1(a). This distribution is characteristic for energy levels distributed at random and with no correlations. If, on the other hand, chaotic systems with time-reversal symmetry are considered within the framework of the random-matrix theory then one obtains [Boh89] $P(s) \simeq \frac{\pi}{2} s \exp[-\pi s^2/4]$, see Fig. 1.1(a). For comparison we also mention the result given by the GAUSSian unitary ensemble (GUE) which represents systems without time reversal symmetry [Boh89]: $P(s) \simeq 32\pi^{-2} s^2 \exp[-4s^2/4]$. The meaning of these results is that chaotic systems should exhibit level repulsion while integrable systems do not if BOHIGAS' conjecture applies.

Another important quantity when studying statistical properties of the energy spectrum is the spectral form factor $K(\tau)$. It is defined as the FOURIER transform of a two-point correlation function with respect to the density of states and thus contains information about the correlations among the energy levels. This spectral form factor is the central object to be studied within this thesis. As it will be thoroughly introduced in Section 2.2 we just briefly state the results obtained by applying random-matrix theory [Boh89, Haa01]. For energy levels distributed according to a POISSONian there are no correlations and the form factor is just a constant. The results for $K(\tau)$ obtained from the random-matrix theory in the GOE and GUE case are shown in Fig. 1.1(b). As one can observe the small $\tau \ll 1$ behavior is significantly different if compared to the case with a POISSONian distribution of the energy levels.

A vast number of experiments and numerical simulations support BOHIGAS' conjecture, e.g. the energy level statistics of a hydrogen atom in a magnetic field, the excitation spectrum of a molecule, billiard systems etc. The observed energy level statistics of these chaotic systems does indeed follow the random-matrix theory predictions, see e.g. [Stö99] and [Haa01] for an overview. However, a complete theoretical link between random-matrix theory and classical chaos could not yet be established. A first step towards a proof of the conjecture was made by BERRY who semiclassically evaluated the spectral form factor using the periodic orbit theory [Ber85]. Since the form factor is related to a two-point correlation function its semiclassical representation contains an infinite double sum over phase-carrying periodic orbits γ which arise from the semiclassical expression of the GREEN's function. The evaluation of these double sums over periodic orbits faces serious technical problems. One way to circumvent these problems is to apply the so-called diagonal approximation. Within this approximation the sum over all possible pairs of periodic orbits (γ, γ') is reduced to those terms where an orbit is only paired with itself which restricts the double sum to the pairs (γ, γ). If time-reversal symmetry is present then the pairs (γ, γ^i), where γ^i represents the time-reversed version of γ, have also to be included. Applying this approximation BERRY derived the form factor $K(\tau)$ and found agreement with the universal random-matrix theory prediction for small τ as shown in

Fig. 1.1(b). As the main objective of this thesis is to go beyond this diagonal approximation we summarize the major steps in BERRY's approach in Section 2.3. After this early attempt by BERRY to deal with the evaluation of multiple infinite sums over phase-carrying classical paths several different attempts trying to tackle this problem followed [AIS93, ADD$^+$93, BK96, Tan99, PS00, Bog00, SR01, Sie02, SV03].

The spectral form factor is a representative of a class of quantum mechanical functions that are based on products of GREEN's functions. Since many other quantities of great physical importance, e.g. matrix element correlations or response functions in linear transport theory, are based on a formally similar structure a profound understanding of the semiclassical treatment of the spectral form factor is essential. If a general scheme for the computation of multiple sums over periodic orbits beyond the diagonal approximation could be developed a more precise semiclassical treatment of many more complicated quantum mechanical objects would be possible.

There have been a number of conceptually different approaches to reveal the relation between spectral statistics and random-matrix theory besides the one based on semiclassical periodic orbit theory. Several attempts were made to transfer well known methods developed in the theory of disordered systems to chaotic yet clean ballistic systems, as for example the non-linear sigma model [Ler03]. The universal features of the spectrum were studied in [SA93, SSA93] while non-universal contributions were investigated in [AA95]. The relation between chaotic and disordered systems was discussed in [AAA95, GM02a, GM02b]. However, in most of these approaches the physical framework was different as ensembles of systems instead of single systems were considered. This implies for example that an additional average, e.g. over the disorder, can be applied which is not the case for a clean chaotic system.

1.3 Model systems in quantum chaos

Billiard systems are frequently used model systems when classical or quantum chaos is studied [Bäc98]. They are based on the free motion of a particle with a given boundary. The shape of the boundary then determines the nature of the classical dynamics. Prominent examples for integrable billiards are the rectangular or the circular billiard while the stadium billiard [Bun74, Ber81], the SINAI billiard [Sin63, Sin70] and the family of LIMAÇON billiards [Rob83, Rob84] are frequently investigated chaotic billiards. The family of LIMAÇON billiards is obtained by a specific continuous deformation of the boundary of the circular billiard. The two limiting cases are thus the completely chaotic cardioid billiard and the completely integrable circular billiard. As the deformation of the boundary can be described by a single parameter this family of billiards is suitable to study the transition be-

tween integrable and chaotic dynamics. One advantage of billiard systems is that their classical properties can be rather easily calculated numerically as the motion inside the billiard follows straight lines while the reflections at the boundary are simply such that the angle of the incoming path with the boundary equals that of the outgoing path. Another useful tool applicable to billiards is that of symbolic dynamics [AY81, BD97, Bäc98] which allows to find all periodic orbits via an associated symbol code.

Besides studying the classical dynamics of billiard systems much effort has been put into the investigation of the quantum mechanical properties. The eigenvalue problem for the LIMAÇON billiards was studied in [Rob84, PR93a, PR93b, BS94, Bäc98, BBR99]. Furthermore the semiclassical quantization was applied to the stadium billiard [Tan97], billiards with mixed boundary conditions [SPS$^+$95] and others (see [Bäc98] and references therein). The eigenfunctions for different billiards were investigated for example in [BSS98] and [CVL02].

In addition to the billiard systems that are based on the motion in a bounded region of a plane a slightly different model was intensively considered: the motion on a two-dimensional surface with constant negative curvature [BV86, AS88]. Although this system is less intuitive because of its non-euclidean metric it has a very simple uniform phase-space structure. This implies for example that all periodic orbits share the same LYAPUNOV exponent. A semiclassical treatment is thus greatly simplified and a recent attempt to go beyond BERRY's diagonal approximation for the spectral form factor of such a system was performed by SIEBER and RICHTER. Their approach [SR01, Sie02] is based on the identification of off-diagonal pairs of correlated periodic orbits which are associated with each other via self-crossings in configuration space. They found agreement with the universal predictions of random-matrix theory. However, the question remained open whether these results are specific for the uniformly hyperbolic system or whether they pertain also for more general chaotic systems with different periodic orbits having different LYAPUNOV exponents. As this thesis aims at a solution of this problem we summarize the configuration-space approach of SIEBER and RICHTER in Section 2.5 and Section 3.1. There have been rather intense research activities in the last few years in order to verify and extend this approach based on off-diagonal orbit pairs [Heu01, BHH02, BHMH02, RS02, NS03, TR03, Spe03, Mül03].

Another yet somewhat more artificial model to mimic quantum chaos is that of quantum graphs [KS01, KS03]. A graph is a network of bonds and vertices. The quantum mechanical approach for the graphs is based on the assumption that the bonds cause a simple free wave evolution in one dimension while the vertices are associated with scattering matrices. Similarly to HAMILTONian systems a periodic orbit theory for quantum graphs was developed and the spectral statistics studied [KS99]. The ideas of the SIEBER and RICHTER approach for the evaluation of the semiclassical spectral form factor beyond the diagonal approximation

could also be successfully applied to quantum graphs [BSW02b, BSW02a, Ber03]. Recently, a scattering theory for quantum graphs was formulated [KS03] and transport properties such as shot noise investigated [SPG03]. However, as the dynamics of quantum graphs does not have a deterministic chaotic classical limit we restrict our considerations to classical HAMILTONian systems and their quantum mechanical counterparts.

1.4 Purpose and outline of the work

This thesis aims at an extension of the configuration-space approach of SIEBER and RICHTER for the computation of off-diagonal contributions in the semiclassical form factor $K(\tau)$ [SR01, Sie02]. We propose a canonically invariant formulation of this approach which naturally allows for an extension to non-uniformly hyperbolic systems with more than two degrees of freedom.

To this end we first introduce the necessary concepts in the theory of dynamical systems and define the statistical quantities under consideration in Chapter 2. Furthermore we summarize the semiclassical approach based on the periodic orbit theory. Finally, we briefly review the configuration-space approach to go beyond the diagonal approximation. In its original version the approach applies to two-dimensional uniformly hyperbolic systems with time-reversal symmetry.

We study the crossing angle distribution of classical trajectories in a non-uniformly billiard system in Chapter 3. This crossing angle distribution is one of the crucial ingredients in the approach by SIEBER and RICHTER. To this end we numerically investigate the family of LIMAÇON billiards in detail. As a result we find that the crossing angle distribution is qualitatively unaltered compared to the uniformly hyperbolic system if a certain class of crossings is neglected. However, it also turns out that for non-uniformly hyperbolic systems a phase-space approach is more suitable than a configuration-space approach based on the crossing angle distribution.

Therefore, the purpose of Chapter 4 is to present the phase-space approach we developed for two-dimensional ($f = 2$) non-uniformly hyperbolic systems. We explain in detail why the crossings in configuration space have to be replaced by 'encounter regions' in phase space. Furthermore we present results for the action difference of the off-diagonal orbit pairs and discuss the issue of the MASLOV indices. Finally we develop a phase-space concept that replaces the crossing angle distribution and provides an alternative way to count the partner orbits. Putting all these ingredients together we proof that (similarly to the uniformly hyperbolic system) the universal random-matrix theory prediction can be reproduced for non-uniformly hyperbolic systems as well.

The phase-space approach allows us in a natural way to extend the method

to systems with more than two degrees of freedom, i.e. $f > 2$. This extension is presented in Chapter 5. Furthermore we check whether the transition between systems with time-reversal symmetry and systems where this symmetry is broken also follows the predictions of the random-matrix theory. In the last section of Chapter 5 we then present an application to the problem of the correlations among semiclassical matrix elements.

Chapter 6 gives a summary of our results and a brief outlook concerning open problems.

CHAPTER 2

Chaotic systems and spectral statistics

The main goals of this chapter are the following. First, we review a few necessary mathematical concepts in the context of classical chaotic systems. Then we introduce the quantum spectral correlation functions, especially the form factor $K(\tau)$. We summarize the semiclassical approach using periodic orbit theory in the case of fully chaotic systems including the evaluation of the form factor within the so-called diagonal approximation. Finally, we review the major ingredients for the calculation of the first off-diagonal correction to $K(\tau)$ in a uniformly hyperbolic system and stress in detail why an extension of the theory, as presented in Chapter 4, is inevitable.

2.1 Dynamical systems and chaos

We use this section to introduce the notation and some necessary mathematical methods frequently applied when dealing with chaotic dynamical systems. Starting from the classical equations of motion we consider their linear approximation described by the stability matrix in the vicinity of a given classical trajectory. After a brief description of the properties of the stability matrix we will introduce the LYAPUNOV exponents and the notion of stable and unstable manifolds in the POINCARÉ surface of section. Finally we will specify the systems under investigation in more detail. Most of the definitions and relations presented

in this section can be found in a book by Gaspard [Gas98]. Besides that, the properties of dynamical systems are nicely presented in [Rei96]. Further introductions to chaotic systems and some specific properties of manifolds can be found in [GH02, Wig94, Ott93, LL92, Rue89, BGS85].

Throughout this thesis we consider closed quantum mechanical single particle systems whose classical counterparts are HAMILTONian systems with f degrees of freedom, e.g. two-dimensional billiard systems where $f = 2$. The classical dynamics is governed by the HAMILTONian function

$$H(\mathbf{q}, \mathbf{p}) = \frac{\mathbf{p}^2}{2m} + V(\mathbf{q}) \,. \tag{2.1}$$

Introducing the phase-space coordinates $\mathbf{x} \equiv (\mathbf{q}, \mathbf{p})$ the equations of motion can be written as

$$\frac{\mathrm{d}}{\mathrm{d}t}\mathbf{x} = \Sigma \frac{\partial H(\mathbf{x})}{\partial \mathbf{x}} \quad \text{with} \quad \Sigma \equiv \begin{pmatrix} \mathbf{0} & \mathbf{1} \\ -\mathbf{1} & \mathbf{0} \end{pmatrix} . \tag{2.2}$$

The unique solution to these $2f$ equations of classical motion corresponding to the initial condition $\mathbf{x}_0$ is denoted by $\mathbf{x}_t = (\mathbf{q}_t, \mathbf{p}_t)$. Thus, the dynamics of the system maps any point $\mathbf{x}_0$ in phase space onto another point $\mathbf{x}_t$ after time t. For conservative systems, as considered in this work, the motion is restricted to the constant energy surface $H(\mathbf{x}) = E$ for a given energy E of the particle. A solution of Eq. (2.2) is called a periodic orbit γ of period T_γ if $\mathbf{x}_t^\gamma = \mathbf{x}_{T_\gamma + t}^\gamma$. If the considered system exhibits time-reversal symmetry the equations of motion (2.2) are invariant under the time-reversal operation $\mathcal{T}\mathbf{x} = \mathcal{T}(\mathbf{q}, \mathbf{p}) = (\mathbf{q}, -\mathbf{p})$ together with $t \to -t$. This is the case if $H(\mathcal{T}\mathbf{x}) = H(\mathbf{x})$. Besides this conventional time-reversal symmetry represented by $\mathcal{T}$ there are also non-conventional time-reversal symmetries [Haa01]. However, throughout this work, we will consider only the case of conventional time-reversal symmetry. The time-reversed version of a periodic orbit $\mathbf{x}_t^\gamma$ is then given by $\mathbf{x}_t^{\gamma,i} = \mathcal{T}\mathbf{x}_{T_\gamma - t}^\gamma = (\mathbf{q}_{T_\gamma - t}^\gamma, -\mathbf{p}_{T_\gamma - t}^\gamma)$.

A very useful tool in the context of dynamical systems is the concept of POINCARÉ maps [Poi92]. Here, a $2f - 2$ dimensional hypersurface $\mathcal{P}(\mathbf{x}) = 0$ is defined within the constant energy shell. Let us denote the vectors[1] in this hypersurface by $\vec{y}$. The continuous dynamics of the systems can then be described by a discrete map in terms of the set of intersection points $\{\vec{y}_i\}$ of $\mathbf{x}_t$ with the hypersurface $\mathcal{P}(\mathbf{x})$. One particular useful example of a POINCARÉ surface of section (PSS) is constructed by using a local coordinate system defined in each phase space point $\mathbf{x}$ via the solution of Eq. (2.2) through that point. In this case a POINCARÉ surface of section can be defined at every phase point $\mathbf{x}$ by all vectors $\vec{y} \equiv (\mathbf{q}^\perp, \mathbf{p}^\perp)$ perpendicular to the flow, see Fig. 2.1(a).

[1] We will indicate that a vector lies in the $2f-2$ dimensional POINCARÉ surface of section (PSS) by using an arrow, e.g. $\vec{y}$, while vectors in the $2f$ dimensional phase space are written in bold face, e.g. $\mathbf{x}$. Nevertheless all vectors in the POINCARÉ surface of section are of course also vectors in the phase space which implies that for example the addition $\mathbf{x} + \vec{y}$ is well defined.

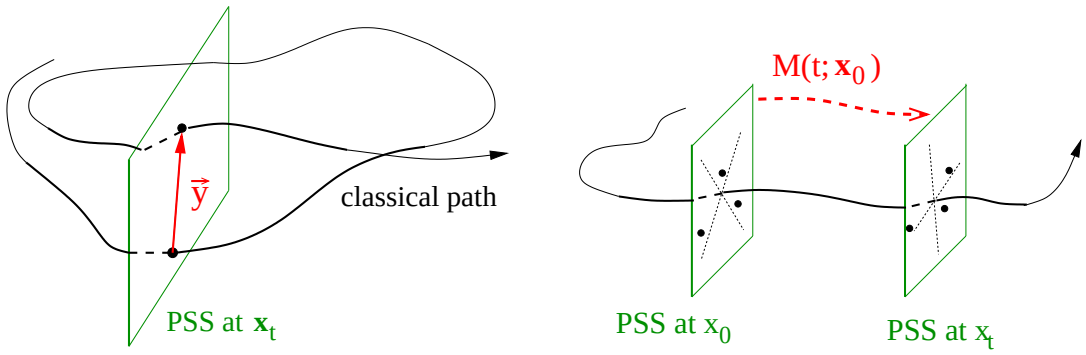

(a) Poincaré surface of section (PSS) (b) Mapping between two PSS

Figure 2.1: (a) *Schematic drawing of a* Poincaré *surface of section (PSS) at* $\mathbf{x}_t$*. It is defined by the perpendicular coordinates of the local coordinate system of a classical path going through* $\mathbf{x}_t$*.* (b) *The stability matrix* $M(t, \mathbf{x}_0)$ *maps the* Poincaré *surface of section at* $\mathbf{x}_0$ *linearly to the one at* $\mathbf{x}_t$*. The dotted lines within the surface represent the local stable and unstable directions while the dots represent the intersection points of another trajectory.*

Each trajectory $\mathbf{x}_t$ is characterized by its linear stability which describes how a small perturbation $\delta\vec{y}$ evolves with time. Thus, for a given classical path the dynamics in the vicinity of that path can be described by the so-called stability matrix[2] $M(t, \mathbf{x})$, see e.g. [Gas98, Rei96]. For any vector $\delta\vec{y} \equiv (\delta\mathbf{q}^\perp, \delta\mathbf{p}^\perp)$ which lies within the constant energy surface and describes a small displacement perpendicular to the trajectory the solution to the equations of motion (2.2) is given by $\delta\vec{y}_t = (\mathbf{x}_0 + \delta\vec{y}_0)_t - \mathbf{x}_t$. Within the range of validity for the linear approximation of Eq. (2.2) it can be approximated by $M(t, \mathbf{x})$:

$$\delta\vec{y}_t(\mathbf{x}) \simeq M(t, \mathbf{x})\ \delta\vec{y}_0(\mathbf{x})\,. \tag{2.3}$$

The meaning of Eq. (2.3) is therefore that the stability matrix $M(t, \mathbf{x})$ maps the Poincaré surface of section defined at $\mathbf{x}_0$ linearly to the Poincaré surface of section at $\mathbf{x}_t$, see Fig 2.1(b). Since the flow of a dynamical system forms a group, i.e. $(\mathbf{x}_\tau)_t = \mathbf{x}_{\tau+t}$, the stability matrix also satisfies a similar relation:

$$M(t + \tau, \mathbf{x}_0) = M(t, \mathbf{x}_\tau) \cdot M(\tau, \mathbf{x}_0)\,. \tag{2.4}$$

For chaotic systems small initial deviations typically grow exponentially with time if considered in the long-time limit. According to Eq. (2.3) this implies that the matrix elements of $M(t, \mathbf{x})$ also grow exponentially. To extract this exponential

[2]Here, we consider the perpendicular directions $(\delta\mathbf{q}^\perp, \delta\mathbf{p}^\perp)$ only while neglecting the neutral direction along the flow.

growth in the stability matrix one can reduce $M(t, \mathbf{x})$ to a diagonal form by the means of a LYAPUNOV homology [Gas98]. In general, the decomposition of $M(t, \mathbf{x})$ has the structure

$$M(t, \mathbf{x}_0) = \sum_{i=1}^{2f-2} \vec{e}_i(\mathbf{x}_t) \Lambda_i(t, \mathbf{x}_0) \vec{f}_i^{\,T}(\mathbf{x}_0) \,, \tag{2.5}$$

where the vector fields $\{\vec{e}_i(\mathbf{x})\}$ and $\{\vec{f}_i(\mathbf{x})\}$ are not growing exponentially. If there is any exponential growth with respect to the time t then it is absorbed in the $\{\Lambda_i(t, \mathbf{x}_0)\}$. That means that one can find a local set of directions $\{\vec{e}_i(\mathbf{x})\}$ and $\{\vec{f}_i(\mathbf{x})\}$ at each phase space point $\mathbf{x}$ so that Eq. (2.5) is fulfilled. However, it is important to realize that the decomposition (2.5) is not identical with a diagonalization of the matrix $M(t, \mathbf{x}_0)$, since the vectors $\{\vec{f}_i(\mathbf{x})\}$ in Eq. (2.5) are evaluated at the initial point $\mathbf{x} = \mathbf{x}_0$ while the set $\{\vec{e}_i(\mathbf{x})\}$ is evaluated at the final point $\mathbf{x} = \mathbf{x}_t$. The vectors $\{\vec{e}_i(\mathbf{x})\}$ and $\{\vec{f}_i(\mathbf{x})\}$ satisfy the relations

$$\sum_i \vec{e}_i(\mathbf{x}) \, \vec{f}_i^{\,T}(\mathbf{x}) = \mathbf{1} \quad \text{and} \quad \vec{f}_i^{\,T}(\mathbf{x}) \cdot \vec{e}_j(\mathbf{x}) = \delta_{ij} \,. \tag{2.6}$$

However, these relations do not imply that the vectors $\{\vec{e}_i(\mathbf{x})\}$ and $\{\vec{f}_i(\mathbf{x})\}$ are mutually orthogonal.

In the decomposition (2.5), there is a stretching factor $\Lambda_i(t, \mathbf{x})$ corresponding to each direction $\vec{e}_i(\mathbf{x})$. From the group property (2.4), the decomposition (2.5) and the relations (2.6) it is clear that $\Lambda_i(t + \tau, \mathbf{x}_0) = \Lambda_i(t, \mathbf{x}_\tau)\Lambda_i(\tau, \mathbf{x}_0)$ also holds, similarly to Eq. (2.4). The stretching factors allow to calculate the LYAPUNOV exponents λ_i associated with the directions $\vec{e}_i$ via the relation

$$\lambda_i \equiv \lambda(\mathbf{x}, \vec{e}_i) = \lim_{t \to \infty} \frac{1}{t} \ln |\Lambda_i(t, \mathbf{x})| \,. \tag{2.7}$$

The equations of motion for the stretching factors follow from a linearization of the original equations of motion (2.2) together with the decomposition (2.5) and the conditions (2.6). They can be written as [Gas98]

$$\dot{\Lambda}_i(t, \mathbf{x}_0) = \chi_i(\mathbf{x}_t) \, \Lambda_i(t, \mathbf{x}_0) \,. \tag{2.8}$$

Solving this differential equation for $\Lambda_i(t, \mathbf{x}_0)$ one finds with Eq. (2.7)

$$\lambda_i(\mathbf{x}_0) = \langle \chi_i(\mathbf{x}_t) \rangle_t \,, \tag{2.9}$$

where $\langle \ldots \rangle_t$ stands for the time average which for any function $f(\mathbf{x})$ is defined by

$$\langle f(\mathbf{x}_0) \rangle_t \equiv \lim_{t \to \infty} \frac{1}{t} \int_0^t \mathrm{d}\tau \, f(\mathbf{x}_\tau) \,. \tag{2.10}$$

The $\chi_i(\mathbf{x})$ introduced in Eq. (2.8) are local growth rates [EY93] which yield the LYAPUNOV exponents when averaged along a trajectory, as in Eq. (2.9). In general

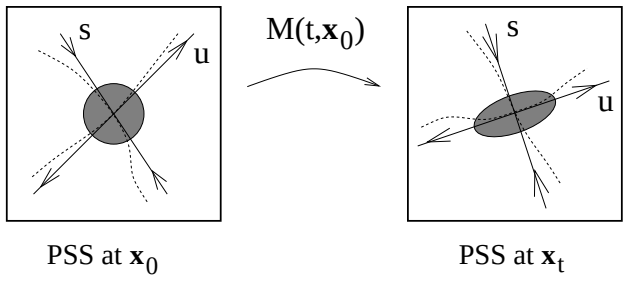

Figure 2.2: *Mapping of the* POINCARÉ *surface of section (PSS) at* $\mathbf{x}_0$ *to the one at* $\mathbf{x}_t$*. The manifolds are represented by the dotted lines. The solid lines are their linear approximations at the origin. All vectors pointing into the unstable direction (u) are stretched while the components with respect to the stable direction (s) become smaller. However, the total volume in phase space is conserved which is reflected in the different sign of* χ *in the pairing rule (2.13).*

they depend on the position in phase space. Only the uniformly hyperbolic system is defined such that $\chi(\mathbf{x}) = \lambda$ independently of $\mathbf{x}$.

Another important concept is that of stable and unstable manifolds, see e.g. [Gas98, Rei96]. The local stable and unstable manifolds $W^{s,u}(\mathbf{x})$ in the POINCARÉ surface of section at $\mathbf{x} = \mathbf{x}_0$ are defined as

$$W^{s,u}(\mathbf{x}) = \{\vec{y}_0 : \|\vec{y}_t\| = \|(\mathbf{x}_0 + \vec{y}_0)_t - \mathbf{x}_t\| \to 0 \quad \text{for} \quad t \to \pm\infty\} \ . \tag{2.11}$$

This definition means the following. Consider a trajectory starting at $\mathbf{x}_0$ and a neighboring trajectory starting at $\mathbf{x}_0^{(n)} = \mathbf{x}_0 + \vec{y}_0$. Then for all $\vec{y}_0$ lying in the stable manifold $W^s(\mathbf{x})$ the neighboring trajectory converges towards the original one when propagated forward in time. This implies that not all initial deviations have to grow exponentially. This exponential growth occurs only if the initial deviation $\vec{y}$ has at least one component which lies outside the stable manifolds. Furthermore, it is clear that the exponential growth is limited by the system size. This means that the initial deviations $\vec{y}_0$ must be small so that the exponential long-time behavior can be seen before $\vec{y}_t$ is of the order of a typical system size. Equivalent arguments hold if the time evolution is reversed, e.g. $t \to -\infty$, leading to the definition (2.11) of the unstable manifold $W^u(\mathbf{x})$.

Because of the mathematical structure of the HAMILTONian system (2.2) the stability matrix is symplectic which means that $M^T \ \Sigma \ M = \Sigma$ with M^T being the transposed matrix. Therefore, the symplectic product defined as $\delta\vec{y}_1^T \, \Sigma \, \delta\vec{y}_2$ is conserved under the evolution of the system, i.e. $\delta\vec{y}_1^T \, \Sigma \, \delta\vec{y}_2 = (M\delta\vec{y}_1)^T \, \Sigma \, (M\delta\vec{y}_2)$ for any two vectors $\delta\vec{y}_{1,2}$. Furthermore, the symplectic property implies a pairing rule for the vector fields $\{\vec{e}_i(\mathbf{x})\}$ and $\{\vec{f}_i(\mathbf{x})\}$ which can most easily be seen by calculating

the inverse of $M(t, \mathbf{x}_0)$:

$$\begin{aligned} M^{-1}(t, \mathbf{x}_0) &= \Sigma \cdot M^T(t, \mathbf{x}_0) \cdot \Sigma \\ &= \sum_{j=1}^{2f-2} \left(\Sigma \vec{f}_j(\mathbf{x}_0)\right) \Lambda_j(t, \mathbf{x}_0) \left(-\Sigma \vec{e}_j(\mathbf{x}_t)\right)^T \\ &= \sum_{i=1}^{2f-2} \vec{e}_i(\mathbf{x}_0) \Lambda_i^{-1}(t, \mathbf{x}_0) \vec{f}_i^T(\mathbf{x}_t) \,. \end{aligned} \tag{2.12}$$

The last representation of M^{-1} can easily be checked with Eqs. (2.5) and (2.6) by verifying $MM^{-1} = M^{-1}M = \mathbf{1}$. Let the vector fields $\{\vec{e}_i(\mathbf{x})\}$ and $\{\vec{f}_i(\mathbf{x})\}$ be fixed for a given system so that Eqs. (2.5) and (2.6) are fulfilled. Then equality (2.12) implies that for each direction i with $\{\chi_i(\mathbf{x}), \vec{e}_i(\mathbf{x}), \vec{f}_i(\mathbf{x})\}$ there is a corresponding direction j for which

$$\left\{\chi_j(\mathbf{x}), \vec{e}_j(\mathbf{x}), \vec{f}_j(\mathbf{x})\right\} = \left\{-\chi_i(\mathbf{x}), S_{\mathrm{cl}} \left(\Sigma \vec{f}_i(\mathbf{x})\right), \frac{1}{S_{\mathrm{cl}}} \left(-\Sigma \vec{e}_i(\mathbf{x})\right)\right\}. \tag{2.13}$$

In order to keep track of the units one has to introduce a classical action denoted by S_{cl} which can be, for example, the action of the shortest periodic orbit in the system. The pairing rule (2.13) also means that because of Eq. (2.9) all the different directions come in pairs (i, j) with $\lambda_i \geq 0$ and $\lambda_j = -\lambda_i \leq 0$. This property is an expression of the fact that the phase space volume is conserved. According to the definition of the LYAPUNOV exponents (2.7) and the definition of the stable and unstable manifolds (2.11) the directions $\vec{e}_i(\mathbf{x})$ with a positive LYAPUNOV exponent $\lambda_i > 0$ are tangent to the unstable manifold, see Fig. 2.2. Therefore they are called local unstable directions and characterized by a superscript u. Similarly, the ones with $\lambda_i < 0$ are the stable directions indicated by a superscript s. This connection between the manifolds $W(\mathbf{x})$ and the vectors $\vec{e}_i(\mathbf{x})$ can most easily be seen by using the linearized equations of motion in the form $(\mathbf{x}_0 + \delta\vec{y}_0)_t \approx \mathbf{x}_t + M(t, \mathbf{x}_0)\delta\vec{y}_0$ in definition (2.11). In terms of stable and unstable directions the pairing rule can then be rewritten as

$$\vec{f}_i^{\,s,u}(\mathbf{x}) = -\frac{1}{S_{\mathrm{cl}}} \Sigma \, \vec{e}_i^{\,u,s}(\mathbf{x}) \tag{2.14}$$

where Σ is the matrix defined in Eq. (2.2) and the index i labels the number of the pair and thus ranges from $i = 1 \ldots (f-1)$.

Throughout the rest of this work we will mostly be concerned with continuously hyperbolic systems. The precise definition of a hyperbolic system can for example be found in [Gas98]. The important properties of a hyperbolic system are: i) all LYAPUNOV exponents (except the one corresponding to the direction along the flow) are strictly nonzero ($\lambda_j \neq 0$) and ii) the angles between the local directions of the manifolds are nonzero in every phase space point $\mathbf{x}$. This ensures that each vector $\delta\vec{y}$ in the POINCARÉ surface of section at $\mathbf{x}$ can be decomposed into its stable and

unstable components

$$\delta\vec{y} \equiv \delta\vec{y}^{\,s} + \delta\vec{y}^{\,u} = \sum_{i=1}^{f-1} s_i\,\vec{e}_i^{\,s}(\mathbf{x}) + u_i\,\vec{e}_i^{\,u}(\mathbf{x})\,. \tag{2.15}$$

Thus it can be characterized by the set of stable coordinates $\{s_i\}$ and unstable coordinates $\{u_i\}$. Using the pairing rule (2.14) the relations (2.6) can be reformulated so that they contain only the vector field $\{\vec{e}_i^{\,u,s}(\mathbf{x})\}$ which are the local directions of the stable and unstable manifolds:

$$\vec{e}_i^{\,u}(\mathbf{x})^T\,\Sigma\,\vec{e}_j^{\,s}(\mathbf{x}) = S_{\mathrm{cl}}\delta_{ij}\;, \quad \vec{e}_i^{\,u}(\mathbf{x})^T\,\Sigma\,\vec{e}_j^{\,u}(\mathbf{x}) = \vec{e}_i^{\,s}(\mathbf{x})^T\,\Sigma\,\vec{e}_j^{\,s}(\mathbf{x}) = 0\,. \tag{2.16}$$

However, these relations (2.16) do not imply that the basis $\{\vec{e}_i^{\,s,u}\}$ is orthogonal since they are based on the symplectic product rather than the usual scalar product.

Furthermore, hyperbolicity implies that after a certain time all initial deviations $\delta\vec{y}$ grow exponentially except when they lie on a stable manifold. This can be illustrated by considering the time evolution of a vector $\delta\vec{y}_0$ by applying the stability matrix $M(t,\mathbf{x})$. By means of the decompositions (2.5), the pairing rule (2.14) and Eq. (2.15) one directly finds

$$\begin{aligned}\delta\vec{y}_t &= \sum_{i=1}^{f-1} s_i(t)\,\vec{e}_i^{\,s}(\mathbf{x}_t) + u_i(t)\,\vec{e}_i^{\,u}(\mathbf{x}_t) \simeq M(t,\mathbf{x}_0)\;\delta\vec{y}_0 \\ &= \sum_{i=1}^{f-1} \Lambda_i(t,\mathbf{x}_0)^{-1}\,s_i(0)\;\vec{e}_i^{\,s}(\mathbf{x}_0) + \Lambda_i(t,\mathbf{x}_0)\,u_i(0)\;\vec{e}_i^{\,u}(\mathbf{x}_0)\,.\end{aligned} \tag{2.17}$$

Thus one can read off the equations of motion for the components $s_i(t)$ and $u_i(t)$ of $\delta\vec{y}_t$. Together with the equations of motion for $\Lambda_i(t,\mathbf{x}_0)$, Eq. (2.8), they can be expressed as

$$u_i(t) = \Lambda_i(t,\mathbf{x}_0)\,u_i(0) \quad \text{and} \quad \dot{u}_i(t) = \chi_i(\mathbf{x}_t)\,u_i(t) \tag{2.18}$$

and similarly for $s_i(t)$. According to the definition of the Lyapunov exponent (2.7) hyperbolicity means that $\Lambda_i(t,\mathbf{x}_0) \sim \exp\lambda_i t$ grows exponentially in the long-time limit. Therefore, all unstable components $u_i(t)$ of any vector $\delta\vec{y}(t)$ also have to grow exponentially on time scales $t \gg \lambda_i^{-1}$ because of Eq. (2.18).

The assumption that the considered system is *continuously* hyperbolic can be expressed by the requirement that

$$\vec{e}^{\,s,u}(\mathbf{x}+\delta\vec{y}) = \vec{e}^{\,s,u}(\mathbf{x}) + \mathcal{O}(\delta\vec{y}) \tag{2.19}$$

is fulfilled for any point in phase space $\mathbf{x}$ and any small displacement $\delta\vec{y}$. This restriction to continuous local stable and unstable directions is not very severe. If for example a hyperbolic billiard system without any singularities of the boundary is

considered then the stability matrix $M(\mathbf{x}, t)$, see Eq. (2.3), is a continuous function of the phase space position $\mathbf{x}$. Since the local stable and unstable directions can be extracted from $M(\mathbf{x}, t)$ via the homological decomposition (2.5) one can conclude that such a system is also continuous hyperbolic. Even if there are isolated singularities of the boundary as it is the case for the cardioid and other billiards the number of phase space points $\mathbf{x}$ where the continuity relation (2.19) is violated is negligible.

Besides being continuously hyperbolic, the systems we consider are also assumed to be mixing which means that

$$\lim_{t\to\infty} \langle a(\mathbf{x}_t)\, b(\mathbf{x})\rangle_{\mathbf{x}} = \langle a(\mathbf{x})\rangle_{\mathbf{x}} \langle b(\mathbf{x})\rangle_{\mathbf{x}} \tag{2.20}$$

for any two functions $a(\mathbf{x})$ and $b(\mathbf{x})$ defined in phase space. The average $\langle \dots \rangle_{\mathbf{x}}$ introduced in Eq. (2.20) is the phase-space average over the constant energy surface, i.e.

$$\langle f(\mathbf{x})\rangle_{\mathbf{x}} \equiv \frac{1}{\Omega(E)} \int\limits_{\substack{\text{phase}\\ \text{space}}} \mathrm{d}\mathbf{x}\; \delta\left(E - H(\mathbf{x})\right)\; f(\mathbf{x}) \tag{2.21}$$

with the normalization $\langle 1\rangle_{\mathbf{x}} = 1$. Thus the volume of the constant energy surface in phase space is given by $\Omega(E) \equiv \int \mathrm{d}\mathbf{x}\; \delta\left(E - H(\mathbf{x})\right)$. The mixing condition basically states that correlations between two different functions at different times decay in the long-time limit. It also implies that a mixing system is ergodic meaning that the time average (2.10) taken along any non-periodic path equals the phase-space average (2.21), i.e. $\langle f(\mathbf{x}_0)\rangle_t = \langle f(\mathbf{x})\rangle_{\mathbf{x}}$ for almost all initial conditions $\mathbf{x}_0$. Ergodicity thus implies that almost all trajectories scan the phase space uniformly in the long-time limit.

Although the above mentioned requirements to the class of systems we consider seem to be rather restrictive they basically just mean that the system shows a strong chaotic behavior. In particular, we are *not* imposing the condition that the system has to be *uniformly* hyperbolic. We stress once more that the systems considered in this work are clean chaotic systems without any disorder.

2.2 Spectral statistics in complex systems

The spectral quantities that are investigated further on are defined in this section. Based on the density of states we introduce the spectral two-point correlation function and its FOURIER transform, the spectral form factor. Finally, we state the results for these quantities that are found by applying random-matrix theory.

The properties of the quantum mechanical spectrum $\{E_n\}$ of the system defined by Eq. (2.1) are determined by the solutions of the corresponding SCHRÖDINGER equation

$$\hat{H}\psi_n(\mathbf{q}) = \left(-\frac{\hbar^2}{2m}\Delta + V(\mathbf{q})\right)\psi_n(\mathbf{q}) = E_n\psi_n(\mathbf{q}) \tag{2.22}$$

subject to the boundary conditions. Based on the corresponding GREEN's function one can define a generalized density of states $d_a(E)$ as

$$d_a(E) \equiv -\frac{1}{\pi}\Im\,\mathrm{tr}\left[\hat{a}\,\hat{G}^+(E)\right] = \sum_n \hat{a}_{nn}\,\delta(E-E_n) \tag{2.23}$$

for a given quantum mechanical operator $\hat{a}$. Here, $\hat{G}^+(E) = 1/(E-\hat{H}+i\varepsilon)$ is the retarded GREEN's function, the E_n denote the eigenenergies of the closed system and $\hat{a}_{nn} \equiv \langle n|\hat{a}|n\rangle$ are the diagonal matrix elements in the energy eigenbasis $\{|n\rangle\}$. Averaging this quantity (2.23) over an energy window of width $\Delta E \ll E$ leads to the average density of states $\bar{d}_a \equiv \langle d_a(E)\rangle_{\Delta E}$. This averaged density of states is a smooth and on quantum scales only slowly varying function of the energy E if the energy average includes many energy levels, i.e. $\Delta E \gg 1/\bar{d}$. If not further specified we will always use an average of the form

$$\langle f(x)\rangle_{\Delta x} = \int_{-\infty}^{\infty} \mathrm{d}x'\, g_{\Delta x}(x'-x)\, f(x')\,. \tag{2.24}$$

The window function $g_{\Delta x}(x)$ can be any normalized, smooth and at $x \sim \pm\Delta x/2$ rapidly decaying function, e.g.

$$g_{\Delta x}(x) = \begin{cases} \exp\left[-\pi\,(x/\Delta x)^2\right]/\Delta x & \text{GAUSSian} \\ \theta_\varepsilon\left(|x|-\Delta x/2\right)/\Delta x & \text{box-like} \end{cases} \tag{2.25}$$

where θ_ε stands for a ε-smoothed step function with $\varepsilon \ll \Delta x$. The usual density of states is retained from Eq. (2.23) by choosing $\hat{a} = 1$ and will be denoted as $d(E) \equiv d_1(E)$.

In terms of the generalized density of states (2.23) the two-point correlation function $C_{ab}(\omega, E)$ is defined as

$$C_{ab}(\omega, E) \equiv \frac{1}{\bar{d}^2}\Big(\big\langle d_a(E+\omega/2)d_b(E-\omega/2)\big\rangle_{\Delta E} - \bar{d}_a\bar{d}_b\Big)\,. \tag{2.26}$$

Again, the energy average $\langle\ldots\rangle_{\Delta E}$ ensures that $C(\omega, E)$ is a slowly varying function of the energy E. Taking the FOURIER transform of Eq. (2.26) with respect to the energy difference ω leads directly to the definition of the generalized form factor

$$K_{ab}(\tau, E) \equiv \bar{d}\left\langle \int_{-\infty}^{\infty} \mathrm{d}\omega\, C_{ab}(\omega, E)\mathrm{e}^{-2\pi\mathrm{i}\omega\bar{d}\tau}\right\rangle_{\Delta\tau}\,. \tag{2.27}$$

Here, the dimensionless time τ is defined in terms of the HEISENBERG time $T_H \equiv 2\pi\hbar\bar{d}$ which represents the time scale associated with the mean level spacing. According to [Pra97] the time average $\langle\ldots\rangle_{\Delta\tau}$ over a small interval $\Delta\tau \ll \tau$ has to be performed in order to obtained a self-averaging spectral form factor. This average

leads effectively to a cutoff in the FOURIER integral over ω at $\omega_{\text{cutoff}} \sim \pm 1/(\bar{d}\,\Delta\tau)$. The special case of the *spectral* form factor $K(\tau)$ is obtained by $\hat{a} = \hat{b} = 1$.

One theory to predict the spectral statistics of complex quantum systems is based on the analysis of fluctuations of eigenvalues of random matrices [Meh90, Por65, Boh89]. It allows for the calculation of the spectral form factor (2.27) in the following way. The underlying assumption is that the HAMILTONian of the quantum system can be represented by a $N \times N$ random matrix. The ensemble of matrices is defined by the general symmetries of the system. In this work we are mainly concerned with the GAUSSian orthogonal ensemble (GOE) which corresponds to HAMILTONians (2.22) that exhibit time-reversal symmetry, e.g. systems with zero magnetic field. This ensemble is defined by all real symmetric matrices such that the ensemble itself is invariant under orthogonal transformations. The linearly independent matrix elements are assumed to be random variables. Another important ensemble is the GAUSSian unitary ensemble (GUE) representing systems without time-reversal symmetry. It contains all hermitian matrices and is invariant under unitary transformations. The random-matrix theory predictions for the spectral form factor (Eq. (2.27) with $\hat{a} = \hat{b} = 1$) in the GOE case are [Meh90, Boh89]

$$K_{\text{GOE}}(\tau) = \left\{ \begin{array}{lll} 2\tau - \tau\ln(1+2\tau) & \text{for} & 0 < \tau < 1 \\ 2 - \tau\ln\left[\frac{2\tau+1}{2\tau-1}\right] & \text{for} & \tau > 1 \end{array} \right\} \approx 2\tau - 2\tau^2 + 2\tau^3 + \ldots \quad (2.28)$$

where the last approximation is a small $\tau \ll 1$ expansion of $K(\tau)$. On the other hand, the GUE result reads

$$K_{\text{GUE}}(\tau) = \left\{ \begin{array}{lll} \tau & \text{for} & 0 < \tau < 1 \\ 1 & \text{for} & \tau > 1 \end{array} \right. \quad (2.29)$$

which is shown in Fig. 1.1(b). Either result is universal in the sense that no system specific parameters enter. The random-matrix theory results (2.28) and (2.29) are valid in the limit of large matrices, i.e. $N \to \infty$.

The transition between the two symmetry classes can be described using a parametric random-matrix theory [PM83]. The basic idea is to introduce a transition parameter α which defines an ensemble of $N \times N$ matrices $H = S + \mathrm{i}\alpha A$. Here, S is a real symmetric matrix with matrix elements S_{ij} that satisfy $\langle S_{ij} \rangle = 0$ when averaged over the ensemble. Furthermore their variance v is fixed so that $\langle S_{ij}^2 \rangle = (1 + \delta_{ij})v^2$. The matrix A is a real antisymmetric matrix with analogous statistical properties. Hence, $\alpha = 0$ yields the GOE case (corresponding to systems with time reversal symmetry) while $\alpha = 1$ gives the GUE case. However, in the limit of large matrices $N \to \infty$ the statistical properties of the eigenvalues of H are non-analytical at $\alpha = 0$ and therefore there is an abrupt transition from the GOE to the GUE case. The proper transition parameter turns out to be $\lambda_{\text{trans}} \equiv \alpha v/\bar{d}$ where $\bar{d}$ is the mean spacing between the eigenvalues and v is the variance [PM83, BGdAS95]. In terms

of this parameter the GOE results are reproduced for $\lambda_{\text{trans}} \to 0$ while the GUE case is given for $\lambda_{\text{trans}} \to \infty$. Within this random-matrix theory framework, the small time limit of the form factor is then given as [PM83, NS03]

$$K_{\text{GOE}\to\text{GUE}}(\tau) \;=\; \tau\left(1+(1-2\tau)\exp\left[-8\pi^2\lambda_{\text{trans}}^2\tau\right]\right) \quad \text{for} \quad \tau \ll 1\,. \tag{2.30}$$

The same universal results that are obtained within the random-matrix theory seem to be applicable for chaotic systems, as conjectured in [BGS84] and supported by a large number of experimental and numerical results [Boh89, Stö99, Haa01]. All further investigations in this thesis are centered around the problem how this statistical behavior described by Eqs. (2.28 – 2.30) in the energy spectrum can be explained for clean chaotic systems. Since the considered clean chaotic systems do not exhibit any disorder the only averages entering Eq. (2.27) are the energy average and the time average but there is no ensemble of systems over which one has to average.

2.3 Semiclassical approach to spectral statistics

In this section we summarize the semiclassical methods and results [Gut90, Haa01, EFMW92] used for the calculation of the spectral correlation functions (2.26, 2.27). This approach is valid in the semiclassical limit $\hbar \to 0$. To be more accurate with the definition of the semiclassical limit one should introduce a dimensionless small parameter instead of using $\hbar$ directly which has the dimensions of an action. If the energy E of the particles is experimentally accessible then the semiclassical approach should be valid for the energy regime where $\bar{d}\,E \gg 1$ meaning that the energy is much bigger than the mean level spacing. Another option is to compare the typical wavelength of the wave functions under consideration with a typical system size. In this case the semiclassical limit is given if the system size is much bigger than the quantum mechanical wavelength of the particle. A third parameter, which we will use frequently, is the ratio between $\hbar$ and a typical classical action S_{cl} of the system, e.g. the action of the shortest periodic orbit as in relation (2.13). Here, the semiclassical limit is described by $S_{\text{cl}}/\hbar \gg 1$.

In order to arrive at a semiclassical approximation for the form factor (2.27) one first evaluates the density of states (2.23) in the semiclassical limit. One way would be to follow the derivation of the Gutzwiller trace formula [Gut90]. This approach can be extended [EFMW92] to the generalized density of states (2.23) by starting from the Wigner transform and its inverse

$$\begin{aligned} a(\mathbf{x}) \equiv a(\mathbf{q},\mathbf{p}) \;&=\; \int \mathrm{d}\bar{\mathbf{q}}\, \left\langle \mathbf{q}+\frac{\bar{\mathbf{q}}}{2}\right| \hat{a} \left|\mathbf{q}-\frac{\bar{\mathbf{q}}}{2}\right\rangle \, \exp\left[-\mathrm{i}\frac{\mathbf{p}\bar{\mathbf{q}}}{\hbar}\right]\,, \\ \langle \mathbf{q}_1 |\hat{a}| \mathbf{q}_2\rangle \;&=\; \frac{1}{(2\pi\hbar)^f}\int \mathrm{d}\mathbf{p}\; a\left(\frac{\mathbf{q}_1+\mathbf{q}_2}{2},\mathbf{p}\right)\, \exp\left[\mathrm{i}\frac{\mathbf{p}(\mathbf{q}_1-\mathbf{q}_2)}{\hbar}\right]\,. \end{aligned} \tag{2.31}$$

This WIGNER transform is a representation of a quantum operator in terms of the classical phase space [Ber77]. Especially, it follows from the definition of the WIGNER transformation (2.31) that the trace of an operator can be written as a phase space integral

$$\mathrm{tr}\left[\hat{a}\,\hat{b}\right] = \frac{1}{(2\pi\hbar)^f} \int\limits_{\substack{\text{phase}\\ \text{space}}} \mathrm{d}\mathbf{x}\, a(\mathbf{x}) b(\mathbf{x}) \tag{2.32}$$

with $a(\mathbf{x})$ and $b(\mathbf{x})$ being the WIGNER transform (2.31) of the operators $\hat{a}$ and $\hat{b}$, respectively. This relation between the trace over quantum operators $\hat{a}$ and $\hat{b}$ on one hand and the associated classical functions $a(\mathbf{x})$ and $b(\mathbf{x})$ on the other hand can be directly applied to the calculation of the semiclassical limit of the generalized density of states (2.23). This limit is then obtained by determining the WIGNER transformation of the GREEN's function and solving all rapidly oscillating integrals, e.g. in Eq. (2.32), in the stationary-phase approximation. It turns out that the occurring phases are stationary for the classical periodic orbits which for hyperbolic systems are unstable and isolated. The result is that the semiclassical expression for the generalized density of states of chaotic systems can be written as a sum of its mean value $\bar{d}_a(E)$ and fluctuations $d_a^{\mathrm{osc}}(E)$ around this mean [Gut90, Wil88, EFMW92, GAB95, CRR99]

$$d_a(E) \equiv \bar{d}_a(E) + d_a^{\mathrm{osc}}(E) \tag{2.33}$$

where

$$\bar{d}_a(E) \approx (2\pi\hbar)^{-f} \int\limits_{\substack{\text{phase}\\ \text{space}}} \mathrm{d}\mathbf{x}\; a(\mathbf{x})\, \delta\left(E - H(\mathbf{x})\right) \tag{2.34}$$

and

$$d_a^{\mathrm{osc}}(E) \approx \frac{1}{\pi\hbar} \Re \sum_{\mathrm{ppo}\{\gamma\}} \sum_{r=1}^{\infty} w_\gamma A_\gamma \exp\left[\mathrm{i}r S_\gamma(E)/\hbar\right] \tag{2.35}$$

with

$$w_\gamma \equiv \frac{T_\gamma \exp(-\mathrm{i}\pi\mu_\gamma r/2)}{\sqrt{\left|\det\left(M_\gamma^r - \mathbf{1}\right)\right|}} \quad \text{and} \quad A_\gamma = A\left(\mathbf{x}_0^\gamma, T_\gamma\right) \equiv \frac{1}{T_\gamma} \int\limits_0^{T_\gamma} \mathrm{d}t\, a(\mathbf{x}_t^\gamma)\,. \tag{2.36}$$

The first contribution $\bar{d}_a(E)$, Eq. (2.34), is the leading order term with respect to $\hbar$ in the so-called WEYL expansion. The function $a(\mathbf{x})$ is the WIGNER function (2.31) of the operator $\hat{a}$. The function $\delta(E - H(\mathbf{x}))$ results from the WIGNER transform of the GREEN's function. The average part $\bar{d}_a(E)$ can be related to the phase space average $\langle a(\mathbf{x})\rangle_{\mathbf{x}}$ by using the fact that the average part of the energy density of states $\bar{d}$ is just given by $\bar{d}(E) = (2\pi\hbar)^{-f}\,\Omega(E)$. Thus, one easily finds

$$\bar{d}_a(E) = \langle a(\mathbf{x})\rangle_{\mathbf{x}}\, \bar{d}(E) \tag{2.37}$$

which is a function that depends only weakly on the energy E.

The second contribution (2.35) to the density of states (2.33) is a rapidly oscillating function of the energy E. The first sum runs over all primitive periodic orbits labeled by γ while the second sum counts the repetitions r of each primitive orbit. The w_γ represent the classical weights (2.36) in terms of the stability matrix M, the MASLOV index μ and the repetition number r. The dependence on the operator $\hat{a}$ enters via A_γ which is the integral (2.36) over its classical phase space representation $a(\mathbf{x})$ along the periodic orbit γ. To simplify the notation we will from now on formally include the number of repetitions r in the label γ when summing over periodic orbits.

Using the definitions of the two-point correlation function (2.26) and the form factor (2.27) we obtain from Eq. (2.35) the semiclassical representation of the generalized form factor [Ber85, EM95] in chaotic systems

$$K_{ab}(\tau) = \left\langle \sum_{\gamma,\gamma'} \frac{(w_\gamma A_\gamma)(w_{\gamma'} B_{\gamma'})^*}{T_H^2} \exp\left[\mathrm{i}\frac{S_\gamma(E) - S_{\gamma'}(E)}{\hbar}\right] \delta_{\Delta\tau}\left(\tau - \frac{T_\gamma + T_{\gamma'}}{2T_H}\right) \right\rangle_{\Delta E} . \tag{2.38}$$

Because of the energy average over ΔE with $1/\bar{d} \ll \Delta E \ll E$ the function $K_{ab}(\tau, E)$ is a smooth and slowly varying function of E. Since the main interest however is in the functional dependence on the rescaled time τ we will drop the argument E in the spectral form factor, i.e. $K_{ab}(\tau, E) \equiv K_{ab}(\tau)$, from now on. The width of the δ-function is due to the time average $\langle \dots \rangle_{\Delta\tau}$ in Eq. (2.27).

As expressed in Eq. (2.38) the form factor in the semiclassical limit is determined by a double sum over pairs of periodic orbits (γ, γ'). The length of the involved orbits is of the order of the HEISENBERG time T_H because of the δ-function in Eq. (2.38). Since $T_H \equiv (2\pi\hbar)\bar{d} = \Omega(E)/(2\pi\hbar)^{f-1}$ and $f \geq 2$ the limit $\hbar \to 0$ implies that all involved periodic orbits are very long compared to the classical length scales as for example the system size. The typical classical actions $S_\gamma(E)$ of these paths are large compared to the quantum mechanical action $\hbar$. This means that the exponential function in Eq. (2.38) is a rapidly oscillating function of the energy E as long as the action difference $S_{\gamma,\gamma'} = S_\gamma - S_{\gamma'}$ is not of the order of $\hbar$. Therefore, the energy average over the quantum mechanically large interval $\Delta E \gg 1/\bar{d}$ strongly suppresses the contributions of most orbit pairs (γ, γ').

The major contribution to the double sum in Eq. (2.38) is therefore due to the terms where a path γ is paired with itself or, if time-reversal symmetry is present, with its time-reversed version γ^i. Then the action difference in Eq. (2.38) vanishes identically. To cover either case we introduce a parameter g such that

$$g = \begin{cases} 1 & \text{if time-reversal symmetry is absent} \\ 2 & \text{if time-reversal symmetry is present} \end{cases} \tag{2.39}$$

assuming that there are no further symmetries among the periodic orbits. Considering only those pairs (γ, γ) and (γ, γ^i), see Fig. 2.3(a), reduces the double sum in

Eq. (2.38) to a single sum. This approximation is known as the diagonal approximation [Ber85, EM95] and we will denote the resulting form factor by $K_{ab}^{(1)}(\tau)$. Within this approximation it is furthermore $T_\gamma = T_{\gamma^i}$ and $w_\gamma = w_{\gamma^i}$ (see e.g. [FR97] for a study of the MASLOV indices under time-reversal) so that one finds

$$\begin{aligned} K_{ab}^{(1)}(\tau) &= \tau \big\langle A_\gamma B_\gamma + (g-1) A_\gamma B_{\gamma^i} \big\rangle_{\gamma, \tau T_H} \\ &= \tau \left\langle \frac{1}{T_\gamma^2} \int_0^{T_\gamma} \mathrm{d}t\, a(\mathbf{x}_t^\gamma) \int_0^{T_\gamma} \mathrm{d}t' \, \left[b(\mathbf{x}_{t+t'}^\gamma) + (g-1) b(\mathbf{x}_{t+t'}^{\gamma,i}) \right] \right\rangle_{\gamma, \tau T_H} \end{aligned} \tag{2.40}$$

where the average over periodic orbits $\langle \dots \rangle_{\gamma,T}$ contains all periodic trajectories of a given length $T_\gamma \simeq T = \tau T_H$ each weighted by $|w_\gamma|^2$, Eq. (2.36). It is defined by

$$\big\langle \dots \big\rangle_{\gamma,T} \equiv \frac{1}{T} \sum_\gamma \dots |w_\gamma|^2 \, \delta_{\Delta T}(T - T_\gamma) \,. \tag{2.41}$$

In order to further evaluate Eq. (2.40) one has to perform this average over periodic orbits. This can be done by means of a sum rule for periodic orbits [HA84]. The last equation in (2.40) is already written such that it allows to employ the specific form of the sum rule given by [PP90]

$$\left\langle \frac{1}{T_\gamma} \int_0^{T_\gamma} \mathrm{d}t\, f(\mathbf{x}_t^\gamma) \right\rangle_{\gamma,T} \approx \frac{1}{T} \int_0^{T} \mathrm{d}t\, f(\mathbf{x}_t) \approx \langle f(\mathbf{x}) \rangle_{\mathbf{x}} \quad \text{for} \quad T \to \infty \,. \tag{2.42}$$

The left hand side is an average of any function $f(\mathbf{x})$ over all periodic orbits of given length while the integral on the right hand side goes along any non-periodic ergodic path starting at any initial condition $\mathbf{x}_0$. Physically it means that a set of all periodic orbits with given long period T fills the phase space uniformly if the weights w_γ are included appropriately. However, this does not necessarily imply that a single periodic orbit is ergodic. The sum rule (2.42) is based on the fact that the classical weights are exponentially small, i.e. $|w_\gamma|^2 \approx T_\gamma^2 \exp\left[-\lambda T_\gamma\right]$, which is compensated by an exponentially large number of periodic orbits. This large number of periodic orbits then allows to replace the sum in Eq. (2.41) by an integral, i.e. $\sum_\gamma \to \int \mathrm{d}T_\gamma \exp\left[\lambda T_\gamma\right] / T_\gamma$.

Applying the sum rule (2.42) to the diagonal approximation (2.40) then leads to the semiclassical result

$$K_{ab}^{(1)}(\tau) = g\, \tau \, \langle a(\mathbf{x}) \rangle_{\mathbf{x}} \, \langle b(\mathbf{x}) \rangle_{\mathbf{x}} \qquad \text{for} \quad \hbar \to 0 \,. \tag{2.43}$$

The long-time limit required for the sum rule (2.42) is automatically fulfilled in the semiclassical limit because the δ-function in Eq. (2.41) ensures orbit lengths of the order of the HEISENBERG time T_H. If the random-matrix theory results (2.28) in

the GOE ($g = 2$) case and (2.29) in the GUE ($g = 1$) case are compared with the semiclassical approach based on the diagonal approximation yielding Eq. (2.43) then one finds that the leading small $\tau \ll 1$ behavior of the spectral form factor $K(\tau)$ is reproduced, see Fig. 1.1(b). However, a detailed explanation of the complete functional shape of $K(\tau)$ can not be given within the diagonal approximation. The reason is that one has neglected all off-diagonal terms in the double sum over periodic orbits in the semiclassical expression for the form factor (2.38). These off-diagonal terms are related to correlations between the actions of classical periodic orbits. If one assumes that the spectral statistics exactly follows the random-matrix theory then one can draw conclusions about these action correlations [ADD+93]. Several works aimed at an extraction of these action correlations from the underlying classical dynamics, see e.g. [Tan99] and [SV03]. However, a complete derivation of the spectral form factor for any value of τ could not be found yet.

It is worth noting that a small but fixed *rescaled* time τ still implies large *unscaled* times $T = \tau T_H$ in the semiclassical limit. The time scale on which we study the form factor is thus given by $t_{\mathrm{erg}} \ll T \ll T_H$ where t_{erg} is the time after which the systems typically reaches its ergodic behavior. For shorter times $T \lesssim t_{\mathrm{erg}}$, the spectral form factor shows non-universal features which are determined by the short periodic orbits. In case of the diagonal approximation this can be immediately seen from Eqs. (2.40) and (2.41) which just give a sum over δ-peaks as the application of the sum rule (2.42) is not justified for short times, see also [AAA95].

2.4 Matrix element statistics

In this section we briefly discuss the relation between matrix element fluctuations and correlation functions such as the form factor (2.27). This problem is related to the statistical properties of wave functions in chaotic systems. A frequently used assumption supported by Shnirelman's theorem [Shn74, Pec83, Zel87, dV85] is that wave functions in chaotic systems tend to be uniformly distributed in the semiclassical limit. More specifically, the theorem states that in the semiclassical limit almost all matrix elements of an operator $\hat{a}$ converge to the microcanonical phase space average of the associated Wigner function (2.31), i.e.

$$\hat{a}_{nn} \equiv \langle n|\hat{a}|n\rangle \approx \langle a(\mathbf{x})\rangle_{\mathbf{x}} \quad \text{for} \quad \hbar \to 0 \quad \text{and} \quad E_n \simeq E = const \tag{2.44}$$

where $|n\rangle$ is the energy eigenstate corresponding to the eigenvalue E_n. This relation applies to almost all eigenstates $|n\rangle$. There are exceptions like Heller's scarred wave functions [Hel84] but the set of these exceptional states is of measure zero if compared to all eigenstates.

One possibility to study the accuracy of the estimate (2.44) is to consider fluctuations of the matrix elements around their expected mean value. An early step

into this direction is described in [FP86] where the relation

$$\sum_m \exp\left[\mathrm{i}\frac{E_n - E_m}{\hbar}t\right]|a_{nm}|^2 = \langle n|\hat{a}(t)\hat{a}(0)|n\rangle \approx \langle a(\mathbf{x}_t)a(\mathbf{x}_0)\rangle_{\mathbf{x}} = \mathcal{C}_{aa}(t) + \langle a(\mathbf{x})\rangle_{\mathbf{x}}^2 \tag{2.45}$$

between the $\hat{a}_{nm}$ and the classical correlation function $\mathcal{C}_{aa}(t)$ was derived. This classical correlation function is defined as

$$\mathcal{C}_{ab}(t) \equiv \langle a(\mathbf{x})b(\mathbf{x}_t)\rangle_{\mathbf{x}} - \langle a(\mathbf{x})\rangle_{\mathbf{x}}\langle b(\mathbf{x})\rangle_{\mathbf{x}} \tag{2.46}$$

where the phase-space average is taken over the initial conditions $\mathbf{x} = \mathbf{x}_0$. The relation given above can be used to consider the fluctuations of the matrix elements by applying a FOURIER transformation to Eq. (2.45). A similar analysis is presented in [Wil87] where the spectral correlation function

$$S(E,\omega) \equiv \sum_{n,m} |\hat{a}_{nm}|^2\, \delta\left(\omega - (E_n - E_m)\right)\, \delta\left(E - \frac{E_n + E_m}{2}\right) \tag{2.47}$$

was related to the FOURIER transform of the classical correlation function $\mathcal{C}_{aa}(t)$.

A slightly different approach was suggested in [EM95, Eck97] where the form factor (2.27) was associated with the matrix element fluctuations in the following way. The two-point correlation function (2.26) can be rewritten as

$$\begin{aligned}\overline{d}^2 C_{ab}(\omega) = &\sum_n \hat{a}_{nn}\hat{b}_{nn}\, \langle\delta(E - E_n)\rangle_{\Delta E}\, \delta(\omega) \\ &+ \sum_{n,m\neq n}\left[\hat{a}_{nn}\hat{b}_{mm}\left\langle\delta\left(E - \frac{E_n + E_m}{2}\right)\right\rangle_{\Delta E}\delta\left(\omega - [E_n - E_m]\right)\right] - \bar{d}_a\bar{d}_b\end{aligned} \tag{2.48}$$

if the diagonal terms are separated from the off-diagonal terms. The long-time limit of the form factor (2.27), i.e. the time averaged FOURIER transform of Eq. (2.48), is hence given as

$$K_{ab}(\tau \gg 1) \approx \overline{d}^{-1} \sum_{\substack{n \\ |E-E_n|<\Delta E/2}} \hat{a}_{nn}\hat{b}_{nn}\, \langle\delta(E - E_n)\rangle_{\Delta E} \approx \frac{1}{\Delta N}\sum_n \hat{a}_{nn}\hat{b}_{nn} \tag{2.49}$$

with $\Delta N = \bar{d}\,\Delta E$ being the number of states with $|E_n - E| < \Delta E/2$. Based on this relation and on the assumption that $K_{ab}(\tau = 1) \approx K_{ab}(\tau \gg 1)$ the variance of the matrix element fluctuations was semiclassically estimated using the diagonal approximation [EM95]. Similarly, one can average the two-point correlation function (2.48) over ω with $\Delta\omega \ll \overline{d}^{-1}$ and then set $\omega = 0$. This gives the variance [EFK+95]

$$\sigma_a^2 \;\equiv\; \frac{1}{\Delta N}\sum_{\substack{n \\ |E-E_n|<\Delta E/2}} \hat{a}_{nn}^2 \;\approx\; \bar{d}\,\Delta\omega\,\left\langle C_{aa}(\omega = 0, E)\right\rangle_{\Delta\omega} \tag{2.50}$$

where we have assumed that $\hat{a} = \hat{b}$ and that the matrix elements $\hat{a}_{nn}$ fluctuate around 0, i.e. $\overline{\hat{a}_{nn}} = 0$. The ω-average corresponds to a smearing of the energy levels on a scale much smaller than the mean level spacing. The accuracy of this approximated relation depends on the type of the window function chosen for the energy average. A recent application of the techniques presented above to cross-section correlations is described in [EFV00, EVP01].

These relations between the correlation function $C_{ab}(\omega)$ or its FOURIER transform $K_{ab}(\tau)$ on one hand and the matrix element fluctuations on the other hand are a motivation to extend the semiclassical evaluation of the spectral form factor $K(\tau) = K_{11}(\tau)$ to the generalized form factor $K_{ab}(\tau)$. In Section 5.3, we will show that to leading order in $\hbar$ the relation $K_{ab}(\tau) = \langle a(\mathbf{x})\rangle_{\mathbf{x}}\langle b(\mathbf{x})\rangle_{\mathbf{x}} K_{11}(\tau)$ holds. We then focus on the special case $\langle a(\mathbf{x})\rangle_{\mathbf{x}} = \langle b(\mathbf{x})\rangle_{\mathbf{x}} = 0$ and determine the next order correction in $\hbar$ which turns out to be related to the classical correlation function $\mathcal{C}_{ab}(t)$.

2.5 Beyond the diagonal approximation: configuration-space approach

The first attempt [SR01] to include off-diagonal contributions to the small τ behavior of the spectral form factor $K(\tau)$ based on orbit pairs with correlated actions is briefly reviewed in this section. The starting point is once more the semiclassical expression (2.38) with $A_\gamma = B_\gamma \equiv 1$ for the spectral form factor. The derivation in [SR01] is restricted to two-dimensional, i.e. $f = 2$, *uniformly* hyperbolic systems [BV86, AS88]. Time-reversal symmetry is assumed to be present. The basic idea is that there are further pairs (γ, γ^p) of classical periodic orbits with small action differences besides the ones considered in the diagonal approximation (2.40). The contribution of these pairs to the spectral from factor is denoted by $K^{(2)}(\tau)$. The total result for the spectral form factor in the semiclassical approach is then a sum of the contribution calculated in the diagonal approximation and the contribution due to the first off-diagonal terms, i.e. $K(\tau) = K^{(1)}(\tau) + K^{(2)}(\tau) + \ldots$. The derivation [SR01] which is summarized in this section aims at a calculation of $K^{(2)}(\tau)$.

First, it is shown that a self-intersecting periodic orbit γ with a small crossing angle $\varepsilon \ll 1$ has a corresponding partner γ^p avoiding this crossing. Then the action difference $S(\varepsilon)$ is derived for this orbit pair as a function of the crossing angle. In order to calculate the contribution of all these orbit pairs (γ, γ^p) in the spectral form factor (2.38) one needs to know how many crossings of a given crossing angle ε there are for a certain periodic orbit γ. This number of crossings is estimated via the crossing angle distribution $P(\varepsilon, T)$ in the limit of long orbits $T \sim T_H \to \infty$. It is shown that the deterministic dynamics of the system (2.1) is responsible for a small correction to the crossing angle distribution that one obtains by assuming ergodicity

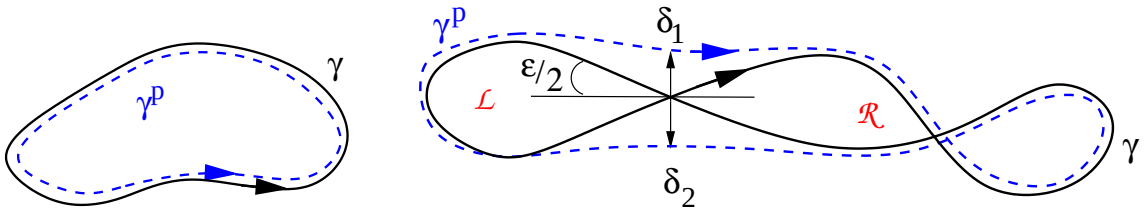

(a) Diagonal approximation (b) Orbit pair for off-diagonal contribution

Figure 2.3: (a) *Orbit pair* $(\gamma, \gamma^p) = (\gamma, \gamma)$ *as considered in the diagonal approximation (2.43). If time-reversal symmetry is present then one also has to include the pair* (γ, γ^i). (b) *Schematic drawing of a periodic orbit* γ *(solid line) and the corresponding partner orbit* γ^p *(dashed line) which are considered for the first off-diagonal correction in the configuration-space approach. For each crossing with a small crossing angle* $\varepsilon \ll 1$ *there is a partner. Here, only the partner for the left crossing is shown. The distance in configuration space between* γ *and* γ^p *at the crossing is denoted by* δ_1 *and* δ_2*. The stability matrices of the left loop* $\mathcal{L}$ *and the right loop* $\mathcal{R}$ *are denoted as* L *and* R*, respectively.*

only. However, it turns out that it is exactly this small correction which eventually reproduces the small $\tau \ll 1$ expansion of the spectral form factor as expected from the random-matrix theory prediction (2.28), namely $K^{(2)}(\tau) = -2\tau^2$.

The derivation of $K^{(2)}(\tau)$ in [SR01] was based on the assumption that the two-dimensional system under consideration is uniformly hyperbolic, e.g. the motion on RIEMANN surfaces of constant negative curvature is considered [BV86, AS88]. The calculation is significantly simplified if it is restricted to these special systems for the following reasons. The phase space does not have an internal structure and the local growth rate is constant, i.e. $\chi(\mathbf{x}) = \lambda$. Therefore all periodic orbits share the same LYAPUNOV exponent $\lambda^\gamma = \lambda$. The stability matrix as defined in Eq. (2.3) can be explicitly determined and is given by

$$M(\mathbf{x}, t) = M(t) = \begin{pmatrix} \cosh \lambda t & (m\lambda)^{-1} \sinh \lambda t \\ (m\lambda) \sinh \lambda t & \cosh \lambda t \end{pmatrix} . \tag{2.51}$$

The local stable and unstable directions (2.15) are $\vec{e}^{(u,s)}(\mathbf{x}) \sim (\pm 1, m\lambda)$ independently of the position $\mathbf{x}$ in phase space. There are no MASLOV indices in the uniformly hyperbolic system.

The orbit pairs (γ, γ^p) entering the first off-diagonal correction to the form factor (2.38) can be characterized as follows. Consider a periodic orbit γ which has a self-intersection. As it will turn out in due course it is sufficient to consider small crossing angles $\varepsilon \ll 1$ only. In this case there is a second periodic orbit γ^p which avoids this crossing but otherwise follows the original orbit γ closely in configuration space.

This implies that the partner orbit γ^p follows the original orbit γ during one loop while having a different orientation during the second loop, see Fig. 2.3(b). Since the crossing angle ε is assumed to be small one can employ the linearized equations of motion (2.3) to determine the geometry of the partner γ^p. In terms of the stability matrix L (R) of the left (right) loop these equations read

$$\begin{aligned} \begin{pmatrix} \delta_2 \\ p(\alpha_2 + \varepsilon/2) \end{pmatrix} &= R \begin{pmatrix} \delta_1 \\ p(\alpha_1 - \varepsilon/2) \end{pmatrix}, \\ \begin{pmatrix} -\delta_2 \\ p(\alpha_2 - \varepsilon/2) \end{pmatrix} &= L \begin{pmatrix} -\delta_1 \\ p(\alpha_2 + \varepsilon/2) \end{pmatrix}. \end{aligned} \tag{2.52}$$

This set of equations is correct up to first order in the small parameter ε. The geometrical meaning of the parameters δ_1 and δ_2 is shown in Fig. 2.3(b). The remaining geometry related parameters α_1 and α_2 describe the angle between the momentum of the partner orbit at the crossing and the horizontal line. Thus one has four independent equations for the four parameters $\delta_{1,2}$ and $\alpha_{1,2}$. Solving these equations in terms of the parameters uniquely defines the geometry of the partner orbit within the linear approximation.

The action difference between the two classical orbits γ and γ^p is then calculated by expanding the action of the original path in terms of the small parameters $\delta_{1,2}$ and $\alpha_{1,2}$. It turns out that the second-order terms are of the same order of magnitude as the first-order terms. Including first and second order corrections then leads to the resulting action difference $S_{\gamma,\gamma^p} = p\varepsilon(\delta_1+\delta_2)/2$, where the $\delta_{1,2}$ have to be determined by solving Eqs. (2.52). Because of the special structure of the stability matrix (2.51) one finds the result

$$S_{\gamma,\gamma^p} = S(\varepsilon) = \frac{p^2}{2m\lambda}\varepsilon^2 \tag{2.53}$$

which shows a quadratic dependence of the action difference on the small parameter ε. Because only pairs (γ, γ^p) with small action differences contribute significantly to the form factor (2.38) it is consistent to restrict the above considerations to small crossing angles $\varepsilon \sim \sqrt{\hbar}$.

The contribution of the pairs (γ, γ^p) in the double sum occurring in the spectral form factor (2.38) is calculated in the following way. The first sum over periodic orbits in Eq. (2.38) remains unaltered while the second sum is arranged in such a way that all partner orbits are sorted according to their corresponding crossing angles. If the number $P_\varepsilon(T_\gamma) = P(\varepsilon, T_\gamma)\mathrm{d}\varepsilon$ of crossings with an angle in the range $\varepsilon \ldots \varepsilon + \mathrm{d}\varepsilon$ were known then the expression (2.38) could be rewritten as

$$\begin{aligned} K^{(2)}(\tau) &= 2\tau \frac{2}{T} \Re \left\langle \sum_\gamma \sum_\varepsilon P_\varepsilon(T_\gamma) |w_\gamma|^2 \exp\left[\mathrm{i}\frac{S(\varepsilon)}{\hbar}\right] \delta_{\Delta\tau}(T - T_\gamma) \right\rangle_{\Delta E} \\ &= 4\tau \Re \left\langle \left\langle \int_0^\pi \mathrm{d}\varepsilon\, P(\varepsilon, T_\gamma) \exp\left[\mathrm{i}\frac{S(\varepsilon)}{\hbar}\right] \right\rangle_{\gamma,T} \right\rangle_{\Delta E} \end{aligned} \tag{2.54}$$

for the uniform system. In the second line of Eq. (2.54) the average over periodic orbits (2.41) was formally introduced in addition to the energy average. One factor of two appears because of time-reversal symmetry. The second factor of two is due to the fact that one has to count the pair (γ, γ^p) as well as the pair (γ^p, γ). Only the first pair is associated with a crossing while the second pair is associated with an avoided crossing. But since the action difference of these two pairs differs only in sign, one can include this by taking twice the real part of the sum over all orbits. In the semiclassical limit $\hbar \to 0$ the major contribution to the integral in Eq. (2.54) is due to small angles $\varepsilon \sim \sqrt{2m\lambda\hbar}/p \ll 1$ which are associated with an action difference $S(\varepsilon) \sim \hbar$. Therefore, it is also sufficient to determine the crossing angle distribution $P(\varepsilon, T)$ for small values of ε only. Furthermore, any length difference of the orbits is neglected in the prefactor of the exponential in Eq. (2.54) since it changes on a much larger scale than the exponential. Therefore, the correction obtained by considering $T_{\gamma^p} = T_\gamma + \Delta T \neq T_\gamma$ in the prefactor would be small in the limit of small crossing angles. This implies that the weights w_γ and w_{γ^p} can also be treated as equal because there are no MASLOV indices in the uniformly hyperbolic system.

The crossing angle distribution is defined as

$$P(\varepsilon, T) = \left\langle \frac{1}{2} \int_0^T \mathrm{d}t \int_0^T \mathrm{d}t' \, |J| \, \delta(\mathbf{q}_t - \mathbf{q}_{t'}) \delta(\varepsilon - |\angle[\mathbf{p}_t, \mathbf{p}_{t'}]|) \right\rangle_{\mathbf{x}_0 = (\mathbf{q}_0, \mathbf{p}_0)} \tag{2.55}$$

with the average taken over different initial conditions $\mathbf{x}_0 = (\mathbf{q}_0, \mathbf{p}_0)$. The angle between the two momenta $\mathbf{p}_t$ and $\mathbf{p}_{t'}$ is denoted by $\angle[\mathbf{p}_t, \mathbf{p}_{t'}]$. The Jacobian of the variable transformation is given by $|J| = m^{-2} |\mathbf{p}_t \times \mathbf{p}_{t'}|$. Analytical considerations for the uniformly hyperbolic system [SR01, Sie02] yield that the long-time limit $T\lambda \gg 1$ of Eq. (2.55) can be written as a sum of a leading contribution and a smaller correction

$$P(\varepsilon, T) = P^{(\mathrm{lead})}(\varepsilon, T) + P^{(\mathrm{corr})}(\varepsilon, T) = \frac{T^2 \, |\mathbf{p}|^2}{2\pi \, m^2 \, A} \sin\varepsilon \left(1 + \frac{4}{\lambda T} \ln \left[\frac{\varepsilon}{c} \right] \right). \tag{2.56}$$

Here, c is a constant of order unity. The leading term can be obtained by using ergodicity and neglecting the classical dynamics of the system. The correction is of the order of $\hbar \ln \hbar$ compared to the leading term since the times involved are of the order of the HEISENBERG time, i.e. $T \sim T_H \sim \hbar^{-1}$, while $\varepsilon \sim \sqrt{\hbar}$. For the uniform system numerical calculations showed excellent agreement with above result [SR01]. The physical reason for the small deviations $P^{(\mathrm{corr})}(\varepsilon, T)$ from the leading contribution lies in the following fact [Sie02]. Consider two paths starting at the crossing with a small crossing angle $\varepsilon \ll 1$. If these two paths are to form a loop they must have a certain minimal loop length. This minimal loop length is determined by the fact that the deviation between the two almost parallel momenta

has to grow so that the loop actually closes. This means that the momenta have to point in exactly opposite direction when the loop closes. Quantitatively this time $T_{\min}$ can therefore be estimated for small ε by assuming an exponential growth of the initial deviation $p\varepsilon$ until it reaches a given value determined by the constant $c \sim 1$. Thus, the minimal loop time is given by $T_{\min} = -2\lambda^{-1} \ln(c\varepsilon)$. If this minimal loop time is included in the derivation of the crossing angle distribution one is lead to the result (2.56) given above.

The knowledge of the crossing angle distribution (2.56) allows to proceed with the calculation of the spectral form factor (2.54). Since only the small crossing angle limit of $P(\varepsilon, T)$ is important one can expand $\sin \varepsilon \approx \varepsilon$. Applying the sum rule (2.42) to Eq. (2.54) and solving the integral over ε one finds that the energy average suppresses the contribution coming from $P^{(\mathrm{lead})}(\varepsilon, T)$ and yields $K^{(2)}(\tau) = 0$. This means that one indeed must not neglect the dynamics of the system which gives rise to the small correction $P^{(\mathrm{corr})}(\varepsilon, T)$ in Eq. (2.56). If the contribution to Eq. (2.54) due to this correction is evaluated one finds $K^{(2)}(\tau) = -2\tau^2$ in the limit $\hbar \to 0$. Thus the method described above to include off-diagonal terms in the derivation of the semiclassical spectral form factor (2.38) does indeed reproduce the next order term in the expansion of the universal random-matrix theory result (2.28).

It is clear that the procedure described so far works only in systems where time-reversal symmetry is present. If this is not the case, e.g. if a magnetic field is applied, then the action difference between the original orbit γ and its partner is not only due to the geometric deviations in the region around the crossing. An additional action difference is accumulated while going along the loop that is traversed in opposite directions, e.g. during the left loop in Fig. 2.3(b). Therefore, in this case the constructed partners (γ, γ^p) do not necessarily have small action differences. This implies that their contribution to the double sum (2.38) also vanishes after averaging over the energy. Therefore, the total correction to the diagonal approximation of the form factor (2.43) can be written as $K^{(2)}(\tau) = -2(g-1)\tau^2$.

In conclusion, the derivation reviewed in this section provides a first step in the direction of proving the applicability of the random-matrix theory results (2.28) and (2.29) to chaotic systems. However, a few essential assumptions were necessary in order to construct the theory based on the loops. First of all, the approach described above is restricted to the uniformly hyperbolic system, e.g. the precise knowledge of the stability matrix (2.51) was necessary to derive the action difference (2.53). Furthermore, Maslov indices are not present in uniformly hyperbolic systems. However, in general the phase in Eq. (2.38) does not only contain the action difference but also the difference in Maslov indices of the two periodic orbits. The second point is that above scheme for the calculation of $K^{(2)}(\tau)$ is based on a configuration-space approach rather than on phase-space methods. Therefore the formulation presented in [SR01] is not invariant under canonical transformations. As we show in Chapter 4, the assumption that each single crossing corresponds to

a partner orbit is in general also incorrect for non-uniformly hyperbolic systems. This means that the crossing angle distribution is not necessarily the quantity that enters the spectral form factor. However, an extension from the configuration-space formulation towards a phase-space approach clarifies this question as well. Finally, one would expect that the random-matrix theory result (2.28) is not restricted to two-dimensional systems with $f = 2$. It is clear that one cannot use the formulation based on crossings in the case of systems with more degrees of freedom since the concept of two paths crossing each other is adapted to the motion in a plane. Nevertheless, in Chapter 3 we first investigate to which extent the theory sketched above can be generalized to non-uniformly hyperbolic systems and where exactly the limitations for its applicability occur. To this end we first study a specific two-dimensional non-uniformly hyperbolic system within the configuration-space approach. In particular, we investigate the crossing angle distribution $P(\varepsilon, T)$ as it is a major ingredient for the configuration space approach. Then, in Chapter 4, we present a phase-space generalization which provides a canonically invariant formulation of this approach. Eventually, our formulation makes an extension of the theory to systems with more than two degrees of freedom possible, see Section 5.1.

CHAPTER 3

Crossing angle distribution in billiard systems

In this chapter the crossing angle distribution for a non-uniformly hyperbolic system is investigated numerically. First we review the crossing angle distribution of the uniformly hyperbolic billiard. Then we introduce a specific non-uniformly hyperbolic system: we choose the family of Limaçon billiards as an example. We present numerical results concerning the crossing angle distribution and extract the corrections to the leading ergodic contribution. We show that these corrections are indeed due to the dynamics of the system and furthermore have a logarithmic dependence on the crossing angle as in the case of the uniformly hyperbolic system. However, we also present arguments why an extension of the approach for uniform systems to non-uniform systems should be based on phase-space objects rather than on crossings in configuration space.

3.1 Crossing angle distribution in the uniformly hyperbolic billiard

In Section 2.5 we reviewed a semiclassical method for the calculation of off-diagonal contributions to the form factor. This method is based on classical periodic orbits with correlated actions. These correlations were expressible in terms of orbit pairs

(γ, γ^p) with a small action difference. The geometrical basis for the identification of these pairs are crossings in configuration space with small crossing angles ε. The total contribution of all these pairs to the double sum over periodic orbits in the semiclassical form factor (2.38) can then be evaluated in terms of the classical crossing angle distribution $P(\varepsilon, T)$, Eq. (2.54). As the leading term in this distribution, see Eq. (2.56), gives a vanishing result for the off-diagonal contributions to the form factor one has to consider the next order correction $P^{(\mathrm{corr})}(\varepsilon, T)$. Including this correction then leads to the random-matrix theory prediction $K^{(2)}(\tau) = -2\tau^2$. It is crucial for the derivation of this *universal* result that the system specific LYAPUNOV exponent occurring in the crossing angle distribution (2.56) exactly cancels the LYAPUNOV exponent in the prefactor of the action difference (2.53). Hence the approach in Section 2.5 is restricted to uniform systems as for them there is only a single LYAPUNOV exponent associated to all periodic orbits, i.e. $\lambda^\gamma = \lambda$. In contrast to this basic system all *non-uniform* hyperbolic systems are characterized by a whole distribution of LYAPUNOV exponents $\{\lambda^\gamma\}$ or, equivalently, a non-constant local growth rate $\chi(\mathbf{x})$, see Eq. (2.8), that depends on the position $\mathbf{x}$ in phase space. Therefore, one expects that a universal result for the form factor must be due to a somewhat different and more subtle mechanism as the one proposed in Section 2.5.

Before presenting our numerical results on the cardioid billiard in the following sections, we give a short review of the arguments leading to Eq. (2.56) as they were presented in [SR01, Sie02, RS02, BHH02]. Especially we focus on $P^{(\mathrm{corr})}(\varepsilon, T)$ in Eq. (2.56) as this correction determines the final result for the form factor $K^{(2)}(\tau) = -2\tau^2$. It is worth stressing once more the fact that this crossing angle distribution is a purely classical quantity.

The number of self-crossings with a certain angle $\varepsilon \ldots \varepsilon + \mathrm{d}\varepsilon$ is given by

$$P(\varepsilon, T)\,\mathrm{d}\varepsilon = \frac{2|\mathbf{p}|^2}{m} \int_{T_{\min}}^{T-T_{\min}} \mathrm{d}t_{\mathrm{loop}}\,(T - t_{\mathrm{loop}})\,\sin\varepsilon\; p_{\mathrm{erg}}\,\mathrm{d}\varepsilon\,. \tag{3.1}$$

This expression can be understood as follows. The integration goes over all possible loop lengths and adds the probabilities that a crossing with angle $\varepsilon \ldots \varepsilon + \mathrm{d}\varepsilon$ and corresponding loop length t_{loop} occurs. This probability is proportional to the length of the remaining trajectory $(T - t_{\mathrm{loop}})$ times the ergodic return probability $p_{\mathrm{erg}} = 1/(2\pi m A)$ if ergodicity is assumed. Furthermore, the angular dependence enters via the $\sin\varepsilon$ as small crossing angles are less likely than larger angles, see Fig. 3.1(a). The leading ergodic part $P^{(\mathrm{lead})}(\varepsilon, T)$ is given by setting the minimal loop time $T_{\min} = 0$ in Eq. (3.1) and is derived in detail in [SR01]. However, the most important part of the crossing angle distribution for our purpose is determined by exactly this minimal loop time $T_{\min}$ in Eq. (3.1). It accounts for the fact that a loop starting and ending at the crossing needs a certain time to close itself. Therefore each loop has a minimal length $T_{\min}$ and a maximal length $T - T_{\min}$. This time $T_{\min}$

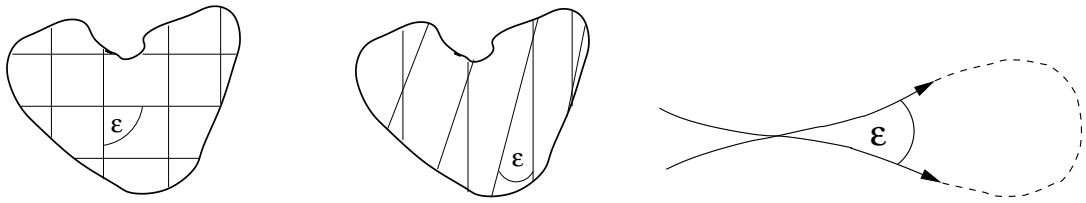

(a) Ergodic model for crossings (b) Minimal loop time

Figure 3.1: (a) *Simple model for the ergodic behavior of a billiard system with respect to the crossing angle. We assume that a path of a fixed length can be represented by its single segments that fill the phase space uniformly. Then it is clear that for fixed path length there are more large crossing angles (situation depicted in the left part of the figure) than small ones (right part of the figure). Subfigure* (b)*: If two classical paths leave a crossing with small angle ε it takes a certain time $T_{\min}(\varepsilon)$ until they can form a closed loop. This time depends logarithmically on the crossing angle if hyperbolicity is assumed.*

depends logarithmically on the crossing angle ε as was confirmed in detailed numerical [SR01] and analytical studies [Sie02, BHH02] for the uniform hyperbolic system. The logarithmic dependence on ε is due to the hyperbolicity and can be seen easily by the following argument [Sie02, RS02, BHH02]. Assume that two classical paths leave a crossing with $\varepsilon \ll 1$, Fig. 3.1(b). Their initial deviation with respect to the momentum is therefore $\delta p^{\perp}_{\text{init}} \sim \varepsilon|\mathbf{p}|$. In order to form a closed loop this deviation has to increase so that $\delta p^{\perp}_{\text{final}} \sim c\,|\mathbf{p}|$ with the constant c being of order unity. This means that the minimal loop length is determined by $c \simeq \varepsilon \exp[\lambda T_{\min}/2]$. Hence the minimal loop length is given by

$$T_{\min}(\varepsilon) = -\frac{2}{\lambda} \ln\left[\frac{\varepsilon}{c}\right]. \tag{3.2}$$

As in the semiclassical limit the total orbit length T increases like the Heisenberg time T_H one finds $T_{\min} \ll T$ for not too small angles ε, i.e. $\exp(-\lambda T) \ll \varepsilon \ll 1$. Thus, Eq. (3.2) together with Eq. (3.1) yields the result (2.56) given in the previous chapter.

In the following section we study whether this argument can be extended to non-uniformly hyperbolic systems. Especially it is important to analyze whether the minimal loop time (3.2) is present in a more general system and what its dependence on the crossing angle ε and the Lyapunov exponent λ is.

3.2 Model system: LIMAÇON billiards

The goal of this chapter is to verify to which extent the specific structure of the distribution $P(\varepsilon, T)$ given in Eq. (2.56) can be reproduced in a more general system than the motion on a surface with constant negative curvature. As a model we choose a two-dimensional billiard. Billiard systems are defined by a specific boundary with a vanishing potential $V(\mathbf{q}) = 0$ inside this boundary while it diverges outside. Therefore, the classical motion of a particle in a billiard is determined by hard wall reflections at the boundary and free motion between these reflections. Billiard systems have been studied as models for classical and quantum chaos in detail (see for example [Bäc98, Gas98] and references therein). They show a classical behavior ranging from integrable to chaotic depending on the shape of the boundary. Typical examples for integrable billiard systems are the rectangular or the circular billiard. Some well studied chaotic billiards include the SINAI billiard [Sin63, Sin70], the BUNIMOVICH stadium billiard [Bun74, Bun79] and the cardioid billiard [Rob83, BS94].

For the investigations in this chapter we choose the family of LIMAÇON billiards introduced in [Rob83], see also [Rob84, BS94, Bäc98]. Their boundary shape is defined by a conformal mapping $z \to w(z)$ of the circle $z = r\mathrm{e}^{\mathrm{i}\theta}$ in the complex plane

$$\begin{aligned} w(z) &= \frac{1}{a}\left(z + bz^2 + br^2\right) \\ &= \varrho(\theta, r)\, \exp\left[\mathrm{i}\theta\right] = \frac{r}{a}\left[1 + 2br\cos\theta\right]\exp\left[\mathrm{i}\theta\right] \\ &= u(\theta, r) + \mathrm{i}v(\theta, r) = \frac{r}{a}\left[\cos\theta + br\cos(2\theta) + br\right] + \mathrm{i}\frac{r}{a}\left[\sin\theta + br\sin(2\theta)\right] \end{aligned} \tag{3.3}$$

where $0 \leq \theta < 2\pi$. The parameter r just defines the length scale in the system while $\varrho(\theta, r)$ is the actual distance of the boundary from the center of the billiard. The parameter b describes the deformation of the boundary. The range of valid values starts at $b = 0$ corresponding to the circular billiard, see Fig. 3.3(a), and ends with $b = 1/(2r)$ which gives the cardioid billiard, see Fig. 3.4(a). Thus the change of this parameter produces an entire family of billiards whose classical dynamics ranges from integrable and non-ergodic to completely chaotic. The normalization a is chosen such that the area of the billiard is given in terms of $\varrho(\theta, r)$ as

$$A = \int_0^{2\pi} \mathrm{d}\theta \int_0^{\varrho(\theta,r)} \mathrm{d}r'\, r' = r^2 \frac{\pi(1 + 2b^2r^2)}{a^2} = r^2 \tag{3.4}$$

for any value of the parameter b. Therefore the parameter a has to be chosen as $a = \sqrt{\pi\left(1 + 2b^2r^2\right)}$. This choice is convenient as setting $r = 1$ immediately gives $A = 1$ for the area (3.4). In these units, the unit circle is obtained by taking $b = 0$

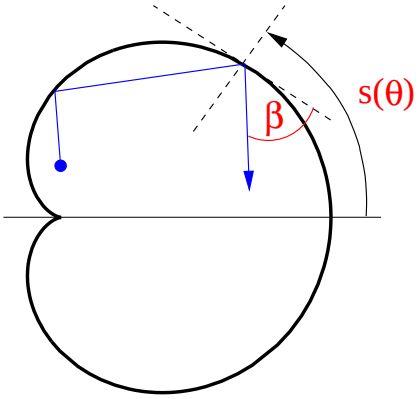

Figure 3.2: *The description of the classical dynamics in terms of the* POINCARÉ *surface of section defined through the boundary of the billiard is based on the coordinates $s(\theta)$ and $\mathcal{P}(\beta)$. Here, $s(\theta)$ represents the position coordinate and is given by the normalized arc length when going along the boundary. The associated momentum coordinate is $\mathcal{P}$ which is determined by the angle β as $\mathcal{P}(\beta) = \cos\beta$.*

and $r = \sqrt{\pi}$. The choice (3.4) for the parameter b (such that the area is independent of b) ensures that the mean level spacing in a quantum mechanical treatment of the billiard system does not change when tuning b. Furthermore one can expect that the ergodic prefactor in the classical crossing angle distribution (2.56) also remains the same no matter which billiard of the family is considered.

The normalized arc length $s(\theta)$ turns out to be an appropriate quantity for a description of the dynamics in the POINCARÉ surface of section defined by the boundary [BB97, Bäc98]. It can be calculated using the total arc length

$$S(\theta, r) = \int_0^\theta \mathrm{d}\theta' \left\| \frac{\mathrm{d}w(\theta', r)}{\mathrm{d}\theta'} \right\| = \frac{2r(1+2br)}{a} E\left(\frac{\theta}{2}\,,\, \frac{\sqrt{8br}}{1+2br}\right) \tag{3.5}$$

where $E(\varphi, k)$ is the elliptic integral of the second kind [GR00]. In order to render this coordinate position independent of the system under consideration we define the normalized arc length $s(\theta)$ such that $0 < s(\theta) < 1$ for $\theta = 0 \ldots 2\pi$ and for any value of b:

$$s(\theta) \equiv \frac{S(\theta)}{S(2\pi)} = E\left(\frac{\theta}{2}\,,\, \frac{\sqrt{8br}}{1+2br}\right) \Big/ E\left(\pi\,,\, \frac{\sqrt{8br}}{1+2br}\right). \tag{3.6}$$

The mean free path $\bar{l}$ in the billiard is now easily obtained [Bäc98] from the area (3.4) and the circumference $S(2\pi)$ as[1] $\bar{l} = \pi A / S(2\pi)$. The conjugated momentum variable to $s(\theta)$ is proportional to the projection of the momentum on the tangent of the boundary at the point of reflection, see Fig. 3.2. It is given by $\mathcal{P} = \cos\beta$ where

[1] To simplify the notation we set $r = 1$ from now on.

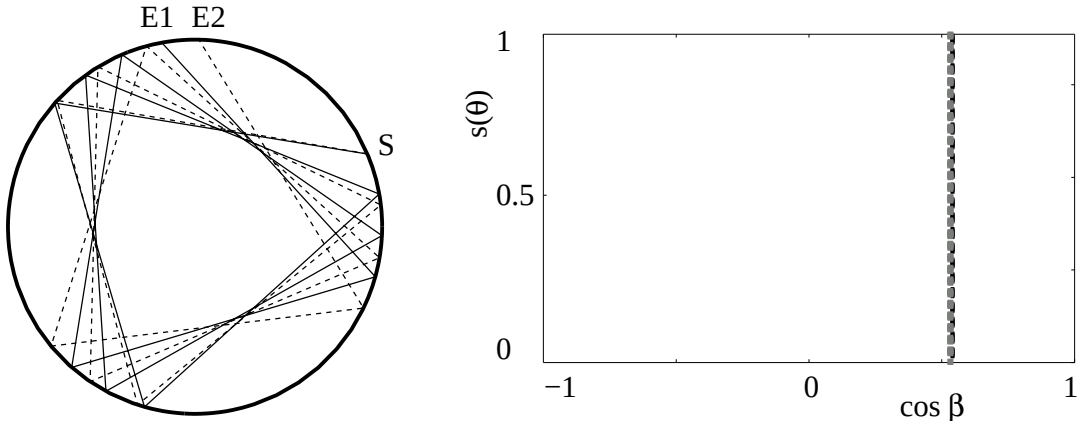

(a) Two classical paths

(b) POINCARÉ surface of section

Figure 3.3: *Circular billiard in the integrable regime* $b = 0.0$*:* (a) *The two classical trajectories (solid and dashed line) start off at point* S *given by* $(\theta = 0.4, \beta = 1.0)$ *with a small initial deviation regarding their momentum. The path length is ten bounces in either case.* (b) *The two trajectories of subfigure* (a) *were calculated for 200 reflections. Each point in the* POINCARÉ *surface of section [which is represented by the* $(s = s(\theta), \mathcal{P} = \cos\beta)$*-plane] corresponds to one reflection of the respective trajectory at the boundary.*

β is the angle between the trajectory and the tangent. Therefore, each coordinate pair $(s = s(\theta), \mathcal{P} = \cos\beta)$ uniquely defines a position in the POINCARÉ surface of section.

In order to illustrate the transition from integrability to chaos as the deformation parameter b is changed from 0 to 0.5 we present three examples: $b = 0$ (completely integrable), $b = 0.5$ (completely chaotic) and finally $b = 0.2$ (intermediate case). For either case we study the motion of a particle in configuration space as well as in phase space represented by the POINCARÉ surface of section. The first example $b = 0$ yields the integrable circular billiard. A typical property of the dynamics in integrable systems is that a small initial deviation between two paths grows rather slowly, e.g. algebraically, with the length of the trajectory. As can be seen in Fig. 3.3(a) two trajectories starting off at the same point S with a slightly different direction remain close together for the shown ten reflections. The underlying regular character of the motion becomes even more obvious in the POINCARÉ surface of section, Fig. 3.3(b), where the coordinates $s = s(\theta)$ and $\mathcal{P} = \cos\beta$ are plotted for successive reflections. As the angular momentum is conserved due to the rotational symmetry of the system all reflection angles remain the same no matter where the reflection occurs. Hence the motion in the POINCARÉ surface of section is restricted to a line corresponding to this fixed reflection angle. This immediately implies that

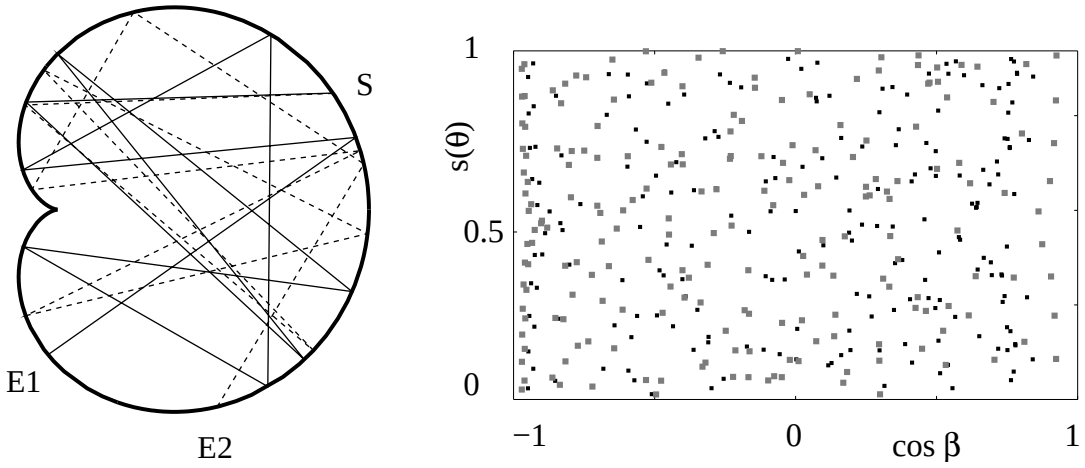

(a) Two classical paths

(b) POINCARÉ surface of section

Figure 3.4: *Cardioid billiard in the chaotic regime with* $b = 0.5$*:* (a) *The two classical trajectories (solid and dashed line) start off with a small initial deviation with respect to the momentum at point* S *given by* $(\theta = 0.4, \beta = 1.0)$*. The path length is ten bounces in either case. Due to the chaotic dynamics of the system they end up at two entirely different points* $E1$ *and* $E2$*.* (b) *The* POINCARÉ *surface of section is uniformly filled by the points of intersection belonging to the classical paths. The two trajectories of subfigure* (a) *were calculated for 200 reflections.*

the system is not ergodic at all.

The billiard resulting in the case $b = 0.5$ is the so-called cardioid. It has been shown to be ergodic and mixing [Sza92, Mar93]. If the geometry of the two trajectories with the same initial conditions as in Fig. 3.3(a) is considered one finds a completely different picture as compared to the integrable case. As shown in Fig. 3.4(a) the two trajectories follow each other for the first few bounces but then the deviation between the two paths becomes of the order of the system size. This example clearly shows that the same small initial deviation grows much faster than in the circular billiard because of the chaotic character of the system. The growth is exponential (as described in Section 2.1) after $5 \ldots 10$ reflections already. The difference between the integrable and chaotic dynamics is even more evident in the POINCARÉ surface of section, Fig. 3.4(b). Either trajectory spreads throughout the entire phase space which is already uniformly filled after a not too long time — in this example 200 reflections. This is a consequence of the ergodic property of the cardioid billiard.

As the third example we present an intermediate case given by $b = 0.2$. The two trajectories in configuration space, see Fig. 3.5(a), look rather similar to the integrable case. The motion still seems quite regular and the initial deviation does

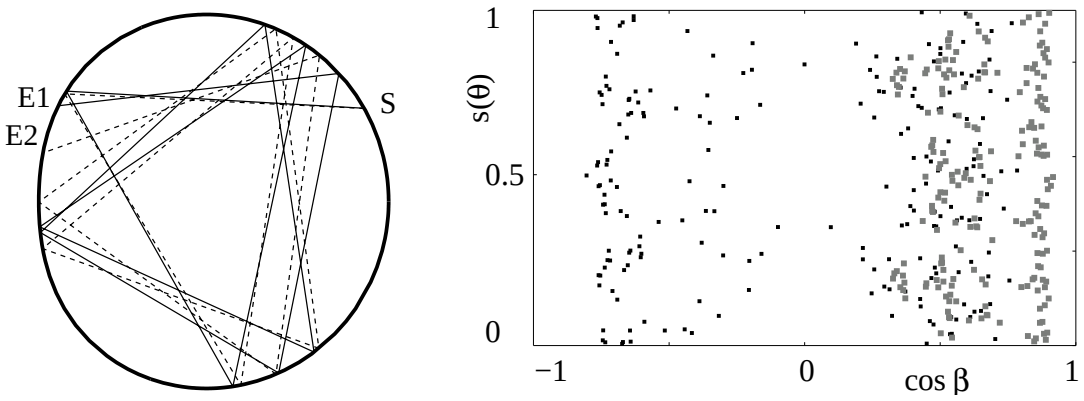

(a) Two classical paths

(b) POINCARÉ surface of section

Figure 3.5: *Billiard ($b = 0.2$) with mixed phase space:* (a) *The two classical trajectories (solid and dashed line) start off with a small initial deviation at point S given by ($\theta = 0.4, \beta = 1.0$). The path length is ten bounces in either case. Similarly to the integrable case, Fig. 3.3(a), they stay rather close together for the length considered.* (b) *The two trajectories of subfigure* (a) *were calculated for 200 reflections. The resulting structure in the* POINCARÉ *surface of section can be clearly distinguished from the integrable case, Fig. 3.3(b). One the other hand, the distribution of intersection points is still more structured and less uniform than in the completely chaotic case, Fig. 3.4(b).*

not grow as fast as in the chaotic case. However, when the POINCARÉ surface of section, see Fig. 3.5(b), is considered more information about the dynamics is revealed. Although the two paths stay close together for quite some time they eventually deviate as one of the paths changes its orientation from counter-clockwise to clockwise. This means that the reflection angles vary around a few preferred values and are not restricted by the conservation of momentum as in the integrable case. In the POINCARÉ surface of section this is reflected by a non-uniform density of intersection points which reveals a system specific structure in the long-time limit. There are islands of regular motion as well as regions corresponding to chaotic motion in the phase space. Therefore, this example corresponds to a dynamical system with a so-called mixed phase space.

A quantitative measure of the chaoticity of the system is the LYAPUNOV exponent λ. As described in Section 2.1 it defines the time scale on which small initial deviations typically grow in the long-time limit. Here we give the values[2] for a few specific parameters b:

[2]In all further considerations concerning the dynamics of a particle in a billiard we set $|\mathbf{p}| = |\mathbf{v}| = 1$.

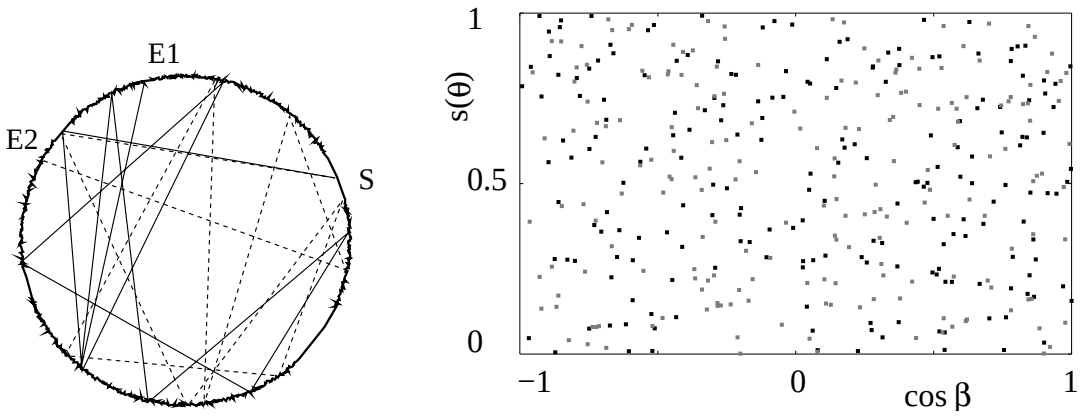

(a) Random paths

(b) POINCARÉ surface of section

Figure 3.6: *A circular billiard with a rough boundary:* (a) *Example of two random trajectories with small deviations in the initial conditions. They are starting at* S *and ending at* $E1$ *and* $E2$ *respectively.* (b) *The* POINCARÉ *surface of section is uniformly filled by the points of intersection belonging to either path. The trajectories of subfigure* (a) *were calculated for 200 reflections.*

b	0.50	0.48	0.46	0.44	0.42	0.40	0.38	0.36	0.34	0.32	0.30
λ	0.78	0.76	0.75	0.74	0.73	0.72	0.71	0.69	0.68	0.66	0.65
$\bar{l}$	0.85	0.86	0.86	0.87	0.87	0.87	0.87	0.88	0.88	0.88	0.88

We conclude this section by presenting one more yet somewhat different model, namely a circular billiard with a rough boundary, see Fig. 3.6(a). This boundary randomizes the classical motion of the particle so that the mechanism which governs the system dynamics is stochastic rather than deterministic. This implies that two trajectories evolve completely independently from each other already after the first reflection no matter how small the initial deviations are, Fig. 3.6(a). Therefore, this system is ergodic as can be seen in the POINCARÉ surface of section, Fig. 3.6(b). However, in clear contrast to the previous three examples this model does not represent a dynamical system and the theoretical methods summarized in Section 2.1 can in general not be applied. One expects that a model like this is well described within the theory of disordered systems [SA93, SSA93, GM02a, GM02b].

In the following investigations we always restrict ourselves to dynamical systems with a completely or almost completely chaotic phase space. This means that there are no or at most very small islands of stability in the POINCARÉ surface of section. For the family of billiard systems chosen that means that we consider either the cardioid billiard itself or at least values close to $b = 1/2$. In the next section we present numerical results for the crossing angle distribution $P(\varepsilon, T)$ for this specific

billiard geometry which represents a dynamical non-uniformly hyperbolic system.

3.3 Crossing angle distribution in the cardioid

The purpose of this section is to present the results of detailed numerical studies on the crossing angle distribution $P(\varepsilon, T)$ for the cardioid billiard. This crossing angle distribution is a very important ingredient for the derivation of the semiclassical form factor (2.54) in the configuration-space approach as presented in Section 2.5. More precisely speaking, a detailed knowledge of the functional dependence of the correction $P^{(\mathrm{corr})}(\varepsilon, T)$ on the crossing angle ε, see Eq. (2.56) for the uniform system, is necessary to obtain a non-vanishing result for $K^{(2)}(\tau)$. Especially we study the changes that occur in $P(\varepsilon, T)$ if a *non-uniform* hyperbolic system like the cardioid billiard is considered instead of a uniform hyperbolic system as in Section 2.5 and 3.1. Although one expects that this change does not affect the leading term $P^{(\mathrm{lead})}(\varepsilon, T)$ as it is determined by the long-time ergodic behavior we first test this property for the cardioid billiard. Then we investigate the correction $P^{(\mathrm{corr})}(\varepsilon, T)$ finding that its scaling with length T is the same as in Eq. (2.56) for uniform systems. We show that this correction contains information about the deterministic dynamics of the system. Furthermore we find that the dependence on the crossing angle ε is indeed logarithmic. However, this is only the case if a certain class of loops is excluded. This class is given by all almost self-retracing loops. Finally we determine the prefactor of the logarithm in Eq. (2.56) as it is responsible for the numerical prefactor of the τ^2 term in the final result $K^{(2)}(\tau) = -2\tau^2$.

For the following numerical tests we use non-periodic trajectories of lengths between 50 and 500 reflections. As we are interested in the statistical properties of long orbits we expect that these are correctly reflected in the properties of non-periodic trajectories [SR01] which is also supported by the shadowing-theorem [ASY96]. In principle one should also measure the length of the trajectories directly instead of using the number of reflections. However, as the system is ergodic and the trajectories are already rather long the deviations between the real lengths of all paths with fixed number of reflections are small, i.e. indirectly proportional to the square root of the length. As we eventually study the small correction $P^{(\mathrm{corr})}(\varepsilon, T)$ on the large background $P^{(\mathrm{lead})}(\varepsilon, T)$ it is necessary to have very good statistics. Thus we typically average over ensembles of half a million trajectories up to twenty million trajectories with random initial conditions when calculating the crossing angle distribution. The number of crossings then scales with the length as T^2 and linearly with the ensemble size. The trajectories have to be long enough, i.e. $\lambda T \gg 1$, to be approximately ergodic and to ensure that the correction term $P^{(\mathrm{corr})}(\varepsilon, T)$ is indeed small compared to the leading term $P^{(\mathrm{lead})}(\varepsilon, T)$.

First, we study the leading term $P^{(\mathrm{lead})}(\varepsilon, T)$ in the crossing angle distribution

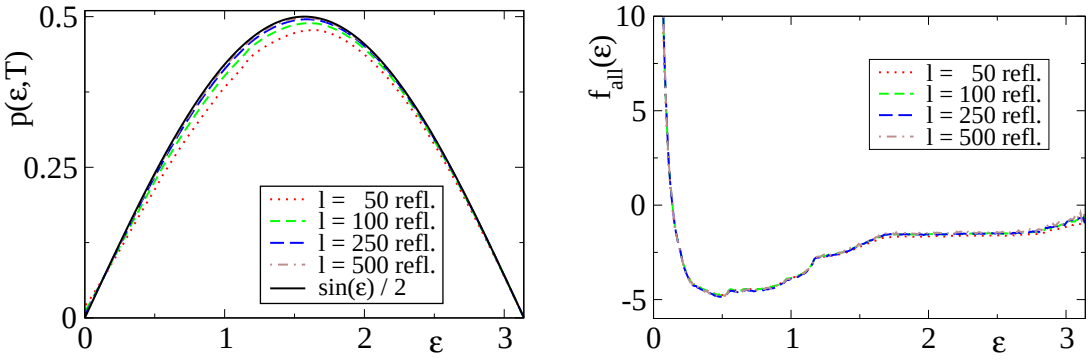

(a) Leading contribution: $p(\varepsilon, T)$

(b) Correction: $f_{\text{all}}(\varepsilon)$

Figure 3.7: *Crossing angle distribution for the cardioid billiard* ($b = 0.5$). *All loops (in particular the almost self-retracing ones) are still included. The four different ensembles are characterized by the length of the trajectories: twenty million trajectories with* 50 *reflections (dotted), ten million trajectories with* 100 *reflections (short dashed), five million trajectories with* 250 *reflections (long dashed) and one million trajectories with* 500 *reflections (dashed – dotted). In subfigure* (a) *the rescaled crossing angle distribution* $p(\varepsilon, T)$ *of all four ensembles is compared to the long-time ergodic prediction given by* $\sin(\varepsilon)/2$. *Subfigure* (b) *shows a comparison of the rescaled correction* $f_{\text{all}}(\varepsilon)$ *to the crossing angle distribution for the four different ensembles.*

of the cardioid and show that it is given by the uniform result (2.56). For a better comparison of different systems or loop lengths we introduce the rescaled distribution

$$p(\varepsilon, T) \equiv \frac{\pi\, m^2\, A}{T^2\, |\mathbf{p}|^2} P(\varepsilon, T)\,. \tag{3.7}$$

According to (2.56) one expects the rescaled distribution to be $p(\varepsilon, T) \simeq \sin(\varepsilon)/2$ independently of the lengths of the trajectories. This expectation is nicely confirmed as can be seen in Fig. 3.7(a). The result for the numerically determined crossing angle distribution so far is therefore that it scales with T^2 and follows a sine function:

$$P_{\text{num}}(\varepsilon, T) \simeq \frac{T^2\, |\mathbf{p}|^2}{2\pi\, m^2\, A} \sin\varepsilon\,. \tag{3.8}$$

However, one can also immediately conclude from Fig. 3.7(a) that there are indeed small corrections to this result. These corrections decrease with increasing length of the trajectory. This confirms the assumption that the leading ergodic contribution is indeed dominant in the long-time limit. In order to study the correction in more detail we divide $p(\varepsilon, T)$ by $\sin(\varepsilon)/2$ and rescale it once more by T. The result is denoted by the function $f(\varepsilon)$ so that

$$P(\varepsilon) = P^{(\text{lead})}(\varepsilon, T) + P^{(\text{corr})}(\varepsilon, T) = \frac{T^2\, |\mathbf{p}|^2}{2\pi\, m^2\, A} \sin\varepsilon \left[1 + \frac{f(\varepsilon)}{T}\right]. \tag{3.9}$$

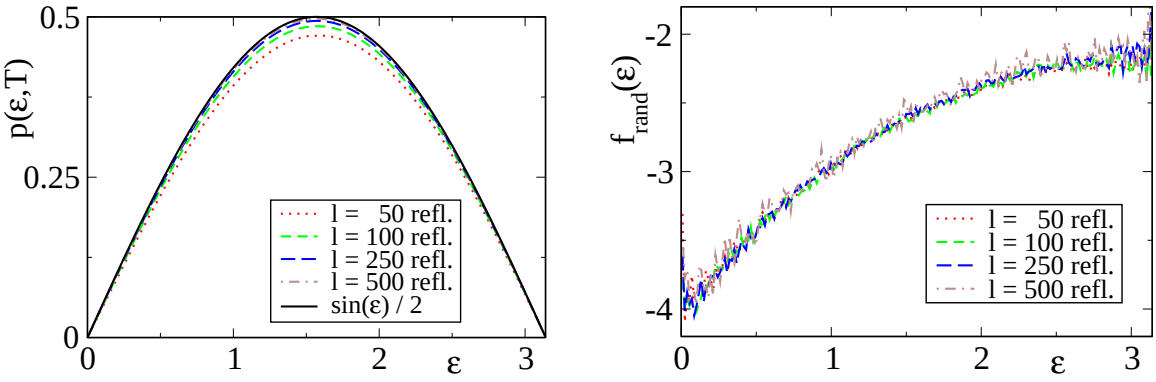

(a) Leading contribution: $p(\varepsilon, T)$

(b) Correction: $f_{\text{rand}}(\varepsilon)$

Figure 3.8: *Crossing angle distribution for the billiard with random reflections. The four different ensembles are defined by the length of the trajectories: two million trajectories with* 50 *reflections (dotted), one million trajectories with* 100 *reflections (short dashed), one million trajectories with* 250 *reflections (long dashed) and half a million trajectories with* 500 *reflections (dashed-dotted). Subfigure* (a) *shows the rescaled crossing angle distribution* $p(\varepsilon, T)$ *of all four ensembles compared to the long-time ergodic prediction* $\sin(\varepsilon)/2$*. In subfigure* (b) *the rescaled correction to the crossing angle distribution* $f_{\text{rand}}(\varepsilon)$ *is compared for the four different ensembles.*

This form is adapted to the structure of the analytical prediction (2.56) and will be used to characterize the numerical results by the introduced function $f(\varepsilon)$. In terms of the rescaled crossing angle distribution $p(\varepsilon, T)$ on thus finds

$$f(\varepsilon) \equiv T \left[2 \frac{p(\varepsilon, T)}{\sin \varepsilon} - 1 \right] . \tag{3.10}$$

Hence the main purpose of the following numerical studies is to confirm the structure (3.9) and to specify the functional dependence of $f(\varepsilon)$ on the crossing angle for $\varepsilon \ll 1$. More specifically, if non-uniform systems behave similarly to uniform systems one should find that the expression on the right hand side in Eq. (3.10) is indeed independent of the length T and diverges logarithmically for $\varepsilon \to 0$.

As we have not yet excluded any kind of loops in the numerical simulations we denote the corresponding function by $f_{\text{all}}(\varepsilon)$. The result for $f_{\text{all}}(\varepsilon)$ is presented in Fig. 3.7(b) which clearly shows that $f_{\text{all}}(\varepsilon)$ does not depend on the length T anymore. This confirms the correct scaling of the correction with the length of the trajectories in the model (3.9). However, one can also immediately check that the correction $f_{\text{all}}(\varepsilon)$ we found numerically does not have the logarithmic small ε behavior as for the uniformly hyperbolic system, see Eq. (2.56).

Before proceeding with a detailed analysis of what exactly causes an increased number of small crossing angles in $f_{\text{all}}(\varepsilon)$ we give the corresponding numerical result

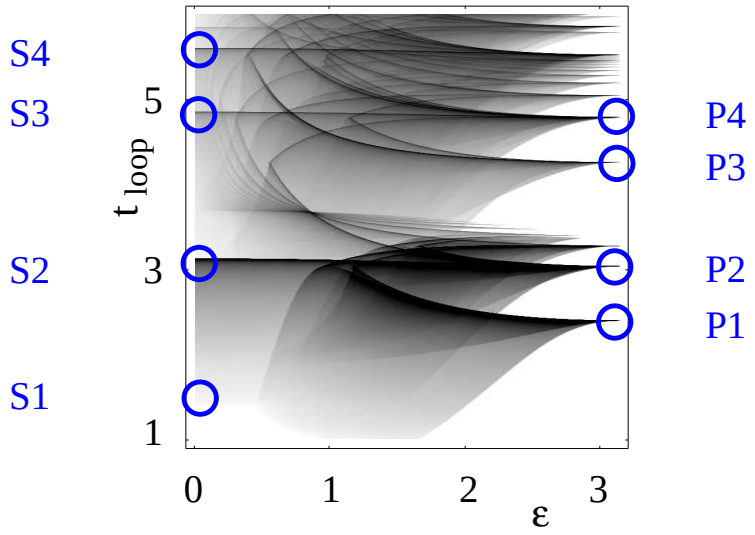

Figure 3.9: *Number of crossings with given crossing angle ε and given loop length t_{loop} as a grey-scale density plot. The higher the number of crossings the darker the corresponding regions are. For this plot we used two million trajectories with* 100 *reflections each. Crossing angles $\varepsilon = \pi$ correspond to periodic orbits. As the periodic orbits are unstable and isolated they form a discrete set. The first four are indicated by* P1 *($t_{\text{loop}} \simeq 2.4$),* P2 *($t_{\text{loop}} \simeq 3.0$),* P3 *($t_{\text{loop}} \simeq 4.3$) and* P4 *($t_{\text{loop}} \simeq 4.8$). For small crossing angles $\varepsilon \approx 0$ we indicated four more regions by* S1 *($t_{\text{loop}} \simeq 1.8$),* S2 *($t_{\text{loop}} \simeq 3.1$),* S3 *($t_{\text{loop}} \simeq 4.8$) and* S4 *($t_{\text{loop}} \simeq 5.6$). The associated orbit and loop geometries are shown in Fig. 3.10 and Fig. 3.11, respectively.*

$f_{\text{rand}}(\varepsilon)$ for the non-deterministic system with random reflections at the boundary, see Fig. 3.6(a). The purpose of this analysis is to show that it makes an important difference regarding the correction $P^{(\text{corr})}(\varepsilon, T)$ if a deterministic or a stochastic system is considered. As the stochastic system is also ergodic one expects that the leading term is given by Eq. (3.8) so that $p(\varepsilon, T) \simeq \sin(\varepsilon)/2$ for large T. This is clearly confirmed by the numerical results shown in Fig. 3.8(a). Again, there are small corrections to this leading term which decrease for increasing lengths of the involved trajectories. Using once more the definition (3.10) we determine the correction $f_{\text{rand}}(\varepsilon)$ for the stochastic system which is shown in Fig. 3.8(b). Although the results for $p(\varepsilon, T)$ for the chaotic system, Fig. 3.7(a), and for the stochastic system, Fig. 3.8(a), look rather similar the rescaled small corrections $f_{\text{all}}(\varepsilon)$ and $f_{\text{rand}}(\varepsilon)$ differ significantly from each other. The result so far is therefore twofold. First of all, we have found that the crossing angle distribution does follow the general form (3.9) for both the chaotic and the stochastic system. This means that the leading contribution is only related to ergodicity but not to the deterministic character of the system. Second, we found that this leading contribution is corrected by small deviations that are proportional to the inverse of the length T. The dependence

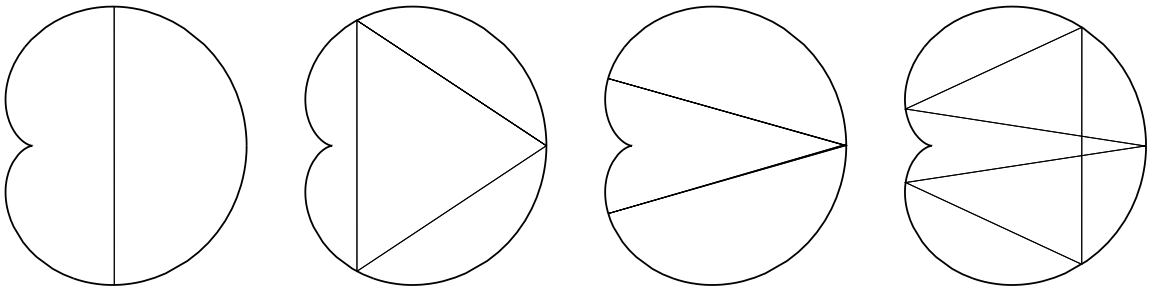

(a) P1 (b) P2 (c) P3 (d) P4

Figure 3.10: *Geometries of the four periodic orbits indicated in Fig. 3.9. If these orbits are slightly deformed their periodicity breaks down and a crossing with crossing angle* $\varepsilon \lesssim \pi$ *appears. The subfigures* (a) *to (d) correspond to the cases* P1 *to* P4 *in Fig. 3.9.*

of the correction $P^{(\mathrm{corr})}(\varepsilon, T)$ on the crossing angle ε is significantly different if the chaotic cardioid is compared to the randomized billiard, i.e. $f_{\mathrm{all}}(\varepsilon) \neq f_{\mathrm{rand}}(\varepsilon)$. This implies that the dynamical properties are indeed of relevance for $f(\varepsilon)$.

As explained in Section 3.1, the proposed logarithmic dependence of $f(\varepsilon)$ on the crossing angle in chaotic systems is due to a lack of short loops with small crossing angles. Fig. 3.7(b) indicates that this argument does not seem to apply to the non-uniform cardioid billiard. As it turns out there is indeed a large class of loops with small crossing angles ε and short loop lengths $t_{\mathrm{loop}} \sim \overline{l}$. This means that for this class the argument of a minimal loop time being a function of ε, see Eq. (3.2), does not hold. It is possible to form loops with arbitrary small crossing angles in the cardioid whose lengths do not increase logarithmically as $\varepsilon \to 0$. In order to identify and characterize this class of loops we calculate numerically the number of crossing angles ε with given loop length t_{loop}. The numerical result of this approach for the cardioid is presented in Fig. 3.9 as a grey-scale plot. In this plot a higher number of crossings with given angle ε and given loop length t_{loop} is indicated by darker points. The plot has to be understood as follows. Large crossing angles $\varepsilon \lesssim \pi$ characterize loops that are very close to periodic orbits. The periodic orbits in the chaotic cardioid form a discrete set as they are isolated and can therefore not be continuously deformed into each other. We have labeled the first few of them by P1 to P4 in Fig. 3.9. The corresponding orbit geometries are shown in Fig. 3.10. As the geometries of these periodic orbits are deformed the associated crossing angles become smaller than π meaning that the periodic orbits start to form loops. For smaller ε one finds that the geometry of certain loops seems to be related to the original periodic orbits via continuous deformations as they are connected by non-interrupted black lines in Fig. 3.9. The loop lengths either increase or decrease as the

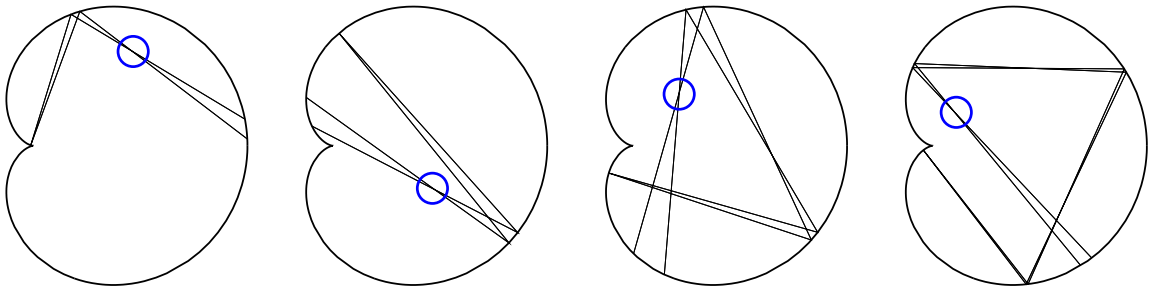

(a) S1 (b) S2 (c) S3 (d) S4

Figure 3.11: *Examples for the geometries of the four types of short loops indicated by S1 to S4 in Fig. 3.9. The small circles mark the considered crossings. The subfigures* (a) *to (d) represent the cases S1 to S4 in Fig. 3.9.*

crossing angle ε becomes smaller. On the other hand also new loops seem to appear when going towards smaller crossing angles ε possibly due to bifurcations or related processes. However it also appears that certain types of loops can be deformed so that the corresponding crossing angles approach zero while the loop lengths do not change significantly. This implies that many short loops with $t_{\text{loop}} \sim \overline{l}$ and crossing angles $\varepsilon \approx 0$ exist. Fig. 3.9 suggests that there are different types of these short loops with small crossing angles: the first type with lengths $t_{\text{loop}} \simeq 1.8 \ldots 3.1$ is represented by S1 and S2. Then follows the next class with loop lengths up to $t_{\text{loop}} \simeq 4.8$ indicated by S3 and so on.

As only the small ε behavior of $P(\varepsilon, T)$ is relevant for the calculation of the form factor (2.54) in the configuration space approach we investigate the short loops with small crossing angles in more detail. It turns out that all the classes S1, S2, ... are based on almost self-retracing loops as shown in Fig. 3.11. Their common feature is that a trajectory hits the boundary almost perpendicular in the middle of the loop. Due to the focusing nature of the billiard two trajectories that start off the boundary with angles $\beta_{1,2}$ close to $\pi/2$ cross each other after one reflection and the crossing angle ε is of the same order as the difference $\beta_2 - \beta_1$, see Fig. 3.12(a). In other words, two almost parallel trajectories starting off perpendicular to the boundary can form short loops with arbitrary small crossing angles ε while the length of the loops remains almost constant. The difference between loops associated to the first class, see for example Fig. 3.11(a) and Fig. 3.11(b), is only in the way they are positioned within the billiard. If any of these loops is extended by two more segments after the first crossing one obtains geometries as the one shown in Fig. 3.11(c) which is characteristic for the second class. This basically means that two almost parallel trajectories starting off perpendicular to the boundary can form a whole family of small crossings. The associated loop lengths do not increase logarithmically with ε

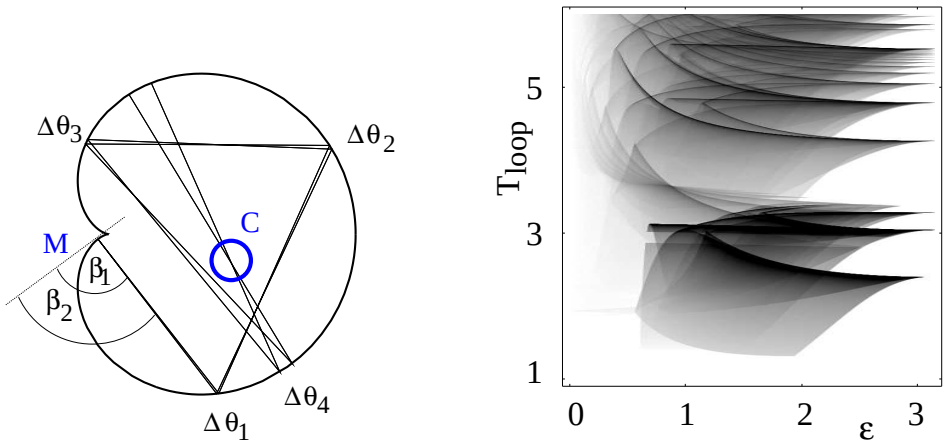

(a) Almost self-retracing loop

(b) Loop length distribution

Figure 3.12: *Excluding almost self-retracing loops:* (a) *An almost self-retracing loop gives rise to a whole family of crossings with arbitrary small crossing angles. It is characterized by two trajectories starting almost perpendicular at the same position M on the boundary ($\beta_1 \approx \beta_2 \approx \pi/2$). As their initial deviation is small they will stay close together for the first few reflections implying small differences $\Delta\theta_i \ll 1$ of the position on the boundary. The average of all $\Delta\theta_i$ is then used to identify almost self-retracing loops by means of the criterion Eq. (3.11). Subfigure* (b) *shows the same type of grey-scale plot as Fig. 3.9 however the almost self-retracing loops are excluded by applying the exclusion criterion (3.11) with* $c_{\text{cutoff}} = 0.3$.

as the crossing angles become smaller, see Fig. 3.11(d) for a further example. The result of the analysis given above is therefore that the set of all almost self-retracing loops causes an increased number of small crossing angles as compared to the result (2.56) for the uniform system. The reason for this lies in the geometry of the cardioid billiard as it has a focusing boundary.

As we prove in Chapter 4 it turns out that one cannot find a partner orbit for a crossing that is associated to an almost self-retracing loop. Before explaining this effect in more detail we first want to present the same type of numerical results as in Fig. 3.7 and Fig. 3.9 if the class of self-retracing loops is excluded. The idea how to decide whether a loop is almost self-retracing is the following. Starting in the middle M of the loop we follow the two almost parallel parts until they reach the crossing C that is considered, see Fig. 3.12(a). Each time the two trajectories are reflected we determine their closeness on the boundary by calculating the difference $\Delta\theta_i$ of the angles θ as specified in Fig. 3.2. The criterion for the loop being counted

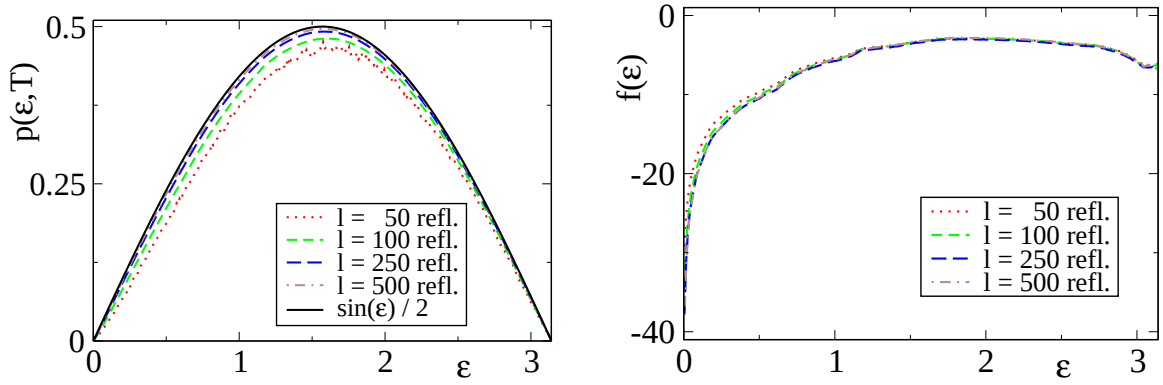

(a) Leading contribution: $p(\varepsilon, T)$

(b) Correction: $f(\varepsilon)$

Figure 3.13: *Crossing angle distribution for the cardioid billiard* ($b = 0.5$) excluding *the almost self-retracing loops. The four different ensembles are the same as in Fig. 3.7: twenty million trajectories with* 50 *reflections (dotted), ten million trajectories with* 100 *reflections (short dashed), five million trajectories with* 250 *reflections (long dashed) and one million trajectories with* 500 *reflections (dashed – dotted). In subfigure* (a) *the rescaled crossing angle distribution* $p(\varepsilon, T)$ *of all four ensembles is compared to the long-time ergodic prediction* $\sin(\varepsilon)/2$. *Subfigure* (b) *shows the rescaled correction* $f(\varepsilon)$ *to the crossing angle distribution for the four different ensembles.*

as self-retracing is then given in the form

$$\frac{1}{n}\sum_{i=1}^{n}\Delta\theta_i < c_{\text{cutoff}} \tag{3.11}$$

where $2n+1$ is the number of reflections with the boundary during the loop, see Fig. 3.12(a). The cut-off c_{cutoff} is a small but finite number. As we show in the next paragraphs the main conclusions concerning the crossing angle distribution $P(\varepsilon, T)$ are independent of this cut-off if the relevant small angle limit $\varepsilon \ll 1$ is considered. The results we presented so far, i.e. Fig. 3.7, thus correspond to $c_{\text{cutoff}} = 0$. The first result of the numerical analysis excluding the almost self-retracing loops is presented in Fig. 3.12(b). In this figure we again plotted the loop length distribution as a function of the crossing angle as in Fig. 3.9. However this time the almost self-retracing loops where neglected by employing the criterion (3.11) and choosing $c_{\text{cutoff}} = 0.3$. Having excluded this class of loops one can indeed not find short loops with small crossing angles anymore. This is a clear indication that this class of loops formed by the almost self-retracing trajectories is the only reason for the appearance of short loops with arbitrarily small crossing angles.

Having identified the class of almost self-retracing loops as the reason for the appearance of many short loops with small crossing angles we now proceed by pre-

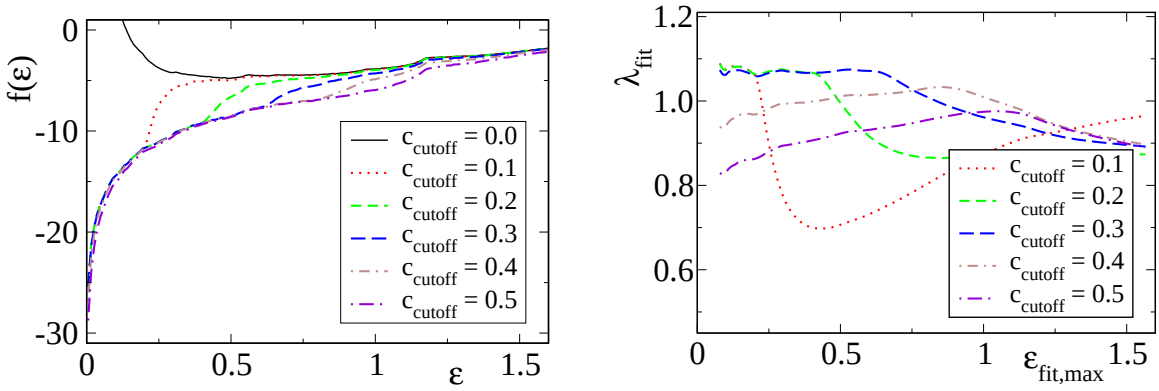

(a) Correction: $f(\varepsilon)$

(b) Prefactor: $\lambda_{\text{fit}}(\varepsilon_{\text{fit,max}}, c_{\text{cutoff}})$

Figure 3.14: *Verification of the valid range for the cut-off parameter* c_{cutoff} *entering the criterion (3.11): Subfigure* (a) *shows the correction* $f(\varepsilon)$*, Eq. (3.10), for different values of* c_{cutoff}*. In subfigure* (b) *we plotted the dependence of the numerically fitted prefactor* λ_{fit} *on the range of* ε *values used for the fit, i.e.* $0.08 < \varepsilon < \varepsilon_{\text{fit,max}}$*. For either plot we considered an ensemble contained five million trajectories with 100 reflections each.*

senting the numerical results for the crossing angle distribution if exactly this class of loops is excluded. By applying this procedure one has to replace the crossing angle distribution in Fig. 3.7 by the result shown in Fig. 3.13. As one can see in Fig. 3.13 the leading ergodic term given by $p(\varepsilon, T)$ as well as the length scaling of the correction fit again perfectly to the proposed form (3.9). However, in clear contrast to $f_{\text{all}}(\varepsilon)$ the modified result $f(\varepsilon)$, Fig. 3.13(b) obtained by the exclusion of the self-retracing loops shows a logarithmic dependence on the crossing angle for small ε, see also Fig. 3.15(a).

In order to verify that our numerical method of excluding the self-retracing loops is indeed consistent and independent of the cut-off parameter we calculate $f(\varepsilon)$ for different values c_{cutoff} ranging from $c_{\text{cutoff}} = 0.1$ to $c_{\text{cutoff}} = 0.5$. The result is presented in Fig. 3.14(a) where we have included the case $c_{\text{cutoff}} = 0$ for comparison. We thus find that the small ε dependence of the function $f(\varepsilon)$ is not changed if different values of $c_{\text{cutoff}} > 0$ are used. Only the size of the ε range showing the logarithmic dependence changes with c_{cutoff}. As an example, one can read off this range for $c_{\text{cutoff}} = 0.3$ from Fig. 3.14(a) to be $0 < \varepsilon \lesssim 0.6$.

As we found that the correction $P^{(\text{corr})}(\varepsilon, T)$ to the crossing angle distribution in the cardioid does indeed show a logarithmic dependence on ε the next step is to determine the numerical prefactor and check whether it is determined by the LYAPUNOV exponent. This means, in order to verify whether our model (3.9) can be casted into the form (2.56) obtained for the uniformly hyperbolic system we write

the function $f(\varepsilon)$ as

$$f(\varepsilon) = \frac{4}{\lambda_{\text{fit}}} \ln \left[\frac{\varepsilon}{c_{\text{fit}}} \right] \tag{3.12}$$

and determine λ_{fit} from the numerical data. As we described in Section 2.5 the second parameter c_{fit} does not play a role in the semiclassical evaluation of the spectral form factor. Therefore, it is sufficient to consider λ_{fit}. In Fig. 3.14(b) we show the resulting values for λ_{fit} as a function of the upper limit $\varepsilon_{\text{fit,max}}$ of the ε interval used to fit the logarithm. Furthermore we checked again whether the resulting prefactor in Eq. (3.12) depends on the artificially introduced cut-off c_{cutoff}. The results in Fig. 3.14(b) can be understood as follows. For a given value of $c_{\text{cutoff}} = 0.1 \ldots 0.3$ the obtained prefactor λ_{fit} does not depend on the size of the fit interval if the involved crossing angles are not too big. We find that the logarithmic dependence approximately breaks down at crossing angles $\varepsilon_{\text{fit,max}} \simeq 2c_{\text{cutoff}}$. This means that one should not use a cut-off parameter which is too small as in this case the range of ε values that can be used for the fit (3.12) is also very small. On the other hand, one must not choose the cut-off parameter too large as this also changes the final result for the prefactor λ_{fit}, see Fig. 3.14(b). Hence, we draw the following conclusions. The exclusion of almost self-retracing orbits by means of the criterion (3.11) yields a crossing angle distribution in accordance with the proposed structure (3.9). The small correction $P^{(\text{corr})}(\varepsilon, T)$ is given by the function $f(\varepsilon)$ which depends logarithmically on ε, see Eq. (3.12). Using the procedure described above to exclude almost self-retracing orbits one can determine the logarithmic prefactor λ_{fit} in a consistent and numerically stable way. Here, the optimal parameter range for the cut-off is $c_{\text{cutoff}} \approx 0.1 \ldots 0.3$. The range of crossing angles that are used to fit Eq. (3.12) has to be adapted accordingly so that $\varepsilon_{\text{fit,max}} \lesssim 2c_{\text{cutoff}}$. In this range of parameters one obtains values for the prefactor λ_{fit} that are independent of c_{cutoff} and $\varepsilon_{\text{fit,max}}$, see Fig. 3.14(b).

In the last step we repeat the numerical calculations for different values of the deformation parameter b. In this way we check whether the prefactor λ_{fit} is indeed determined by the LYAPUNOV exponent λ of the system that is presented in Section 3.2. First of all we find that the model (3.9) including the specific form (3.12) for the function $f(\varepsilon)$ perfectly describe the numerical results for different shapes of the billiard, see Fig. 3.15(a). We then determined the corresponding prefactor λ_{fit} for many different billiard shapes. They are compared to the LYAPUNOV exponents in Fig. 3.15(b). Although our numerical method allows only for a certain precision in the determination of λ_{fit} (indicated by the error bars in Fig. 3.15(b)) we nevertheless find a clear indication that the numerical results λ_{fit} overestimate the system specific LYAPUNOV exponents λ. As can be clearly seen in the inset of Fig. 3.15(b) the ratio of λ and λ_{fit} is always slightly smaller than 1. This effect appears to be most pronounced for the cardioid ($b = 0.5$) itself. With decreasing deformation parameter b one expects that at some point small stability islands appear in the

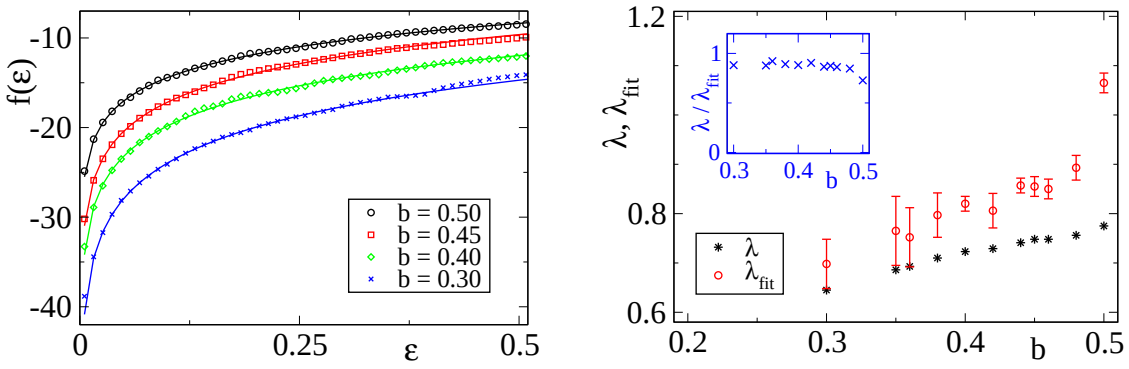

(a) Correction: $f(\varepsilon)$

(b) Prefactor: $\lambda_{\text{fit}}(b)$

Figure 3.15: *Crossing angle distribution for different values of the deformation parameter b. In subfigure* (a) *we present the numerically determined correction $f(\varepsilon)$ compared to the fit according to Eq. (3.12). The values of b range from $b = 0.50$ (circles) over $b = 0.45$ (squares) and $b = 0.40$ (diamonds) to $b = 0.30$ (crosses). Subfigure* (b) *shows the prefactor λ_{fit} (circles) as obtained in accordance with Eq. (3.12) for different values of b. The corresponding* LYAPUNOV *exponents as given in Section 3.2 are included for comparison (stars). The inset shows the ratio $\lambda/\lambda_{\text{fit}}$ as a function of b. For the numerical calculations we used ensembles of 20 million trajectories with 100 reflections. The almost self-retracing orbits were excluded ($c_{\text{cutoff}} = 0.3$).*

phase space [Bäc98]. This can explain why the numerical evaluation of λ_{fit} becomes more unstable and erroneous for the smaller values of b, i.e. $b \lesssim 0.4$. It is worth noting that an increased ensemble size does not bring the calculated λ_{fit} closer to the expected value λ.

The results of our numerical investigations can be summarized as follows. The crossing angle distribution of *non-uniformly* hyperbolic billiards — in our studies the chaotic members of the family of LIMAÇON billiards — follows the form (3.9). For small crossing angles ε it includes a logarithmic correction with respect to ε, see Eq. (3.12). These results are thus qualitatively analogous to the crossing angle distribution of a *uniformly* hyperbolic billiard, see Eq. (2.56). We can therefore conclude that the logarithmic correction to the crossing angle distribution for small ε does not rely on a uniform phase space. However, due to the focusing nature of the cardioid billiard one has to exclude a certain class of loops namely the almost self-retracing loops to find this result. We show in the next chapter why this type of loops does not yield a partner orbit and thus does not contribute to the semiclassical evaluation of the form factor $K(\tau)$. The almost self-retracing loops contain a whole family of crossings, see Fig. 3.11(d), and all these crossings have to be neglected. The reason is that all of these crossings can be related to each other be means of the stability matrix. In this way one can show that if one of the crossings within

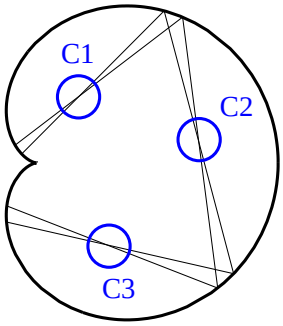

Figure 3.16: *Example for a family of successive small crossings in the cardioid billiard.*

a family does not have a partner then neither do all the other crossings. A similar argument can actually be applied to successive small crossings within a single family that do not form a self-retracing loop, see Fig. 3.16. Also for this case we show that the crossings are related to each other via the linearized equations of motion. This implies that there is just *one* partner orbit for the whole set of crossings. As a consequence one would need a refined formulation of the configuration-space approach where not single crossings but only families of crossings are counted for the calculation of the spectral form factor. However, in the next chapter we proceed in a different way be developing a phase-space approach which resolves these problems concerning the almost self-retracing loops and the families of crossings in a rather straightforward and elegant manner. In due course we then explain how exactly the logarithmic prefactor depends on the properties of the phase space of the system.

CHAPTER 4

Phase-space approach for two-dimensional systems

In this chapter we present a phase-space generalization of the configuration-space approach which was developed for uniformly hyperbolic systems [SR01, Sie02]. First we will show how the relation between a periodic orbit γ and its partner orbits γ^p can be described in phase space. In particular, we will explain in detail how the concept of self-crossings can be replaced by a method based on 'encounter regions' to be defined in phase space. Then we will derive the action difference of the orbit pair (γ, γ^p) in terms of local phase-space properties instead of the crossing angle ε used in [SR01, Sie02]. We show that the semiclassical weights and the MASLOV indices for the orbit γ and its partners γ^p are equal. Finally we provide a new method to count the partner orbits γ^p for a given periodic orbit γ which is based on considerations regarding the flow in phase space. We show how one can use this new framework to compute the off-diagonal contribution $K^{(2)}(\tau)$ of the spectral form factor in *non-uniformly* hyperbolic systems.

4.1 Correlated orbits and the 'encounter region'

The purpose of the following section is to provide the main ideas how the configuration-space approach [SR01] is reformulated in terms of phase-space methods [TR03]. Especially we will show that the relevant objects to specify the partner

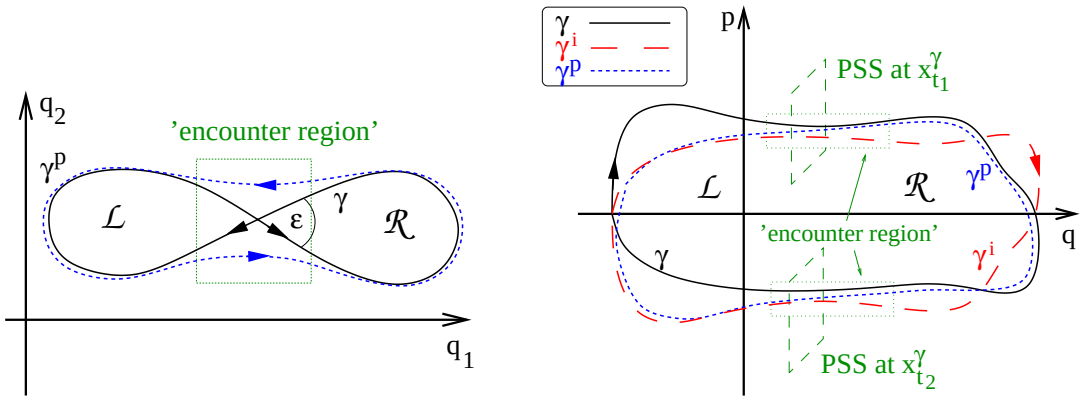

(a) Configuration space (b) Phase space

Figure 4.1: (a) *Periodic orbit γ (solid line) with self-crossing in configuration space and corresponding partner orbit γ^p (dashed line) which avoids the crossing.* (b) *Sketch of a correlated orbit pair in phase space (shown is a projection of the four-dimensional space). The original periodic orbit γ, the time-reversed orbit γ^i, and the partner orbit γ^p are represented by the solid, dashed and dotted line, respectively. Due to time-reversal symmetry each 'encounter region' appears twice – first at time t_1 and again at $t_2 = t_1 + t_{\rm loop}$. The* POINCARÉ *surfaces of section (PSS) defined by the perpendicular coordinates $(\delta q^\perp, \delta p^\perp)$ at $\mathbf{x}^\gamma_{t_1}$ and $\mathbf{x}^\gamma_{t_2}$ are indicated in the 'encounter region'.*

orbits of a given orbit are so-called 'encounter regions' in phase space instead of crossings in configuration space. The approach we propose is canonically invariant. It provides a natural way to describe non-uniform systems as considered in Chapter 3 as well as more than two-dimensional systems to be described in Section 5.1.

The theory formulated in the framework of the configuration space, Section 2.5, is based on the small parameter ε, the crossing angle. Therefore we first identify the relevant quantity in phase space that replaces the crossing angle ε. Consider a periodic orbit having a self-crossing with a small crossing angle ε, see Fig. 4.1(a). The orbit enters the crossing twice: at time t_1 and then again at t_2. The lengths of the two loops are then given by $t_{\rm loop} = t_2 - t_1$ and $t'_{\rm loop} = T_\gamma - t_{\rm loop}$. Because of the small crossing angle $\varepsilon \ll 1$ the two momenta $\mathbf{p}_{t_1}$ and $\mathbf{p}_{t_2}$ point in almost exactly opposite directions, i.e. $|\mathbf{p}_{t_1} + \mathbf{p}_{t_2}| \approx p\varepsilon \ll p$. Thus a crossing with a small crossing angle means that the orbit γ comes close to its time-reversed version γ^i at the time t_1 and again at time t_2 if considered in phase space, see Fig. 4.1(b). The phase-space coordinates $\mathbf{x}^{\gamma,i}_t$ of the time-reversed orbit γ^i are given in terms of the original orbit $\mathbf{x}^\gamma_t = (\mathbf{q}^\gamma_t, \mathbf{p}^\gamma_t)$ as

$$\mathbf{x}^{\gamma,i}_t = (\mathbf{q}^{\gamma,i}_t, \mathbf{p}^{\gamma,i}_t) = (\mathbf{q}^\gamma_{T_\gamma - t}\,, -\mathbf{p}^\gamma_{T_\gamma - t}) = \mathcal{T}\,\mathbf{x}^\gamma_{T_\gamma - t}. \tag{4.1}$$

The time-reversal transformation $\mathcal{T}$ implies for the local stable and unstable directions introduced in Section 2.1 the relation

$$\vec{e}^{\,s,u}(\mathbf{x}^{\gamma}_{t_1}) = F\,\vec{e}^{\,u,s}(\mathbf{x}^{\gamma,i}_{T_\gamma - t_1}) = F\,\vec{e}^{\,u,s}(\mathcal{T}\mathbf{x}^{\gamma}_{t_1}) \quad \text{with} \quad F \equiv \begin{pmatrix} \mathbf{1} & 0 \\ 0 & -\mathbf{1} \end{pmatrix}. \tag{4.2}$$

In order to quantify how close the two orbits γ and γ^i are we introduce a vector $\delta\vec{y}$ pointing from the original orbit γ to the time-reversed orbit γ^i:

$$\delta\vec{y}(\mathbf{x}^{\gamma}_{t_1}, t_{\text{loop}}) = \delta\vec{y}(\mathbf{x}^{\gamma}_{t_1}, t_2 - t_1) \equiv \mathcal{T}\mathbf{x}^{\gamma}_{t_2} - \mathbf{x}^{\gamma}_{t_1} = \mathbf{x}^{\gamma,i}_{T_\gamma - t_2} - \mathbf{x}^{\gamma}_{t_1}, \tag{4.3}$$

see Fig. 4.2(a). The time t_2 is chosen such that this vector $\delta\vec{y}$ lies in the POINCARÉ surface of section at $\mathbf{x}^{\gamma}_{t_1}$. The additional parameter t_{loop} indicates that the vector $\delta\vec{y}$ corresponds to an intersection of γ^i with the POINCARÉ surface of section at $\mathbf{x}^{\gamma}_{t_1}$ after a certain loop time. Although, strictly speaking, the part of the periodic orbit γ between t_1 and $t_2 = t_1 + t_{\text{loop}}$ does not form a loop in phase space, see Fig. 4.1(b), we will still use this terminology as it is based on the intuitive configuration-space picture, see Fig. 4.1(a). In principle, definition (4.3) would yield a different $\delta\vec{y}$ if the POINCARÉ surface of section were defined at $\mathbf{x}^{\gamma,i}_{T_\gamma - t_2}$ instead of $\mathbf{x}^{\gamma}_{t_1}$ because of a different local coordinate system. But since the two points are close to each other the relation (4.3) between $\mathbf{x}^{\gamma}_{t_1}$, $\mathbf{x}^{\gamma,i}_{T_\gamma - t_2}$ and $\delta\vec{y}$ is correct up to higher-order corrections in $\delta\vec{y}$ for either choice of the position of the POINCARÉ surface of section. The orbit γ enters the crossing after the right loop $\mathcal{R}$ once more. That means that the orbit γ and the time-reversed γ^i are once more close to each other in phase space, see Fig. 4.1(b), with a difference vector $\delta\vec{y}\,'$. Formally this can be written as $\delta\vec{y}\,' = \mathbf{x}^{\gamma,i}_{T_\gamma - t_1} - \mathbf{x}^{\gamma}_{t_2}$, see Fig. 4.2(b). However, the two difference vectors $\delta\vec{y}$ and $\delta\vec{y}\,'$ are not independent of each other. In the case of a crossing where $\delta\vec{y}$ represents the crossing angle this is immediately clear since the crossing angle ε is the same no matter whether one considers the first passing of the crossing at t_1 or the second one at t_2. This connection between $\delta\vec{y}$ and $\delta\vec{y}\,'$ is due to the time reversal symmetry expressed in Eq. (4.1) and can be written as $\delta\vec{y}\,' = F\delta\vec{y}$. Again, the relations given above are correct if higher order terms in $\delta\vec{y}$ can be neglected.

To have a better understanding what it means when the two orbits γ and γ^i are coming close to each other we decompose the vector $\delta\vec{y}$ according to Eq. (2.15) into its components with respect to the local stable and unstable directions $\vec{e}^{\,s,u}(\mathbf{x})$:

$$\delta\vec{y}(\mathbf{x}) = u\,\vec{e}^{\,u}(\mathbf{x}) + s\,\vec{e}^{\,s}(\mathbf{x}) \quad \text{with} \quad s = \frac{(\vec{e}^{\,u})^T\,\Sigma\,\delta\vec{y}}{(\vec{e}^{\,u})^T\,\Sigma\,\vec{e}^{\,s}} \quad \text{and} \quad u = \frac{(\vec{e}^{\,s})^T\,\Sigma\,\delta\vec{y}}{(\vec{e}^{\,s})^T\,\Sigma\,\vec{e}^{\,u}}\,. \tag{4.4}$$

The equations for the components s and u follow directly from Eq. (2.16). In terms of these components the two orbits are considered as being close if $s, u \ll 1$. It will again – as for the crossing angle ε – turn out that it is sufficient to consider only the case $s, u \ll 1$ as long as the conditions for a semiclassical treatment are fulfilled.

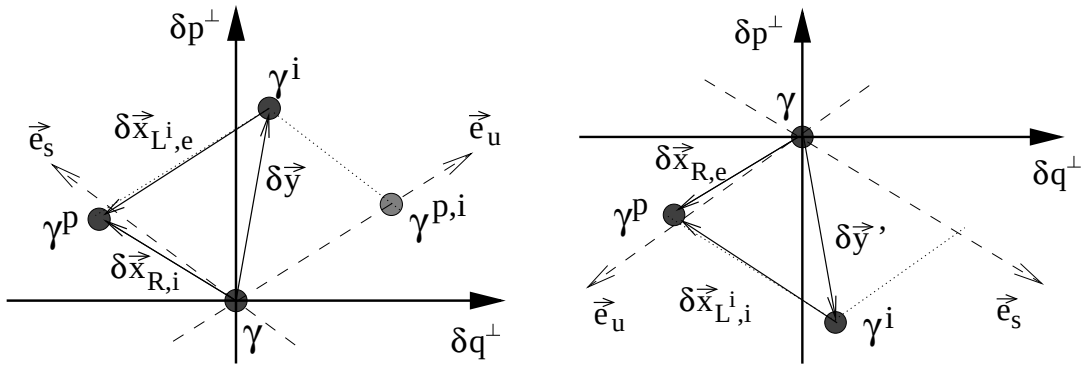

(a) PSS at $\mathbf{x}^{\gamma}_{t_1}$ (b) PSS at $\mathbf{x}^{\gamma}_{t_2}$

Figure 4.2: (a) POINCARÉ *surface of section shortly after the crossing at* t_1. *The difference in position space is almost zero, i.e.* $\delta q^{\perp} \approx 0$, *while the difference in momentum space is given by the crossing angle, i.e.* $\delta p^{\perp} \approx \varepsilon p$, *see Fig. 4.1.* (b) POINCARÉ *surface of section shortly before the reentry through the crossing at* t_2. *The difference in position space is almost zero again, i.e.* $\delta q^{\perp} \approx 0$, *while the difference in momentum space is given by the crossing angle, i.e.* $\delta p^{\perp} \approx -\varepsilon p$.

It is important to realize that the choice of the time t_1 and the corresponding $\delta\vec{y} = \delta\vec{y}(\mathbf{x}^{\gamma}_{t_1}, t_{\text{loop}})$ is not unique. One could have chosen a different $\bar{t}_1 = t_1 + \Delta t$ slightly before or after the original t_1 and the two orbits would still be in the vicinity of each other, see Fig. 4.3(a). However, we will prove later on in this section that such a shift of the POINCARÉ surface of section does not alter the partner orbit. Therefore a partner orbit is not associated with a single point in phase space (as it was the case in the configuration space formulation, Section 2.5) but with an entire region. This 'encounter region' is defined by all vectors $\delta\vec{y}_{\Delta t}(\mathbf{x}^{\gamma}_{t_1}, t_{\text{loop}})$ that can be connected to each other within the linear approximation as Δt is varied. To give a more specific definition of an 'encounter region' consider a small $\delta\vec{y} = \delta\vec{y}_0(\mathbf{x}^{\gamma}_{t_1}, t_{\text{loop}})$. If the POINCARÉ surface of section is shifted along the orbit by a small Δt forward or backward in time this vector changes to

$$\delta\vec{y} = \delta\vec{y}_{\Delta t}(\mathbf{x}^{\gamma}_{t_1}, t_{\text{loop}}) = \delta\vec{y}_0(\mathbf{x}^{\gamma}_{t_1+\Delta t}, t_{\text{loop}} - 2\Delta t) \ ,$$

see Fig. 4.3(a). As long as Δt is not too large the components of the vector $\delta\vec{y}_{\Delta t}(\mathbf{x}^{\gamma}_{t_1}, t_{\text{loop}})$ will still be small and the linear approximation (2.3) is still valid.

However, there is a certain Δt^u forward in time and Δt^s backward in time for which the linear approximation $\delta\vec{y}_{\pm\Delta t^{u,s}}(\mathbf{x}) \simeq M(\pm\Delta t^{u,s}, \mathbf{x})\delta\vec{y}_0(\mathbf{x})$ breaks down. These critical times $\Delta t^{s,u}$ defining the start and the end of the 'encounter region' can be determined by an implicit equation for the stable and unstable components of any vector $\delta\vec{y}_0(\mathbf{x})$. Let us denote the time dependent stable component of $\delta\vec{y}_{\Delta t}(\mathbf{x})$

as $s(\Delta t; \delta\vec{y}_0, \mathbf{x})$ and similarly for $u(\Delta t; \delta\vec{y}_0, \mathbf{x})$. Then the implicit equations for $\Delta t^{s,u}$ read

$$|s(-\Delta t^s; \delta\vec{y}_0, \mathbf{x})| = c^s(\mathbf{x}) \quad \text{and} \quad |u(\Delta t^u; \delta\vec{y}_0, \mathbf{x})| = c^u(\mathbf{x}) \; . \tag{4.5}$$

Here, the $c^{s,u}(\mathbf{x})$ describe the maximum values s and u can reach before the linear approximation breaks down. They are solely defined by the classical dynamics of the system and can, in principle, depend on the position $\mathbf{x}$ in phase space. In general, they might also depend on $\delta\vec{y}_0$ itself. However, as we consider only small $\delta\vec{y}_0$ one can take the limiting value $\lim_{\delta\vec{y}_0 \to 0} c^{s,u}(\mathbf{x}, \delta\vec{y}_0) = c^{s,u}(\mathbf{x})$. Even more, it will turn out that the final result for the spectral form factor $K^{(2)}(\tau)$ does not depend on $c^{s,u}(\mathbf{x})$ at all in the semiclassical limit. The Eqs. (4.5) implicitly determine the times $\Delta t^{s,u} = \Delta t^{s,u}(s, u; \mathbf{x})$ as functions of the coefficients s and u and the position in phase space $\mathbf{x}$. The possible values for Δt thus range from $-\Delta t^s$ to Δt^u. This defines the length of the 'encounter region'

$$t_{en}(s, u; \mathbf{x}) = \Delta t^s(s, u; \mathbf{x}) + \Delta t^u(s, u; \mathbf{x}) \tag{4.6}$$

as a function of $\mathbf{x}$ and $\delta\vec{y} = s\,\vec{e}^{\,s} + u\,\vec{e}^{\,u}$. The definitions (4.6) and (4.5) ensure that the length t_{en} can be determined at any point within a given 'encounter region' and always yields the same value.

To summarize, we have to replace the scalar parameter of the crossing angle ε by a vector $\delta\vec{y}$ lying in the POINCARÉ surface of section defined by the local perpendicular coordinates. A small crossing angle $\varepsilon \ll 1$ then corresponds to the situation where the original orbit γ comes close to its time-reversed orbit γ^i implying that the components s and u of the vector $\delta\vec{y}$, Eq. (4.4), are small, i.e. $s, u \ll 1$. The partner orbit has to be associated with an entire region in phase space – the 'encounter region' – instead of a singular event in configuration space like a crossing. In the next paragraphs we will show how the geometry of the partner orbit can be found quantitatively and that the concept of using 'encounter regions' instead of self-crossings is indeed consistent.

As a next step we demonstrate how the geometry of the partner orbit γ^p can be determined quantitatively. The characteristic feature of the partner orbit in the configuration-space formulation is that it avoids the crossing and therefore traverses one of the loops in a different direction, e.g. the left loop $\mathcal{L}$ as in Fig. 4.1(a). Translated into the phase space picture this means that the partner orbit γ^p has to follow the original orbit γ during the right loop $\mathcal{R}$ between t_1 and t_2. Then it switches to the time-reversed orbit γ^i and follows that one between t_2 and $t_1 + T_\gamma$, see Fig. 4.1(b). Hence, the phase-space coordinates of the partner orbit are given by

$$\mathbf{x}_t^{\gamma,p} \simeq \begin{cases} \mathbf{x}_t^{\gamma} & \text{for} \quad t_1 \le t \le t_2 \qquad (\text{part } \mathcal{R}) \\ \mathcal{T}\mathbf{x}_{t_1+t_2-t}^{\gamma} = \mathbf{x}_{T_\gamma - t_1 - t_2 + t}^{\gamma,i} & \text{for} \quad t_2 \le t \le T_\gamma + t_1 \qquad (\text{part } \mathcal{L}) \end{cases} \; . \tag{4.7}$$

To explicitly construct the partner orbit we analyze the linearized equations of motion around γ in part $\mathcal{R}$ and around γ^i in section $\mathcal{L}$. This linearization is possible if

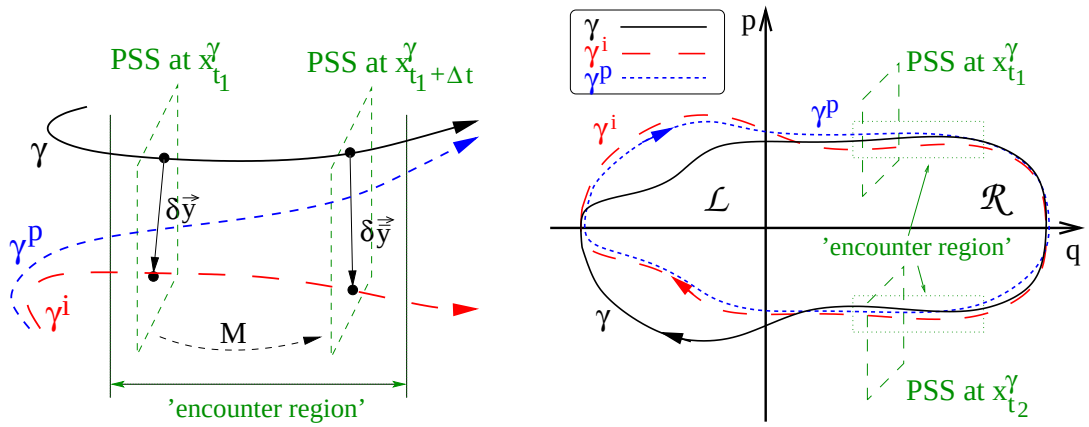

(a) Shifted PSS (b) Short loop $\mathcal{R}$

Figure 4.3: (a) *Enlarged schematic drawing of the 'encounter region' shown in Fig. 4.1(b). If the* Poincaré *surface of section (PSS) used to construct the partner orbit according to Eq. (4.8) is shifted from* $\mathbf{x}^\gamma_{t_1}$ *to* $\mathbf{x}^\gamma_{t_1+\Delta t}$ *the vector* $\delta\vec{y}$ *changes to* $\delta\vec{\bar{y}}$*. However, the solution (4.9) is invariant under this shift and yields the same partner orbit* γ^p *in either case.* (b) *Geometry of the partner orbit* γ^p *(dotted line) according to Eq. (4.8) if the right loop* $\mathcal{R}$ *is short so that the original path* γ *(solid line) stays close to the time-reversed path* γ^i *during the entire loop between the times* t_1 *and* t_2*. The two indicated 'encounter regions' at* t_1 *and* t_2 *should not be treated separately because of the shortness of loop* $\mathcal{R}$*, i.e.* $t_{\rm loop} = t_2 - t_1 < 2\Delta t^u(s, u; \mathbf{x}^\gamma_{t_1})$*.*

the vector $\delta\vec{y}$ is not too long meaning that its components are small, i.e. $s, u \ll 1$. We show that a nontrivial solution to these linearized equations of motion representing the partner orbit γ^p exists under certain conditions. The distance between γ and the partner orbit γ^p at the beginning of the first loop $\mathcal{R}$ is denoted by $\delta\vec{x}_{R,i}$, see Fig. 4.2(a). This vector lies in the Poincaré surface of section defined at the phase space position $\mathbf{x} = \mathbf{x}^\gamma_{t_1}$ before the loop $\mathcal{R}$. Having passed loop $\mathcal{R}$ after a time $t_{\rm loop} = t_2 - t_1$ this distance has changed to $\delta\vec{x}_{R,e}$, see Fig. 4.2(b). For a small $\delta\vec{x}_{R,i}$ the final $\delta\vec{x}_{R,e}$ can be found by means of the stability matrix $R = M(t_{\rm loop}, \mathbf{x}^\gamma_{t_1})$. Before and after the other part of the orbit the difference between the time-reversed path γ^i and the partner γ^p is denoted by $\delta\vec{x}_{L^i,i}$ and $\delta\vec{x}_{L^i,e}$, respectively. Here, L^i indicates that one has to follow the time-reversed loop $\mathcal{L}^i$. Its stability matrix $L^i = F\,L^{-1}\,F$ is determined by the inverse of the stability matrix L of the loop $\mathcal{L}$. In terms of the matrices R and L^i this gives the following set of equations

$$\begin{aligned} \delta\vec{x}_{R,e} &= R\,\delta\vec{x}_{R,i} & \qquad \delta\vec{x}_{R,i} - \delta\vec{x}_{L^i,e} &= \delta\vec{y} \\ \delta\vec{x}_{L^i,e} &= L^i\,\delta\vec{x}_{L^i,i} & \qquad \delta\vec{x}_{R,e} - \delta\vec{x}_{L^i,i} &= F\delta\vec{y}\,. \end{aligned} \tag{4.8}$$

The two vector equations on the left side just determine the two single pieces of

the partner orbit γ^p during $\mathcal{R}$ and $\mathcal{L}^i$ while the equations on the right make sure that the two pieces fit together in the 'encounter region', see Fig. 4.2. This set of equations is the generalization of the relations (2.52) to the phase-space picture. It is correct up to first order in $\delta\vec{y}$ neglecting higher order corrections beyond the linear approximation.

The solution to Eqs. (4.8) can be found by carrying the vectors $\delta\vec{x}$ once around the entire orbit by applying the relations (4.8) in the appropriate order. For a given vector $\delta\vec{y}$ the geometry of the partner is then uniquely defined by the solution

$$\begin{aligned} \delta\vec{x}_{R,i} &= \left[\mathbf{1} - L^i\, R\right]^{-1} \left[\mathbf{1} - L^i\, F\right]\, \delta\vec{y} \qquad & \delta\vec{x}_{R,e} &= F\, \left[\mathbf{1} - L\, R^i\right]^{-1} \left[\mathbf{1} - L\, F\right]\, \delta\vec{y} \\ \delta\vec{x}_{L^i,i} &= \left[\mathbf{1} - R\, L^i\right]^{-1} \left[R\, F - \mathbf{1}\right]\, F\, \delta\vec{y} \qquad & \delta\vec{x}_{L^i,e} &= F\, \left[\mathbf{1} - R^i\, L\right]^{-1} \left[R^i F - \mathbf{1}\right]\, F\, \delta\vec{y}\,. \end{aligned} \tag{4.9}$$

However, it is important to realize that the solution (4.9) to Eqs. (4.8) is valid only if the loops $\mathcal{L}$ and $\mathcal{R}$ are long enough. Let us consider the part $\mathcal{R}$ as an example. Then a long loop length means that it must not be possible to relate the vector $\delta\vec{y}$ in the Poincaré surface of section before $\mathcal{R}$ to the vector $\delta\vec{y}\,' = F\delta\vec{y}$ after $\mathcal{R}$ *within* the linear approximation. For a certain time t' with $t_1 < t' < t_2 = t_1 + t_{\rm loop}$ the linearization $\delta\vec{y}_{t'}(\mathbf{x}^\gamma_{t_1}, t_{\rm loop}) \simeq M(t', \mathbf{x}^\gamma_{t_1})\delta\vec{y}_0(\mathbf{x}^\gamma_{t_1}, t_{\rm loop})$ must break down. This implies that there must be two separate 'encounter regions' at $\mathbf{x}_{t_1}$ and $\mathbf{x}_{t_2}$ so that the two vectors $\delta\vec{y}$ and $\delta\vec{y}\,'$ do not belong to the same 'encounter region', see Fig. 4.1(b). If this is not the case, i.e. if $R\,\delta\vec{y} = F\,\delta\vec{y}$, then the solution (4.9) for the equations (4.8) has to be replaced by $\delta\vec{x}_{R,i} = \delta\vec{y}$, $\delta\vec{x}_{R,e} = F\delta\vec{y}$, $\delta\vec{x}_{L^i,i} = 0$ and $\delta\vec{x}_{L^i,e} = 0$. But this means that the constructed partner γ^p exactly coincides with the time-reversed orbit γ^i.

This different mathematical result for a short loop $\mathcal{R}$ can be understood intuitively and is demonstrated in Fig. 4.3(b). If the loop $\mathcal{R}$ is short in the sense that one can treat $\delta\vec{y}$ between t_1 and t_2 in the linear approximation then this implies that the original orbit γ and the time-reversed γ^i stay close together between t_1 and t_2. On the other hand, the partner orbit γ^p has to switch from γ^i to γ at t_1 and back to γ^i at t_2. But since γ and γ^i follow each other during $\mathcal{R}$ the partner orbit is also close to γ^i for this part. Thus the partner orbit γ^p coincides with the time-reversed orbit γ^i, see Fig. 4.3(b), because all periodic orbits are isolated and unstable. A similar argument of course holds true for the left loop $\mathcal{L}$, i.e. if $L^i\delta\vec{y}\,' = F\delta\vec{y}\,'$. When calculating the form factor (2.38) one has to make sure that these orbits with $\gamma^p = \gamma^i$ or $\gamma^p = \gamma$ are not included into the calculation of the off-diagonal terms in $K^{(2)}(\tau)$ because they were already accounted for in the diagonal approximation (2.43).

The precise quantitative formulation for which loop lengths $t_{\rm loop} = t_2 - t_1$ and $t'_{\rm loop} = T + t_1 - t_2$ the above solution (4.9) is not valid can be expressed as follows. Depending on the considered vector $\delta\vec{y} = s\,\vec{e}^{\,s} + u\,\vec{e}^{\,u}$ it must be $t_2 > t_1 + 2\Delta t^u(s, u; \mathbf{x})$ and similarly for the other loop $\mathcal{L}$. Therefore we find the condition $2\Delta t^u < t_{\rm loop} < T_\gamma - 2\Delta t^s$ under which a new partner orbit γ^p different from γ and γ^i exists. We

will show that it is exactly this dynamics related restriction which causes the small correction in the crossing angle distribution (2.56) and thus yields the universal result for the form factor $K^{(2)}(\tau)$.

So far we have considered the case where a periodic orbit γ comes close to its time-reversed version γ^i at a certain time t_1 and then again at time t_2. We have shown that if $t_{\rm loop}$ and $t'_{\rm loop}$ are large enough then there is a partner orbit γ^p that can be described in terms of deviations $\delta\vec{x}_{R,i}\ldots$ between γ^p and γ or γ^i, see Eqs. (4.9). However, one could also have chosen a slightly later time $\bar{t}_1 = t_1 + \Delta t$. Because of the deterministic dynamics the two orbits γ and γ^i would still be close together but now with a different coordinate difference $\delta\vec{\bar{y}}$. As we will show in the following one obtains exactly the same partner orbit for the new $\delta\vec{\bar{y}}$ as for the original $\delta\vec{y}$. Mathematically this means that Eqs. (4.8) and their solution (4.9) are invariant under a shift of the Poincaré surface of section, see Fig. 4.3(a), as long as one determines $\delta\vec{y}$ within the same 'encounter region'. Since the time shift Δt is assumed to be sufficiently small the new vector $\delta\vec{\bar{y}}$ can be expressed in terms of the previous one $\delta\vec{y}$ within the linear approximation by the stability matrix $M = M(\Delta t, \mathbf{x}_{t_1})$, i.e. $\delta\vec{\bar{y}} = M\delta\vec{y}$, see Fig. 4.3(a). Similarly all vectors in the previous Poincaré surface of section at $\mathbf{x}^\gamma_{t_2}$ can be mapped to the new one at $\mathbf{x}^\gamma_{t_2-\Delta t}$ via another stability matrix N^{-1}. The new vectors and matrices occurring in Eqs. (4.8) and (4.9) can therefore be obtained via the transformations

$$\begin{aligned} R &\to \bar{R} = N^{-1}\,R\,M^{-1} & \qquad L &\to \bar{L} = M\,L\,N \\ \delta\vec{y} &\to \delta\vec{\bar{y}} = M\,\delta\vec{y} & \qquad \delta\vec{y}\,' &\to \delta\vec{\bar{y}}\,' = N^{-1}\,\delta\vec{y}\,' \\ \delta\vec{x}_{R,i} &\to \delta\vec{\bar{x}}_{R,i} = M\,\delta\vec{x}_{R,i} & \qquad \delta\vec{x}_{R,e} &\to \delta\vec{\bar{x}}_{R,e} = N^{-1}\delta\vec{x}_{R,e} \quad \ldots \quad . \end{aligned} \tag{4.10}$$

Furthermore time-reversal symmetry, e.g. expressed as $\delta\vec{y}\,' = F\delta\vec{y}$, implies $M = N^i$. The Eqs. (4.10) are again correct up to linear order in the coefficients of $\delta\vec{y}$.

It can easily be seen that the structure of the relations (4.8) defining the partner orbit γ^p does not change if they are rewritten in terms of $\delta\vec{\bar{y}}$, $\delta\vec{\bar{x}}_{R,i}$, ... by means of Eqs. (4.10). This also implies that the solution (4.9) does not change by applying the transformation (4.10) and thus yields the same partner orbit for $\delta\vec{\bar{y}}$. Therefore one finds only one partner orbit for each 'encounter region' no matter whether $\delta\vec{y}$ or $\delta\vec{\bar{y}} = M\delta\vec{y}$ is chosen within the 'encounter region'. This fact makes clear that in the configuration-space picture a family of successive small crossings, if present, gives just one partner. On the other hand it is also possible that there is no crossing at all but still a partner can be constructed. This implies that the original orbit γ and the partner orbit γ^p are treated equivalently in the proposed phase-space approach. Hence, the correct way of counting the partner orbits is not to count the self-crossings of a periodic orbit but to determine the number of 'encounter regions'. In the case of the uniformly hyperbolic system each 'encounter region' contains exactly one crossing which is the reason why the crossing angle distribution can be directly used to calculate the spectral form factor.

Finally we want to further simplify the solution (4.9) and give an intuitive interpretation of it. Consider once more the situation where a periodic orbit γ comes close to its time-reversed version γ^i so that the loop times are long, i.e. $t_{\text{loop}}, t'_{\text{loop}} \sim T_H$. Since the partner orbit γ^p has to follow γ during the entire long loop $\mathcal{R}$ the initial deviation $\delta\vec{x}_{R,i}$ has to lie very close the local stable direction $\vec{e}^{\,s}(\mathbf{x}^\gamma_{t_1})$, see Fig. 4.2(a). On the other hand, the deviation $\delta\vec{x}_{L^i,e}$ between γ^p and γ^i is located close to the unstable manifold $\vec{e}^{\,u}(\mathbf{x}^{\gamma,i}_{T_\gamma - t_2})$ of γ^i at $\mathbf{x}^{\gamma,i}_{T_\gamma - t_2}$. This can be seen by propagating $\delta\vec{x}_{L^i,e}$ backwards in time. Therefore, the position of γ^p in the POINCARÉ surface of section at $\mathbf{x}^\gamma_{t_1}$ must be very close to the intersection of the stable manifold of γ with the unstable manifold of γ^i, see Fig. 4.2(a). Hence, to first order in the small quantities u and s one can rewrite the solution (4.9) as $\delta\vec{x}_{R,i} = s_{R,i}\,\vec{e}^{\,s}(\mathbf{x}^\gamma_{t_1})$, $\delta\vec{x}_{L^i,e} = u_{L^i,e}\,\vec{e}^{\,u}(\mathbf{x}^{\gamma,i}_{T_\gamma - t_2}) = u_{L^i,e}\,\vec{e}^{\,u}(\mathbf{x}^\gamma_{t_1})$ and similarly for $\delta\vec{x}_{R,e}$ and $\delta\vec{x}_{L^i,i}$. Together with Eqs. (4.8) and (4.2) these approximations can be used to give a simplified version of the solution (4.9) for long loop lengths

$$\begin{aligned} \delta\vec{x}_{R,i} &= s\;\vec{e}^{\,s}(\mathbf{x}^\gamma_{t_1}) & \delta\vec{x}_{R,e} &= s\;\vec{e}^{\,u}(\mathbf{x}^\gamma_{t_2}) \\ \delta\vec{x}_{L^i,i} &= -u\;\vec{e}^{\,s}(\mathbf{x}^\gamma_{t_2}) & \delta\vec{x}_{L^i,e} &= -u\;\vec{e}^{\,u}(\mathbf{x}^\gamma_{t_1}) \end{aligned} \tag{4.11}$$

describing the partner γ^p in terms of the vector $\delta\vec{y} = s\,\vec{e}^{\,s} + u\,\vec{e}^{\,u}$, see Fig. 4.2. This solution quantitatively determines the partner geometry that we proposed in Eq. (4.7). So far, we have neglected the fact that there is another partner orbit $\gamma^{p,i}$ in addition to γ^p, namely it time reversed version. In the spirit of Eq. (4.11) the geometry of $\gamma^{p,i}$ is given by

$$\begin{aligned} \delta\vec{x}_{R,i} &= u\;\vec{e}^{\,u}(\mathbf{x}^\gamma_{t_1}) & \delta\vec{x}_{R,e} &= u\;\vec{e}^{\,s}(\mathbf{x}^\gamma_{t_2}) \\ \delta\vec{x}_{L^i,i} &= -s\;\vec{e}^{\,u}(\mathbf{x}^\gamma_{t_2}) & \delta\vec{x}_{L^i,e} &= -s\;\vec{e}^{\,s}(\mathbf{x}^\gamma_{t_1}), \end{aligned} \tag{4.12}$$

see Fig. 4.2(a). Thus the time-reversed partner $\gamma^{p,i}$ follows the original orbit γ in part $\mathcal{L}$ and then switches to γ^i in loop $\mathcal{R}$. However, all four orbit pairs (γ, γ^p), $(\gamma, \gamma^{p,i})$, (γ^i, γ^p) and $(\gamma^i, \gamma^{p,i})$ share the same action difference because of their symmetry. The great advantage of the long loop approximations (4.11) and (4.12) is that they are completely independent of the matrix elements of the stability matrices. The expressions for the four $\delta\vec{x}$ in Eqs. (4.11) and (4.12) depend only on the components s and u of the distance vector $\delta\vec{y} = s\,\vec{e}^{\,s} + u\,\vec{e}^{\,u}$ and local phase space properties, namely the local stable and unstable directions $\vec{e}^{\,(u,s)}(\mathbf{x})$.

In this section we have shown that the crossing angle ε defined in configuration space has to be replaced by the vector $\delta\vec{y}$ in phase space. We have generalized the linearized equations of motion (2.52) allowing for a quantitative description of the partner orbit. We have introduced the concept of an 'encounter region' in phase space replacing the crossing in configuration space. Furthermore, we have proved that there is exactly one partner per 'encounter region' if the associated loop lengths are large enough. The condition for the loop lengths can be written

as $2\Delta t^u < t_{\rm loop} < T_\gamma - 2\Delta t^s$ where $t^{s,u}$ are functions of $\delta\vec{y}$. One has to keep in mind that there is always the time-reversed version of an 'encounter region' which yields the time-reversed version of the partner orbit. In the following section we will calculate the action difference of the orbit pair (γ, γ^p) in terms of local phase-space properties.

4.2 Action difference

The aim of this section is to present a generalized expression for the action difference (2.53) valid also for non-uniform hyperbolic systems. The resulting action difference $S_{\gamma^p,\gamma} \equiv S_{\gamma^p} - S_\gamma$ should be a function of the distance vector $\delta\vec{y}$ as this vector now replaces the small parameter ε appearing in the configuration-space approach. Thus one expects the action difference to be a function of second order in the components of $\delta\vec{y}$. In order to calculate the action of the partner orbit γ^p defined by Eq. (4.9) we first expand the action [Sie] of the original orbits γ and γ^i in terms of the small deviations[1] $\delta\vec{x}_{R,i} = (\delta\vec{q}_{R,i}, \delta\vec{p}_{R,i})$, $\delta\vec{x}_{R,e} = (\delta\vec{q}_{R,e}, \delta\vec{p}_{R,e})$, ... introduced in Eqs. (4.8). Then we use the solution in the form (4.11) to rewrite the action difference in terms of the components of $\delta\vec{y} = s\,\vec{e}^{\,s} + u\,\vec{e}^{\,u}$. The following derivation is based on the assumption that s and u are indeed small parameters so that the action difference between γ and γ^p can be expanded in these quantities.

In general, the action S of any classical path can be considered as a function of the initial and the final coordinates $\mathbf{q}$ if the energy of the particle is fixed [LL90]. Using the definition

$$S(\mathbf{q}_{t_2}, \mathbf{q}_{t_1}, E) = \int\limits_{\substack{\text{path} \\ (\mathbf{q}_{t_1} \to \mathbf{q}_{t_2})}} \mathrm{d}\mathbf{q} \quad \mathbf{p}(\mathbf{q}, E) \tag{4.13}$$

where the integration follows the classical path from $\mathbf{q}_{t_1}$ to $\mathbf{q}_{t_2}$ one can show the equality of the action of a path $\mathbf{x}_t$ and its time-reversed version $\mathbf{x}_t^i$, see e.g. Eq. (4.1). This allows to split the periodic orbit γ into the two parts $\mathcal{R}$ and $\mathcal{L}$, see Fig. 4.4. For the right loop $\mathcal{R}$ one can calculate the action difference between γ and γ^p because these two orbits follow each other closely in this part. The action difference accumulated in the second section $\mathcal{L}$ is determined by considering the deviations of γ^p from γ^i. The exact point where to split the orbit is not uniquely defined. However, in order to write the action difference in terms of the perpendicular deviations (4.9) we have chosen the POINCARÉ surface of section at $\mathbf{x}_{t_1}^\gamma$ where the orbit γ is in the middle of the 'encounter region', see Fig. 4.4. This POINCARÉ surface of section is exactly the one presented in Fig. 4.2(a). It is important to take the same POINCARÉ

[1] For two-dimensional systems ($f = 2$) the space of *perpendicular* coordinates is also two-dimensional implying that $\delta\vec{q}$ and $\delta\vec{p}$ are just scalars. However, in order to keep the derivation as general as possible we use the vector notation.

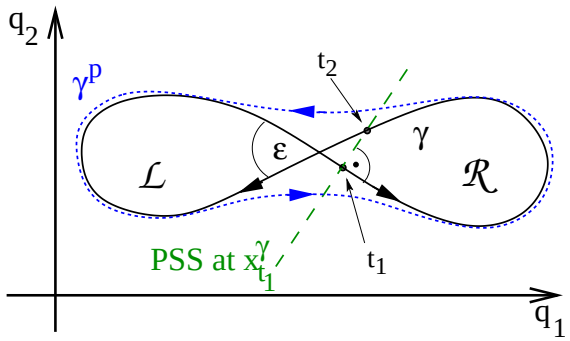

Figure 4.4: *In order to evaluate the action difference between the original orbit γ (solid line) and the partner orbit γ^p (dotted line) the whole trajectory is split in two parts. The first part is loop $\mathcal{R}$ starting at time t_1 and ending at t_2. The rest of the orbit defines loop $\mathcal{L}$. The definition of the two parts is not unique. For technical reasons we have chosen the intersections of the orbit or its time-reverse with the* Poincaré *surface of section at $\mathbf{x}^\gamma_{t_1}$. This* Poincaré *surface of section is the same as shown in more detail in Fig. 4.2(a). Here, we sketch its position in configuration space.*

surface of section as a reference after the traversal of $\mathcal{R}$ because otherwise parts of the orbit are neglected or their contributions enter twice.

As the geometric deviations of the partner orbit γ^p with respect to the original orbit γ are known in terms of the parameter $\delta\vec{y}$, Eqs. (4.9), we can evaluate its action in terms of the original orbit γ by expanding (4.13):

$$\begin{aligned}
\Delta S_R^{(1)} &= \frac{\partial S_R}{\partial \mathbf{q}_{t_2}}\,\Delta\mathbf{q}_{t_2} + \frac{\partial S_R}{\partial \mathbf{q}_{t_1}}\,\Delta\mathbf{q}_{t_1} = (\mathbf{p}_{t_2})^T\,\Delta\mathbf{q}_{t_2} - (\mathbf{p}_{t_1})^T\,\Delta\mathbf{q}_{t_1} \\
\Delta S_R^{(2)} &= \frac{1}{2}\left[\Delta\mathbf{q}_{t_2}^T \frac{\partial^2 S_R}{\partial \mathbf{q}_{t_2}\,\partial \mathbf{q}_{t_2}^T}\,\Delta\mathbf{q}_{t_2} + \Delta\mathbf{q}_{t_2}^T \frac{\partial^2 S_R}{\partial \mathbf{q}_{t_2}\,\partial \mathbf{q}_{t_1}^T}\,\Delta\mathbf{q}_{t_1}\right. \\
&\quad + \left.\Delta\mathbf{q}_{t_1}^T \frac{\partial^2 S_R}{\partial \mathbf{q}_{t_1}\,\partial \mathbf{q}_{t_2}^T}\,\Delta\mathbf{q}_{t_2} + \Delta\mathbf{q}_{t_1}^T \frac{\partial^2 S_R}{\partial \mathbf{q}_{t_1}\,\partial \mathbf{q}_{t_1}^T}\,\Delta\mathbf{q}_{t_1}\right] \\
&= \frac{1}{2}\left[(\Delta\mathbf{q}_{t_2})^T\,\Delta\mathbf{p}_{t_2} - (\Delta\mathbf{q}_{t_1})^T\,\Delta\mathbf{p}_{t_1}\right].
\end{aligned} \tag{4.14}$$

Here, $\Delta S^{(1)}$ denotes the first-order action difference between γ and γ^p while $\Delta S^{(2)}$ is of second order in the small initial and final deviations $(\Delta\mathbf{q}, \Delta\mathbf{p})$. The original orbit is given by the phase-space coordinates $\mathbf{x}_t \equiv (\mathbf{q}_t, \mathbf{p}_t)$ while the partner orbit is described by $\mathbf{x}_t^p \equiv (\mathbf{q}_t^p, \mathbf{p}_t^p)$. The coordinate difference in the beginning and in the end is defined as $\Delta\mathbf{q}_t = \mathbf{q}_t^p - \mathbf{q}_t$ and similarly for the difference in momentum. Along the same lines we can express the action difference in the other part $\mathcal{L}$ as

$$\begin{aligned}
\Delta S_L^{(1)} &= \left(\mathbf{p}^i_{T-t_2}\right)^T \Delta\mathbf{q}^i_{T-t_2} - \left(\mathbf{p}^i_{T-t_1}\right)^T \Delta\mathbf{q}^i_{T-t_1} \\
\Delta S_L^{(2)} &= \frac{1}{2}\left[\left(\Delta\mathbf{q}^i_{T-t_2}\right)^T \Delta\mathbf{p}^i_{T-t_2} - \left(\Delta\mathbf{q}^i_{T-t_1}\right)^T \Delta\mathbf{p}^i_{T-t_1}\right]
\end{aligned} \tag{4.15}$$

with $\mathbf{x}_t^i \equiv (\mathbf{q}_t^i, \mathbf{p}_t^i) = (\mathbf{q}_{T-t}, -\mathbf{p}_{T-t})$ being the coordinates of the time-reversed trajectory. The difference $\Delta\mathbf{q}_t^i = \mathbf{q}_t^i - \mathbf{q}_t^p$ is now to be taken between the orbits γ^i and γ^p and equivalently for $\Delta\mathbf{p}_t^i$.

Since we have chosen the POINCARÉ surface of section defined by the perpendicular coordinates at $\mathbf{x}_{t_1}^\gamma$ we can rewrite Eqs. (4.14) and (4.15) in terms of the vector $\delta\vec{y} = (\delta\vec{y}_q, \delta\vec{y}_p)$ and the four vectors $\delta\vec{x}_{\ldots} = (\delta\vec{q}_{\ldots}, \delta\vec{p}_{\ldots})$ introduced in Eqs. (4.8), see also Fig. 4.2(a). These vectors lie in the POINCARÉ surface of section perpendicular to the flow through $\mathbf{x}_{t_1}$. The result for the action differences (4.14) and (4.15) then reads

$$\begin{aligned}
\Delta S_R^{(1)} &= (\delta\vec{y}_p)^T \;\delta\vec{q}_{R,e} - 0\,, \quad \Delta S_R^{(2)} = \frac{1}{2}\left[(\delta\vec{p}_{R,e})^T \;\delta\vec{q}_{R,e} - (\delta\vec{p}_{R,i})^T \;\delta\vec{q}_{R,i}\right] \quad \text{and} \\
\Delta S_L^{(1)} &= (\delta\vec{y}_p)^T \;\delta\vec{q}_{L^i,e} - 0\,, \quad \Delta S_L^{(2)} = \frac{1}{2}\left[\left(\delta\vec{p}_{L^i,e}\right)^T \;\delta\vec{q}_{L^i,e} - \left(\delta\vec{p}_{L^i,i}\right)^T \;\delta\vec{q}_{L^i,i}\right].
\end{aligned} \tag{4.16}$$

As one now realizes the two contributions $\Delta S^{(1)}$ and $\Delta S^{(2)}$ are of the same order of magnitude. Intuitively this is clear since for example the momentum $\mathbf{p}_{t_2}$ entering $\Delta S_R^{(1)}$ in Eq. (4.14) is almost perpendicular to the difference in positions $\Delta\mathbf{q}_{t_2}$ yielding a small value for the scalar product $(\mathbf{p}_{t_2})^T \cdot \Delta\mathbf{q}_{t_2}$ between the two vectors, see Fig. 4.4. Therefore, one has to keep the second-order contribution $\Delta S^{(2)}$ in addition to the first-order terms $\Delta S^{(1)}$.

The total action difference in terms of the four vectors $\delta\vec{x}_{\ldots}$ describing the partner γ^p can now be calculated by summing all terms in (4.16) and reads

$$S_{\gamma^p,\gamma} = \Delta S_R^{(1)} + \Delta S_L^{(1)} + \Delta S_R^{(2)} + \Delta S_L^{(2)} = \frac{1}{2}\left[\delta\vec{x}_{R,e}^T\,\Sigma\,\delta\vec{x}_{L^i,i} + \delta\vec{x}_{L^i,e}^T\,\Sigma\,\delta\vec{x}_{R,i}\right] \tag{4.17}$$

where the vector $\delta\vec{y}$ was eliminated by using Eqs. (4.8) and Σ is the matrix defined in Eq. (2.2). As shown in Section 4.1 partner orbits exist only for long loops which allows to apply the approximations (4.11) and (4.12). These relations connect the solution for the geometric deviations of γ^p from γ with the local phase-space properties and the components of the distance vector $\delta\vec{y} = s\,\vec{e}^{\,s} + u\,\vec{e}^{\,u}$. Hence the action difference (4.17) can also be rewritten in terms of the components s and u of $\delta\vec{y}$ in the basis of the local stable and unstable directions $\vec{e}^{\,s,u}(\mathbf{x})$:

$$S_{\gamma,\gamma^p} \equiv S_\gamma - S_{\gamma^p} = S(\delta\vec{y}) = S_{\text{cl}}\; s\, u\,. \tag{4.18}$$

This is the central result of this section and provides the generalization of expression (2.53). It can be applied to either orbit pair (γ, γ^p), $(\gamma, \gamma^{p,i})$, (γ^i, γ^p) and $(\gamma^i, \gamma^{p,i})$. The classical action S_{cl} enters because the length of $\vec{e}^{\,s,u}$ was defined on the basis of this quantity, see Eq. (2.16). As can be seen in Eq. (4.18) the final result for the action difference is given solely in terms of the components of the displacement vector $\delta\vec{y} = s\,\vec{e}^{\,s} + u\vec{e}^{\,u}$ but does not contain any specific information about the loops, such as the matrix elements of the stability matrices R and L, anymore. Only local

phase space properties, namely the local stable and unstable manifolds, enter via the components s and u of a given $\delta\vec{y}$.

As we pointed out in Section 2.3, only those orbit pairs having a small action difference $S_{\gamma,\gamma^p} \sim \hbar$ contribute significantly in the semiclassical evaluation of the spectral form factor (2.38). This means that we indeed have to include only the cases where $s, u \sim \sqrt{\hbar/S_{\rm cl}} \ll 1$ meaning that the orbit γ comes very close to its time-reversed version γ^i in phase space. Thus the restriction to $s, u \ll 1$ in all previous considerations is justified in the semiclassical limit and our approach is self-consistent.

The intuitive interpretation of Eq. (4.18) is rather straightforward. The action difference is given by the area enclosed by the four intersection points of γ, γ^i, γ^p and $\gamma^{p,i}$ with the POINCARÉ surface of section at $\mathbf{x}^{\gamma}_{t_1}$, see Fig. 4.2(a). Now we will argue that the evaluation of the action difference resulting in Eq. (4.18) is also consistent with the concept of the 'encounter region' we introduced earlier. In particular, the derived action difference (4.18) does not depend on the position within an 'encounter region' used for its calculation. If the POINCARÉ surface of section at a slightly different time $\bar{t}_1 = t_1 + \Delta t$ is considered then the enclosed area does not change because the volume in phase space is conserved. Formally, this is most easily seen in Eq. (4.17). One could map the POINCARÉ surface of section at $\mathbf{x}_{t_1}$ to $\mathbf{x}_{t_1+\Delta t}$ by applying the corresponding stability matrix $M(\Delta t, \mathbf{x}_{t_1})$. However, due to the symplectic property $M^T \Sigma M = \Sigma$ the symplectic product between any two vectors is conserved, see Section 2.1. As the action difference contains only symplectic products it must also be invariant under this shift from $\mathbf{x}_{t_1}$ to $\mathbf{x}_{t_1+\Delta t}$. Therefore, it is clear that one can choose any position $\bar{t}_1$ within an 'encounter region' to calculate the action difference between γ and γ^p.

In the previous two sections we have shown that if a periodic orbit γ comes close to its time-reversed version γ^i in phase space then a partner orbit γ^p exists if the loop times are large enough, i.e. $2\Delta t^u < t_{\rm loop} < T_\gamma - 2\Delta t^s$. The vector $\delta\vec{y} = s\,\vec{e}^{\,s} + u\,\vec{e}^{\,u}$ describes quantitatively how close the two orbits γ and γ^i are. The geometric deviations of the partner orbit γ^p from the original orbit γ are given by Eqs. (4.11) and the action difference between the two follows from Eq. (4.18). An important conceptual difference between the configuration-space approach, Section 2.5, and the proposed phase-space approach is that the crossings are replaced by 'encounter regions'. These 'encounter regions' are not localized in phase space as crossings are. They extend over a time t_{en} given by Eq. (4.6). In the next section we will argue why the MASLOV indices of the orbits γ and γ^p cancel and why their semiclassical weights are approximately equal. This finally allows to calculate the contribution of the orbit pairs (γ, γ^p) to the spectral form factor (2.38) in Section 4.4.

4.3 MASLOV index and weight of the partner orbit

The purpose of this section is to first show that the semiclassical weights w_γ and w_{γ^p} for the periodic orbits entering the expression for the form factor (2.38) are approximately equal. This can most easily be done by relating the partner orbit γ^p to the original orbit γ in part $\mathcal{R}$ and to γ^i in part $\mathcal{L}$. Then we will demonstrate that the MASLOV indices μ_γ and μ_{γ^p} introduced in Eq. (2.36) cancel each other in the calculation of the semiclassical form factor (2.38) if the orbits pairs (γ, γ^p) are considered. We will show that $\mu_\gamma = \mu_{\gamma^p}$ by using the geometrical interpretation of the MASLOV indices as winding numbers of the stable or unstable manifolds. This interpretation was introduced for two-dimensional systems in [CRL90] to show that the MASLOV index of a periodic orbit entering GUTZWILLER's trace formula (2.33) is canonically invariant. The approach was then extended to systems with f degrees of freedom in [Rob91] and some practical methods of calculation where suggested in [EW91]. Especially useful for the considerations to follow is the proof [FR97] that the MASLOV index of a periodic orbit γ equals that one of its time-reversed version γ^i, i.e. $\mu_\gamma = \mu_{\gamma^i}$.

Before we investigate the MASLOV indices in more detail let us argue why the weights of γ and γ^p are approximately equal, i.e. $w_\gamma \simeq w_{\gamma^p}$. The reason is that the geometric deviations between the orbits γ and γ^p are very small. As only small action differences $|S_{\gamma,\gamma^p}| \sim \hbar$ contribute significantly to $K^{(2)}(\tau)$ the components of the distance vector $\delta\vec{y} = s\,\vec{e}^{\,s} + u\,\vec{e}^{\,u}$ are also very small, i.e. $s, u \sim \sqrt{\hbar/S_{\rm cl}}$, see Eq. (4.18). This implies that the geometric deviations $\delta\vec{x}_{\ldots}$ between γ and γ^p, Eq. (4.11), are also on the order of $\sqrt{\hbar/S_{\rm cl}}$. Hence the difference between the loop lengths T_γ and T_{γ^p} yields a correction to the form factor (2.38) which is small in the semiclassical limit $\hbar \to 0$. A similar argument holds for the weights w_γ which are also geometry related classical quantities. Quantitatively this can be seen as follows. For any smooth function $f(\mathbf{x})$ defined in phase space one finds the following relation using (4.7)

$$\int_0^{T_{\gamma,p}} \mathrm{d}t\, f(\mathbf{x}_t^{\gamma,p}) \simeq \int_{t_1}^{t_2} \mathrm{d}t\, f(\mathbf{x}_t^{\gamma}) + \int_{t_2}^{T_\gamma+t_1} \mathrm{d}t\, f(\mathcal{T}\mathbf{x}_{t_1+t_2-t}^{\gamma}) \tag{4.19}$$

with small corrections on the order of $|s_i|, |u_i| \sim \sqrt{\hbar/S_{\rm cl}}$. The times t_1 and t_2 are related to the loop length via $t_2 = t_1 + t_{\rm loop}$. This means that the integral over any function $f(\mathbf{x})$ along the partner orbit γ^p is approximately given by integrals along parts of γ and γ^i. The corrections in Eq. (4.19) are primarily due to the deviations of the partner orbit γ^p from the original orbit γ or its time-reversed version γ^i within the encounter region. There, the deviations between γ^p and γ or γ^i are most pronounced, see Fig. 4.1(b), but still they are of first order in $\delta\vec{y}$ meaning that they are small. Obviously, Eq. (4.19) yields $T_\gamma \simeq T_{\gamma^p}$ for $f(\mathbf{x}) = 1$. Similarly we can apply (4.19) to the local growth rate, i.e. $f(\mathbf{x}) = \chi(\mathbf{x})$, which results into $\lambda^\gamma \simeq \lambda^{\gamma,p}$,

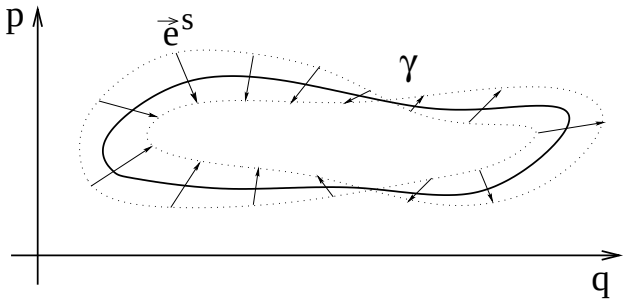

Figure 4.5: *The* MASLOV *index of a periodic orbit γ is given as the winding number of the local stable (or unstable) direction when going once around the orbit. In this figure we sketch an example where the winding number is equal to one.*

see Eq. (2.9). Hence one can conclude that the LYAPUNOV exponent of the partner orbit has to be very similar to that of the original orbit.

Finally we can also identify $f(\mathbf{x})$ with the local change in the winding number of the stable or unstable manifolds. According to [Rob91, FR97] the MASLOV index μ_γ entering GUTZWILLER's trace formula (2.35) can be obtained by considering the winding number $\mathrm{wn}^\gamma\left[\vec{e}^{s,u}(\mathbf{x}_t)\right]$ of the local stable or unstable direction when going along the periodic orbit γ, see Fig. 4.5. For two-dimensional systems ($f = 2$) the vectors $\vec{e}^{s,u}$ associated with the stable and unstable directions can be represented by complex numbers, e.g. $\vec{e}^{s,u} = (q^{s,u}, p^{s,u}) \to q^{s,u} + \mathrm{i}p^{s,u}$. The winding number $\mathrm{wn}_\gamma\left[\vec{e}^{s,u}(\mathbf{x}_t)\right]$ can then be determined by considering the change of the argument of this complex number. Thus the MASLOV index μ_γ is given by

$$\mu_\gamma = \mathrm{wn}\left[\vec{e}^{s,u}(\mathbf{x}_t^\gamma)\right]_0^{T_\gamma} \equiv \frac{1}{2\pi}\int_0^{T_\gamma} \mathrm{d}t\,\frac{\mathrm{d}}{\mathrm{d}t}\arg\left[\vec{e}^{s,u}(\mathbf{x}_t^\gamma)\right]. \tag{4.20}$$

One can choose either the stable or the unstable local direction in Eq. (4.20) as a basis for the calculation of the MASLOV index. Either case yields the same result. The reason is that the manifolds never cross or lie on top of each other so that $\vec{e}^s \neq \vec{e}^u$ is always fulfilled. Formally this is expressed in the relation $\vec{e}^s \Sigma \vec{e}^u \neq 0$, see Eq. (2.16). Hence, the winding numbers based on the stable and the unstable manifolds must be the same, i.e. $\mathrm{wn}\left[\vec{e}^s\right]_0^{T_\gamma} = \mathrm{wn}\left[\vec{e}^u\right]_0^{T_\gamma}$.

Furthermore, one can show that the MASLOV index of a periodic orbit γ is the same as for its time-reversed version γ^i, i.e. $\mu_\gamma = \mu_{\gamma^i}$, [FR97]. To see this one has

to apply Eq. (4.2) to the definition (4.20) which then yields

$$\begin{aligned}\mu_{\gamma^i} &= \mathrm{wn}\left[\vec{e}^{\,s,u}(\mathbf{x}_t^{\gamma,i})\right]_0^{T_\gamma} = \frac{1}{2\pi}\int_0^{T_\gamma} \mathrm{d}t\,\frac{\mathrm{d}}{\mathrm{d}t}\arg\left[\vec{e}^{\,s,u}(\mathbf{x}_t^{\gamma,i})\right] \\ &= \frac{1}{2\pi}\int_0^{T_\gamma} \mathrm{d}t\,\frac{\mathrm{d}}{\mathrm{d}t}\arg\left[F\,\vec{e}^{\,u,s}(\mathbf{x}_{T_\gamma-t}^{\gamma})\right] = \mathrm{wn}\left[\vec{e}^{\,u,s}(\mathbf{x}_t^{\gamma})\right]_0^{T_\gamma} = \mu_\gamma\ . \end{aligned} \tag{4.21}$$

In the second line of Eq. (4.21) the variable transformation $t \to T_\gamma - t$ was performed. As formally expressed in Eq. (4.21) the equality $\mu_\gamma = \mu_{\gamma^i}$ is due to the fact that not only the orientation of the orbit γ is changed due to time reversal but also the manifolds have to be transformed according to Eq. (4.2). These two effects exactly compensate each other if the trajectory is periodic. Finally, the definition (4.20) ensures that the MASLOV index can be interpreted as an additive function of a local quantity implying $\mathrm{wn}\left[\vec{e}^{\,s,u}\right]_0^T = \mathrm{wn}\left[\vec{e}^{\,s,u}\right]_0^{t'} + \mathrm{wn}\left[\vec{e}^{\,s,u}\right]_{t'}^T$ for any time t'.

The following proof of $\mu_\gamma = \mu_{\gamma^p}$ uses the assumption that the local stable and unstable directions are continuous functions with respect to their positions in phase space, Eq. (2.19). In order to evaluate the MASLOV index μ_{γ^p} we again split the original periodic orbit γ into the two parts $\mathcal{R}$ and $\mathcal{L}$, see Fig. 4.1(b) and Fig. 4.4. The first loop $\mathcal{R}$ goes from t_1 to t_2 while the second part $\mathcal{L}$ starts at t_2 and ends at $T_\gamma + t_1$. The MASLOV index μ_{γ^p} of the partner orbit is then evaluated separately for either part by relating it to μ_γ and μ_{γ^i} via the continuity relation (2.19). This yields

$$\begin{aligned}\mu_{\gamma^p} &= \mathrm{wn}\left[\vec{e}^{\,s}(\mathbf{x}_t^{\gamma,p})\right]_{t_1}^{t_2} + \mathrm{wn}\left[\vec{e}^{\,s}(\mathbf{x}_t^{\gamma,p})\right]_{t_2}^{T_\gamma+t_1} \\ &\simeq \frac{1}{2\pi}\int_{t_1}^{t_2} \mathrm{d}t\frac{\mathrm{d}}{\mathrm{d}t}\arg\left[\vec{e}^{\,s}(\mathbf{x}_t^{\gamma})\right] + \frac{1}{2\pi}\int_{T_\gamma-t_1}^{2T_\gamma-t_2} \mathrm{d}t\frac{\mathrm{d}}{\mathrm{d}t}\arg\left[\vec{e}^{\,s}(\mathbf{x}_t^{\gamma,i})\right] \\ &= \mathrm{wn}\left[\vec{e}^{\,s}(\mathbf{x}_t^{\gamma})\right]_{t_1}^{t_2} + \frac{1}{2\pi}\int_{-t_1}^{T_\gamma-t_2} \mathrm{d}t\frac{\mathrm{d}}{\mathrm{d}t}\arg\left[Fe^{u}(\mathbf{x}_{T_\gamma-t}^{\gamma})\right] \\ &= \mathrm{wn}\left[\vec{e}^{\,s}(\mathbf{x}_t^{\gamma})\right]_{t_1}^{t_2} + \mathrm{wn}\left[\vec{e}^{\,u}(\mathbf{x}_t^{\gamma})\right]_{t_2}^{T_\gamma+t_1} \end{aligned} \tag{4.22}$$

if the local stable direction $\vec{e}^{\,s}(\mathbf{x}_t^{\gamma,p})$ is used as a basis for the determination of the winding number. The derivation above has to be understood as follows. During the first loop $\mathcal{R}$ we can express the contribution to the total winding number of γ^p via the corresponding contribution of γ since the two paths follow each other closely. It is important to note that the total difference of these two contributions between t_1 and t_2 is at most $1/2$ since the continuity relation is assumed to be true at all points along the path. A similar argument holds for the second loop so that the error is $\mathcal{O}(\delta\vec{y})$ but does not scale with the loop times t_{loop} and t'_{loop}. Therefore, the second

line in Eq. (4.22) represents only an approximation of μ_{γ^p} but with small corrections $\mathcal{O}(\delta\vec{y})$ only.

On the other hand one can also use the unstable direction $\vec{e}^{\,u}(\mathbf{x}_t^{\gamma,p})$ to determine the winding number. Performing a similar calculation as in Eq. (4.22) results in

$$\mu_{\gamma^p} = \mathrm{wn}\left[\vec{e}^{\,u}(\mathbf{x}_t^{\gamma,p})\right]_{t_1}^{t_2} + \mathrm{wn}\left[\vec{e}^{\,u}(\mathbf{x}_t^{\gamma,p})\right]_{t_2}^{T_\gamma+t_1} = \mathrm{wn}\left[\vec{e}^{\,u}(\mathbf{x}_t^{\gamma})\right]_{t_1}^{t_2} + \mathrm{wn}\left[\vec{e}^{\,s}(\mathbf{x}_t^{\gamma})\right]_{t_2}^{T_\gamma+t_1} \ . \quad (4.23)$$

Therefore, together with (4.22) we find that the two Maslov indices μ_γ and μ_{γ^p} must be approximately equal with an error $\mathcal{O}(\delta\vec{y})$:

$$\begin{aligned}\mu_{\gamma^p} &= \frac{1}{2}\left(\mathrm{wn}\left[\vec{e}^{\,s}(\mathbf{x}_t^{\gamma,p})\right]_0^{T_\gamma} + \mathrm{wn}\left[\vec{e}^{\,u}(\mathbf{x}_t^{\gamma,p})\right]_0^{T_\gamma}\right) \\ &= \frac{1}{2}\left(\mathrm{wn}\left[\vec{e}^{\,s}(\mathbf{x}_t^{\gamma})\right]_0^{T_\gamma} + \mathrm{wn}\left[\vec{e}^{\,u}(\mathbf{x}_t^{\gamma})\right]_0^{T_\gamma}\right) + \mathcal{O}(\delta\vec{y}) \simeq \mu_\gamma \ . \end{aligned} \quad (4.24)$$

Although above derivation (4.22, 4.23, 4.24) only shows the approximate equality of μ_γ and μ_{γ^p} we can now conclude that the two Maslov indices have to be exactly equal. The reason is that the winding number multiplied by two must be an integer number for periodic orbits. Therefore, the smallest non-zero difference between two Maslov indices is at least one half. Hence one arrives at the conclusion that the difference $\mu_\gamma - \mu_{\gamma^p}$, being at most $\mathcal{O}(\delta\vec{y})$ according to (4.24), is exactly zero. This proves that for an orbit pair (γ, γ^p) in a continuous hyperbolic system the Maslov indices are equal, i.e. $\mu_\gamma = \mu_{\gamma^p}$. This is important for the calculation of the semiclassical form factor (2.38) since then the only phase factor entering the exponential is due to the action difference (4.18).

In this section we have shown that the weights and periods of the orbits γ and γ^p are approximately equal, i.e. $w_\gamma \simeq w_{\gamma^p}$ and $T_\gamma \simeq T_{\gamma,p}$, while the Maslov indices are exactly equal, i.e. $\mu_\gamma = \mu_{\gamma,p}$. In the next section we will present a new method of how the partner orbits γ^p can be counted and how their contribution to the form factor is evaluated. This is the final step in the generalization of the configuration-space approach reviewed in Section 2.5 towards a canonically invariant formulation based on phase-space concepts.

4.4 Counting the partner orbits and calculation of the form factor

In the previous sections of this chapter we have shown that among all orbit pairs (γ, γ') entering the semiclassical form factor (2.38) there are certain pairs (γ, γ^p) that have a small action difference. We showed that the criterion for the existence of such pairs can be expressed by employing a vector $\delta\vec{y}$ which describes how close the orbit γ comes to its time-reversed version γ^i in phase space. We derived the geometry of the partner orbit γ^p, Eq. (4.11), and its action difference S_{γ,γ^p}, Eq. (4.18). In the

last section we then showed the equality of the MASLOV indices of the two orbits, i.e. $\mu_\gamma = \mu_{\gamma^p}$. The goal of this section is to perform the summations over these pairs (γ, γ^p) of orbits in the semiclassical form factor (2.38). We will show that their contribution amounts to $K^{(2)}(\tau) = -2\tau^2$ and is thus universal as it was for the uniform hyperbolic system, Section 2.5.

To compute the contribution $K^{(2)}(\tau)$ of the orbit pairs (γ, γ^p) to $K(\tau) = K^{(1)}(\tau) + K^{(2)}(\tau) + \ldots$ we rearrange the double sum over periodic orbits in the semiclassical expression for the form factor (2.38) in the following way. First we rewrite $K^{(2)}(\tau)$ as a sum over periodic orbits γ and a second sum over all the partners γ^p associated with each of the orbits. This procedure is based on the assumption that the dominant off-diagonal contribution to $K^{(2)}(\tau)$ is due to the systematic correlations of actions of the considered orbit pairs (γ, γ^p). Other random correlations are neglected since they would disappear if the system is slightly changed. Therefore they cannot be responsible for universal contributions to the form factor. As opposed to the approach in configuration space, Section 2.5, we then sort the terms in the sums with respect to their action differences $S_{\gamma^p,\gamma}$. The action difference is the correct small parameter for the phase-space approach replacing the crossing angle ε, e.g. in Eq. (2.54). It characterizes the orbit pairs and their associated contribution $\exp(\mathrm{i}S_{\gamma,\gamma^p}/\hbar)$ to the semiclassical form factor uniquely. Furthermore, the action difference S_{γ,γ^p} unlike the crossing angle ε is independent of the choice of coordinates and thus canonically invariant. For the spectral form factor we then find

$$\begin{aligned} K^{(2)}(\tau) &= \frac{1}{T_H} \left\langle \sum_\gamma \sum_{n=0}^{\infty} |w_\gamma|^2 \, \delta_{\Delta\tau}\left(\tau\, T_H - T_\gamma\right) \; N_\gamma(S_n) \, \exp\left[\mathrm{i}\frac{S_n}{\hbar}\right] \right\rangle_{\Delta E} \\ &= \tau \left\langle \int_{-S_{\max}(E)}^{S_{\max}(E)} \mathrm{d}S \, \left\langle \frac{\mathrm{d}N_\gamma(S,T)}{\mathrm{d}S} \right\rangle_{\gamma,\tau T_H} \exp\left[\mathrm{i}\frac{S}{\hbar}\right] \right\rangle_{\Delta E} . \end{aligned} \tag{4.25}$$

In the first step we formally introduced the number of partner orbits $N_\gamma(S_n)$ of a given periodic γ as a function of the action difference S_n. Furthermore we used the approximation $T_\gamma \approx T_{\gamma^p}$ and $w_\gamma \approx w_{\gamma^p}$. The major effect in the double sum over periodic orbits comes from changes in the rapidly oscillating exponential, i.e. the action difference S in Eq. (4.25), since the exponent effectively enters in units of $\hbar$. Therefore, the leading correction to the form factor can be evaluated by considering only the effect of the phase difference between γ and γ^p neglecting any corrections coming from pre-exponential factors. This corresponds to a saddle point approximation. In the second step in Eq. (4.25) we replaced the discrete sum over action differences S_n by a continuous integral and the number of partners $N_\gamma(S_n)$ correspondingly by a partner density per action difference $\mathrm{d}N_\gamma/\mathrm{d}S$. The maximum action difference among the orbit pairs (γ, γ^p) is denoted by $S_{\max}$. The replacement of the sum by an integral is reasonable because of the huge number of partners that

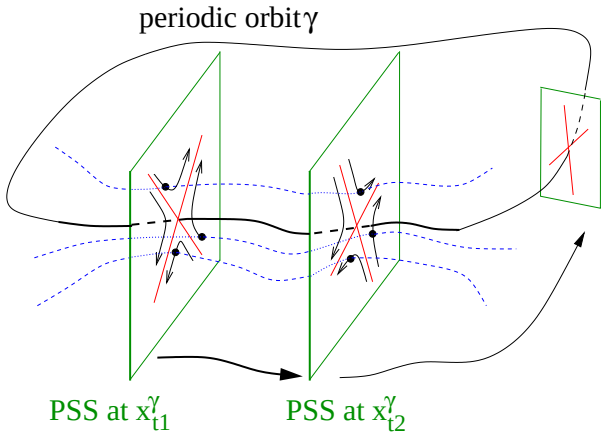

Figure 4.6: *The* Poincaré *surface of section (PSS) is considered as it moves following the phase space flow along the orbit. Neighboring trajectories can then be represented as points* $\{\delta\vec{y}_i\}$ *within the* Poincaré *surface of section. As a function of time these points change their positions in the* Poincaré *surface of section and thus define a flow in this* $2f-2$ *dimensional hypersurface.*

can be expected for large orbit lengths $T_\gamma \approx \tau T_H$. The other sum over periodic orbits together with the weights w_γ and the δ-function can be expressed using the average over periodic orbits $\langle \dots \rangle_{\gamma,T}$ of given length $T_\gamma \approx T = \tau T_H$ as defined in Eq. (2.41). The evaluation of the leading off-diagonal correction to the form factor is thus reduced to the calculation of the density of partners per action difference averaged over all periodic orbits. The major contribution to the integral in Eq. (4.25) is due to the small $|S| \sim \hbar$ behavior of this density in the semiclassical limit. This also implies that the precise knowledge of the largest possible action difference $S_{\max}$ among the orbit pairs (γ, γ^p) is not important for the further calculation of $K^{(2)}(\tau)$. In the following paragraphs we propose a new method how to count the partner orbits and determine $\langle \mathrm{d}N_\gamma/\mathrm{d}S\rangle_\gamma$ which eventually allows to evaluate $K^{(2)}(\tau)$, Eq. (4.25).

The basic idea for the computation of the density of partners per action difference $\mathrm{d}N_\gamma/\mathrm{d}S$ is to consider the dynamical flow within the Poincaré surface of section as it is moved along an orbit, see Fig. 4.6. Each time the time-reversed orbit γ^i comes close to the original periodic orbit γ it intersects the Poincaré surface of section. The set of all intersection points is denoted by $\{\delta\vec{y}_i\}$ where each member can be associated to a different loop time $t_{\mathrm{loop},i}$. As one moves the Poincaré surface of section along the orbit the whole set of intersection points close to the origin changes its position according to the linearized equations of motion (2.3) and thus defines a flow, see Fig. 4.7(a). Because of the requirement that the action difference (4.18) is small the stable and unstable components of all relevant $\delta\vec{y}_i$ must also be small at a certain time (roughly speaking in the middle of the 'encounter region'). But this is only possible if the vectors $\{\delta\vec{y}_i\}$ lie close to the local stable direction in the

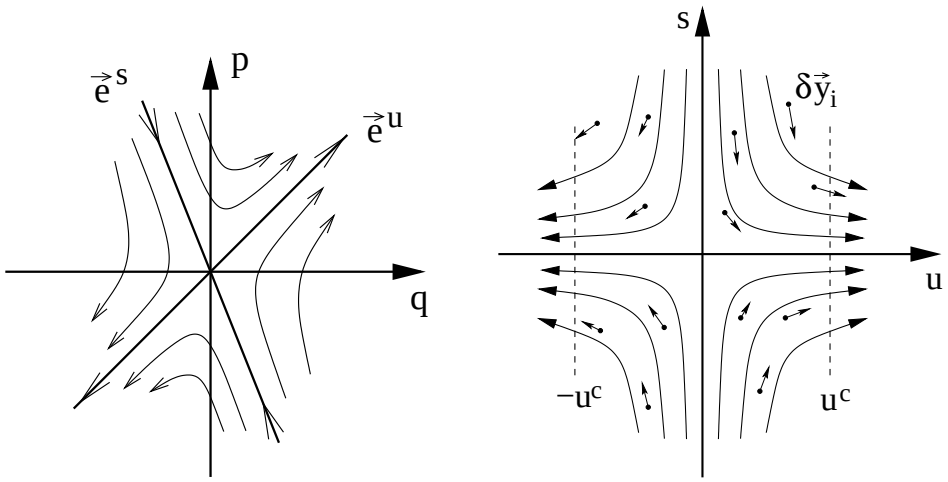

(a) Dynamical flow within the PSS (b) Flux through $u = u^c$ line in PSS

Figure 4.7: (a) *The dynamical flow within the* Poincaré *surface of section in the vicinity of an unstable hyperbolic periodic orbit can be described by hyperbolas. In the long-time limit the stable component of any point in the* Poincaré *surface of section decreases exponentially while the unstable component increases.* (b) *If the* Poincaré *surface of section is shifted once around the periodic orbit each point $\delta\vec{y}_i$ with a positive coefficient u crosses the line $u = u^c$ exactly once from left to right. In principle the flow in the* Poincaré *surface of section could also reverse its direction on short time scales. This can imply that a point having already passed the $u = u^c$ line comes back and crosses the line in the opposite direction from right to left. However, the hyperbolic long-time behavior of the flow ensures that there is an overall exponential growth of the unstable component u so that the point would have to pass the line a third time compensating the second passing from the wrong side. A similar argument also holds for the $u = -u^c$ line.*

beginning, then move towards the origin of the Poincaré surface of section and finally end up close to the local unstable direction. To be more specific, as a function of time all points $\{\delta\vec{y}_i\}$ corresponding to partner orbits move on hyperbolas which converge towards the local stable and unstable directions. This can be most easily seen by decomposing any vector $\delta\vec{y}$ in the Poincaré surface of section into its stable and unstable components, i.e. $\delta\vec{y} = s\,\vec{e}^{\,s} + u\,\vec{e}^{\,u} = \delta\vec{y}^{\,s} + \delta\vec{y}^{\,u}$, see Eq. (2.15). Due to the symplectic nature of the dynamics the symplectic product between any two vectors has to be conserved. This implies $(\delta\vec{y}_s)^T\,\Sigma\delta\vec{y}_u = -S_{\rm cl}\,u\,s = \text{const}$ because of Eq. (2.16). Hence the stable component s of $\delta\vec{y}$ can be written as a function of the unstable component u, i.e. $s \propto 1/u$, or vice versa, see Fig. 4.7(b). The flow which is represented in Fig. 4.7 is then obtained by assigning different values to const.

In this flow based picture the number of partners γ^p is given by the number of

points $\{\delta\vec{y}_i\}_p$ crossing a certain line $u = \pm u^c$ in the POINCARÉ surface of section while the surface is shifted once around the entire periodic orbit. The parameter u^c therefore fixes the position within an 'encounter region' that is used to identify and count it. This means that one has to evaluate the flux through the lines $u = \pm u^c$ between $t = 0 \dots T_\gamma$, see Fig. 4.7(b). It is clear that the final result for the number of partners should not depend on the specific value of u^c as long as it is chosen small enough for the linear approximation to hold. Let us denote the density of points $\{\delta\vec{y}_i\}_p$ in the u-s-plane, Fig. 4.7(b), each corresponding to a partner orbit, by $\varrho(s, u; \mathbf{x})$. The number of intersection points crossing the lines $u = \pm u^c$ is then determined by this density $\varrho(u, s; \mathbf{x}_t)$ and the velocity $\dot{u}(u, s; \mathbf{x}_t)$ of each point $\delta\vec{y}_i$ into the unstable direction. Therefore the total density of partners per action difference can be written as

$$\left\langle \frac{\mathrm{d}N_\gamma(S,T)}{\mathrm{d}S} \right\rangle_{\gamma,T} = \frac{1}{S_{\mathrm{cl}}} \left\langle \int_0^{T_\gamma} \mathrm{d}t \; \left[\varrho\left(u^c, \frac{S}{S_{\mathrm{cl}}u^c}; \mathbf{x}_t^\gamma\right) \frac{\dot{u}\left(u^c, \frac{S}{S_{\mathrm{cl}}u^c}; \mathbf{x}_t^\gamma\right)}{u^c} + \right. \right.$$
$$\left. \left. \varrho\left(-u^c, \frac{S}{-S_{\mathrm{cl}}u^c}; \mathbf{x}_t^\gamma\right) \frac{\dot{u}\left(-u^c, \frac{S}{-S_{\mathrm{cl}}u^c}; \mathbf{x}_t^\gamma\right)}{-u^c} \right] \right\rangle_{\gamma,T} . \tag{4.26}$$

Here, we used the fact that for fixed $u = \pm u^c$ the action difference $S = S_{\gamma,\gamma^p}$, Eq. (4.18) is uniquely determined by the component $s = S/(S_{\mathrm{cl}}u^c)$. This allows to perform a variable transformation $s \to S$ which then gives a factor $1/(S_{\mathrm{cl}}u^c)$. The two terms in the integral in Eq. (4.26) represent the $u = +u^c$ and the $u = -u^c$ line, respectively. The products $\varrho(\dots)\,\dot{u}(\dots)$ characterize the flux through these lines. In order to proceed with the calculation of the number of partners (4.26) we have to determine the density $\varrho(s, u; \mathbf{x}_t^\gamma)$ of intersection points $\{\delta\vec{y}_i\}_p$ lying in the POINCARÉ surface of section at $\mathbf{x}_t^\gamma$. As explained in detail in Section 4.1, an intersection point $\delta\vec{y}_i$ corresponds to a partner orbit if and only if the associated loop lengths are larger then the minimal times $\Delta t^{s,u}$, see Eqs. (4.5, 4.6). The density of points $\{\delta\vec{y}_i\}_p$ is therefore given as

$$\varrho(s, u; \mathbf{x}_t) = \int_{2\Delta t^u}^{T-2\Delta t^s} \mathrm{d}t_{\mathrm{loop}} \; \delta\left(\left[\mathbf{x}_t - \mathcal{T}\mathbf{x}_{t+t_{\mathrm{loop}}}\right]_u - u\right) \delta\left(\left[\mathbf{x}_t - \mathcal{T}\mathbf{x}_{t+t_{\mathrm{loop}}}\right]_s - s\right) \times$$
$$\delta\left(\left[\mathbf{x}_t - \mathcal{T}\mathbf{x}_{t+t_{\mathrm{loop}}}\right]_{\|}\right) \tag{4.27}$$

where t_{loop} represents all possible loop lengths. The indices s and u in $[\mathbf{x}]_{s,u}$ denote the perpendicular stable or unstable component of a phase space vector $\mathbf{x}$, respectively. The last δ-function ensures that $\mathcal{T}\mathbf{x}_{t+t_{\mathrm{loop}}}$ lies in the POINCARÉ surface of section at $\mathbf{x}_t$ as the difference of the parallel components has to vanish. The functional dependence of the times $\Delta t^{s,u} = \Delta t^{s,u}(s, u; \mathbf{x})$ on s, u is determined by the

implicit condition (4.5). The choice for the limits of the integration in Eq. (4.27) excludes the short loop times. Hence only those intersection points $\{\delta\vec{y}_i\}_p$ that can be associated with a partner orbit are counted. Therefore, if almost self-retracing loops exist they are excluded as they do not yield a partner orbit.

We continue with the derivation of the density of partners per action difference by rewriting Eq. (4.26) in terms of the local growth rate $\chi(\mathbf{x})$ as

$$\left\langle \frac{\mathrm{d}N_\gamma(S,T)}{\mathrm{d}S} \right\rangle_{\gamma,T} = \frac{1}{S_{\mathrm{cl}}} \int_0^T \mathrm{d}t \left[\varrho\left(u^c, \frac{S}{S_{\mathrm{cl}}u^c}; \mathbf{x}_t\right) + \varrho\left(-u^c, \frac{S}{-S_{\mathrm{cl}}u^c}; \mathbf{x}_t\right) \right] \chi(\mathbf{x}_t) \; . \tag{4.28}$$

This result can be found by using the equations of motion for the component u, Eq. (2.18), and applying of the sum rule for periodic orbits (2.42). The integration now goes along any ergodic path of length $T = \tau T_H$. Hence the density of partners per action averaged over all periodic orbits is reduced to a time average over the density $\varrho(s,u;\mathbf{x}_t)$ of intersection points $\delta\vec{y}_i$ in the Poincaré surface of section multiplied with the local growth rate $\chi(\mathbf{x}_t)$.

As the path length $T = \tau T_H$ is large in the semiclassical limit one can use the ergodic property $\langle f(\mathbf{x}_0)\rangle_t = \langle f(\mathbf{x})\rangle_{\mathbf{x}}$ of the system to determine the density $\varrho(s,u;\mathbf{x})$, Eq. (4.27):

$$\begin{aligned} \varrho(s,u;\mathbf{x}_0) &= (T - 2t_{en}(s,u;\mathbf{x}_0)) \times \\ &\qquad \left\langle \delta\left([\mathbf{x}_0 - F\mathbf{x}]_u - u\right) \, \delta\left([\mathbf{x}_0 - F\mathbf{x}]_s - s\right) \, \delta\left([\mathbf{x}_0 - F\mathbf{x}]_\parallel\right) \right\rangle_{\mathbf{x}} \\ &= S_{\mathrm{cl}} \left(\frac{T}{\Omega(E)} + \frac{-2\,t_{en}(s,u;\mathbf{x}_0)}{\Omega(E)} \right) \equiv \varrho^{\mathrm{lead}} + \varrho^{\mathrm{corr}}(s,u;\mathbf{x}_0) \end{aligned} \tag{4.29}$$

This ergodic approximation yielding a uniform density is justified for the following reason. In the semiclassical limit only small action differences $|S| = S_{\mathrm{cl}}\,|u\,s| \sim \hbar$ are relevant or correspondingly $s, u \sim \sqrt{\hbar/S_{\mathrm{cl}}}$. Since the constants $c^{s,u}(\mathbf{x})$ introduced in the definition for $\Delta t^{s,u}$, Eq. (4.5), are based only on classical quantities they do not scale with $\hbar$ when performing the limit $\hbar \to 0$. Therefore these constants are large compared to quantum mechanical scales, i.e. $c^{s,u}(\mathbf{x}) \gg \sqrt{\hbar/S_{\mathrm{cl}}} \sim s, u$. This implies large times $\lambda\,\Delta t^{s,u} \gg 1$ and thus one can apply the long-time limit $c^u = |u(\Delta t^u)| \approx |u(0)| \exp(\lambda\,\Delta t^u)$ which follows from the equations of motion (2.18) and the definition of the Lyapunov exponent (2.7). Therefore, the points $\mathbf{x}_t$ and $\mathcal{T}\mathbf{x}_{t+t_{\mathrm{loop}}}$ are basically uncorrelated. Hence one can assume the density to be uniform and given by $S_{\mathrm{cl}}/\Omega(E)$ where the factor S_{cl} is due to the coordinate transformation $(s,u) \to (\delta q^\perp, \delta p^\perp)$ in Eq. (4.29). The prefactor $T - 2t_{en}$ stems from the fact that parts of the orbit have to be excluded as they cannot yield a partner orbit. The density $\varrho(s,u;\mathbf{x})$ can thus be written as a sum of two terms ϱ^{lead} and ϱ^{corr}. The first contribution ϱ^{lead} represents the leading ergodic properties of the system. The second

term ϱ^{corr} is a small correction due to the deterministic character of the motion of the particle. It depends not only on the coordinates s and u in the POINCARÉ surface of section but also on the position $\mathbf{x}$ in phase space. If the result (4.29) is inserted in the expression (4.28) for the density of partners per action difference one immediately realizes that $\langle \mathrm{d}N/\mathrm{d}S\rangle_\gamma$ is indeed independent of the specific value assigned to u^c.

However, in order to actually compute the time integral in Eq. (4.28) one still needs to find the asymptotic expression for $t_{en}(s,u;\mathbf{x})$, Eq. (4.6). Using a similar argument for Δt^s as the one given above for Δt^u we find for the length $t_{en}(s,u;\mathbf{x})$ of an 'encounter region' the following asymptotic result

$$\lambda\, t_{en}(s,u;\mathbf{x}) \approx \ln\left[\frac{c^u(\mathbf{x})\, c^s(\mathbf{x})}{|u|\ |s|}\right] = \ln\left[c^u(\mathbf{x})\, c^s(\mathbf{x})\frac{S_{\mathrm{cl}}}{|S|}\right] = \lambda\, t_{en}(S;\mathbf{x}) \tag{4.30}$$

in the limit of small action differences $S \sim \hbar$, see Eq. (4.18). This result is consistent with the requirement that the length $t_{en}(s,u,\mathbf{x})$ of a given 'encounter region' is constant within this region. It does not depend on s or u separately but only on their product $s\,u$ as this quantity is a constant of motion. Furthermore, Eq. (4.30) implies a weak dependence of $t_{en}(s,u;\mathbf{x})$ on the actual position $\mathbf{x}$ in phase space if the limit $S \sim \hbar \to 0$ is considered. The reason is that $c^{s,u}(\mathbf{x})$ are defined on a purely classical basis independently of the semiclassical limit. As we will show in Section 5.1 it is not even of crucial importance to explicitly calculate the asymptotic form of t_{en} as in Eq. (4.30). However, the approach chosen in this chapter is the most straightforward extension of the configuration-space approach towards a phase-space formulation. It also makes clear that time scales on the order of the EHRENFEST time[2] T_E must not be neglected although they are much smaller than the orbits lengths given by the HEISENBERG time T_H, i.e. $t_{en} \sim T_E \ll T_H \sim T_\gamma$.

The asymptotic expression (4.30) for the time t_{en} together with result (4.29) for the density $\varrho(s,u;\mathbf{x})$ allows for a determination of the density of partner orbits per action difference (4.28) as follows:

$$\left\langle \frac{\mathrm{d}N_\gamma(S,T)}{\mathrm{d}S}\right\rangle_{\gamma,T} = \left\langle \frac{\mathrm{d}N_\gamma^{\mathrm{lead}}(S,T)}{\mathrm{d}S}\right\rangle_{\gamma,T} + \left\langle \frac{\mathrm{d}N_\gamma^{\mathrm{corr}}(S,T)}{\mathrm{d}S}\right\rangle_{\gamma,T} \tag{4.31}$$

where

$$\left\langle \frac{\mathrm{d}N_\gamma^{\mathrm{lead}}(S,T)}{\mathrm{d}S}\right\rangle_{\gamma,T} = \frac{2T}{\Omega(E)}\int_0^T \mathrm{d}t\, \chi(\mathbf{x}_t) \simeq \frac{2\lambda T^2}{\Omega(E)} \tag{4.32}$$

[2]The EHRENFEST time T_E is given by the time it takes for two trajectories with an initial distance $\sim 1/k_F$ to separate so that the final distance is of the order of the system size l, i.e. $T_E \sim \lambda^{-1}\ln k_F l$. Here, λ denotes the LYAPUNOV exponent and k_F is the FERMI wave number.

and

$$\left\langle \frac{\mathrm{d}N_\gamma^{\mathrm{corr}}(S,T)}{\mathrm{d}S} \right\rangle_{\gamma,T} = \frac{4}{\Omega(E)} \int_0^T \mathrm{d}t\, \frac{\chi(\mathbf{x}_t)}{\lambda} \left(\ln \frac{|S|}{S_{\mathrm{cl}}} - \ln c^s(\mathbf{x}_t) c^u(\mathbf{x}_t) \right) \simeq \frac{4T}{\Omega(E)} \ln \frac{|S|}{S_{\mathrm{cl}}} \,. \tag{4.33}$$

The first contribution (4.32) is the dominating one ($\sim \hbar^{-2}$) and describes the ergodic properties of the system. It is corrected by (4.33) involving the logarithm of $|S|$ which is due to the underlying dynamics. This logarithmic correction is therefore of the order of $\sim \hbar^{-1} \ln \hbar$. We neglected all smaller terms $\sim \hbar^{-1}$ in Eqs. (4.32) and (4.33). In principle one could argue that only the first term (4.32) is relevant in the semiclassical limit. However, as we show in the next paragraph, this term does not contribute to the spectral form factor $K^{(2)}(\tau)$. Therefore, one has to keep the small correction (4.33). This set of Eqs. (4.31 - 4.33) is the first major result of this section. It provides the phase-space generalization of the crossing angle distribution $P(\varepsilon, T)$, Eq. (2.56).

In the last step we now determine the contribution of $\langle \mathrm{d}N_\gamma/\mathrm{d}S \rangle_{\gamma,T}$ to the spectral form factor (4.25). Inserting only the first term (4.32) into Eq. (4.25) while neglecting the correction (4.33) gives

$$K^{(2,\mathrm{lead})}(\tau) = \tau^2 \frac{2\lambda T}{\pi} \left\langle \sin \frac{S_{\max}(E)}{\hbar} \right\rangle_{\Delta E} = 0 \,. \tag{4.34}$$

Thus the leading term in the density of partners per action difference yields a vanishing contribution to the spectral form factor. This is due to the energy average performed with respect to the rapidly oscillating sine function which suppresses the prefactor. This prefactor is of the order of $\hbar^{-1}$ and would give a non-universal contribution to the spectral form factor $K(\tau)$ as it contains the LYAPUNOV exponent of the system. However, because of the vanishing contribution (4.34) of the leading order term in $\langle \mathrm{d}N_\gamma/\mathrm{d}S \rangle_\gamma$ one has to evaluate the correction due to (4.33) as well since it turns out that its contribution remains finite for $\hbar \to 0$. The final result for the form factor thus reads

$$\begin{aligned} K^{(2)}(\tau) &= K^{(2,\,\mathrm{lead})}(\tau) + K^{(2,\,\mathrm{corr})}(\tau) \\ &= 0 \;-\; 8\tau^2 \left\langle \frac{\hbar T_H}{\Omega(E)} \int_0^{\frac{S_{\max}(E)}{\hbar}} \mathrm{d}x\, \frac{\sin x}{x} \right\rangle_{\Delta E} = -2\tau^2 \end{aligned} \tag{4.35}$$

in the limit $\hbar \to 0$. It is important to note that the contribution from the correction (4.33) to the form factor does not vanish in the semiclassical limit although $\langle \mathrm{d}N_\gamma^{\mathrm{lead}}/\mathrm{d}S \rangle_\gamma \gg \langle \mathrm{d}N_\gamma^{\mathrm{corr}}/\mathrm{d}S \rangle_\gamma$. This shows that one has to carefully perform the $\hbar \to 0$ limit.

In this chapter we have shown that the method of evaluating off-diagonal terms in the semiclassical spectral form factor (2.38) proposed in [SR01, Sie02] can be

extended to non-uniformly hyperbolic systems. To this end we developed a new approach based on phase-space concepts. We showed that the relevant objects which allow to find the orbit pairs (γ, γ^p) are 'encounter regions' in phase space rather than crossings in configuration space. These 'encounter regions' are characterized by a small distance $\delta\vec{y}$ between a periodic orbit γ and its time-reversed version γ^i. We determined the geometry, Eq. (4.11), and the action of the partner orbit γ^p with respect to the original orbit γ, Eq. (4.18), in terms of local phase space properties. Finally we showed that the crossing angle distribution has to be replaced by a density of partners per action difference, Eq. (4.31). Combining all these results we were able to evaluate the off-diagonal terms in the double sum of periodic orbits in the spectral form factor, Eq. (4.35). It turns out that the result coincides with the τ^2 order appearing in the universal random-matrix theory prediction (2.28). In order to find this result one has to include dynamical properties of the system. This means for example that one must not neglect the fact that two close trajectories stay close to each other for a certain time. This is due to the deterministic equations of motion underlying the system dynamics. In the next chapter we will study some extensions and applications of this new approach.

CHAPTER 5

Extensions and applications of the phase-space approach

In this chapter, we first demonstrate how the phase-space approach for the semiclassical calculation of the spectral form factor $K(\tau)$ in two-dimensional systems can be extended to higher-dimensional systems. We show that all the different time scales given by the whole set of LYAPUNOV exponents do not affect the final result for the spectral form factor which again coincides with the universal random-matrix theory prediction. Furthermore we study the transition from a system with strict time-reversal symmetry towards a system where this symmetry is broken. This corresponds to the GUE – GOE transition in random-matrix theory. Finally we apply our technique to investigate matrix element fluctuations. We derive a relation between the *spectral* form factor and the *generalized* form factor and evaluate the semiclassical approximation.

5.1 Higher-dimensional systems

In this section we extend the proposed technique for evaluating off-diagonal contributions of the spectral form factor $K(\tau)$ to systems with $f \geq 2$ degrees of freedom [TSMR04]. Since the determination of the partner geometry for $f = 2$, as described in Section 4.1, and the evaluation of the action difference S_{γ,γ^p}, see Section 4.2, was already formulated in a rather general framework we just briefly summarize the

corresponding results for $f > 2$. The main focus will be on the statistics of the number of partner orbits. As we showed in Section 4.4, the number of partners in the case $f = 2$ is determined by the phase-space flow, i.e. the local growth rate $\chi(\mathbf{x})$, see Eq. (4.28). In systems with more than two degrees of freedom the POINCARÉ surface of section is a $2f-2$ dimensional hypersurface in the $2f$ dimensional phase space. Hence, according to Eq. (2.8), there are $f-1$ fluctuating local growth rates $\{\chi_i(\mathbf{x})\}$. Their phase-space average yields a set of $f-1$ LYAPUNOV exponents $\{\lambda_i\}$. However, we prove that all these different time scales exactly cancel and thus do not appear in the final result for $K(\tau)$. In this context it is important to realize that a direct extension of the original configuration-space approach based on crossings, see Section 2.5, to systems with more than two degrees of freedom is not possible.

Before we present the extension of the phase space approach to the case $f > 2$ let us make a few remarks concerning semiclassical approximations in systems with more than two degrees of freedom. Traditionally, it has been believed that GUTZWILLER's trace formula is a good approximation for the density of states in systems with $f = 2$ only. The reason is that the mean density of states $\bar{d}(E) = (2\pi\hbar)^{-f}\Omega(E)$ increases like $\sim \hbar^{-f}$ in the semiclassical limit. On the other hand, GUTZWILLER argued that the errors for the semiclassical approximations leading to the trace formula are $\sim \hbar^2$ [Gut90]. Therefore one would expect that $f = 2$ represents an upper critical dimension for the applicability of the trace formula. This issue is thoroughly discussed in [PS98, PS00]. It is shown that the traditional argument mentioned above is too simple and that the semiclassical accuracy measured in units of the mean level spacing depends only weakly on the dimensionality f. More specifically it was argued that the traditional error estimate $\sim \hbar^{2-f}$ has to be replaced (in a 'pessimistic' version, [PS98]) by a *maximum* error bound $\sim \ln\hbar$ which is independent of f. These theoretical arguments were substantiated by numerical studies on the three dimensional SINAI billiard in [Pri95, PS98, PS00]. Further numerical studies on a three dimensional billiard are presented in [Pro97]. The spectral statistics was shown to follow random-matrix theory with small deviations.

In the following we give a semiclassical derivation of the spectral form factor, Eq. (2.38) with $A_\gamma = B_\gamma = 1$, on the grounds of GUTZWILLER's trace formula for $f \geq 2$. In order to go beyond the diagonal approximation one has — in analogy to the case $f = 2$ — to identify orbit pairs which are characterized by a small action difference on the order of $\hbar$. Such an orbit pair (γ, γ^p) can be found if a periodic orbit γ comes close to its time-reversed version γ^i at a certain point $\mathbf{x}^\gamma_{t_1}$ in phase space, see Section 4.1. The distance between γ and γ^i can be quantified by the small vector $\delta\vec{y}$. This vector lies in the $2f-2$ dimensional POINCARÉ surface of section defined by the perpendicular coordinates $(\delta\mathbf{q}^\perp, \delta\mathbf{p}^\perp)$ at $\mathbf{x}^\gamma_{t_1}$. It points from $\mathbf{x}^\gamma_{t_1}$ to $\mathcal{T}\mathbf{x}^\gamma_{t_2}$ and is formally given by Eq. (4.3) independently of the dimensionality f. As described in Section 2.1 this vector can be decomposed into its stable and unstable

components

$$\delta\vec{y}(\mathbf{x}^{\gamma}_{t_1}, t_{\rm loop}) = \sum_{i=1}^{f-1} s_i(\mathbf{x}^{\gamma}_{t_1}, t_{\rm loop})\, \vec{e}^{\,s}_i(\mathbf{x}^{\gamma}_{t_1}) \;+\; u_i(\mathbf{x}^{\gamma}_{t_1}, t_{\rm loop})\, \vec{e}^{\,u}_i(\mathbf{x}^{\gamma}_{t_1}) \tag{5.1}$$

where $t_{\rm loop} \equiv t_2 - t_1$. Relation (5.1) replaces Eq. (4.4). The coefficients s_i can be calculated explicitly using

$$s_i = \frac{\det\left(\vec{e}^{\,s}_1, \ldots, \vec{e}^{\,s}_{i-1}, \delta\vec{y}, \vec{e}^{\,s}_{i+1}, \ldots, \vec{e}^{\,s}_{f-1}, \vec{e}^{\,u}_1, \ldots, \vec{e}^{\,u}_{f-1}\right)}{\det\left(\vec{e}^{\,s}_1, \ldots, \vec{e}^{\,s}_{f-1}, \vec{e}^{\,u}_1, \ldots, \vec{e}^{\,u}_{f-1}\right)} \tag{5.2}$$

and similarly for u_i.

We say that the vector $\delta\vec{y}$ is small if its components $\{s_i, u_i\}$ are small, i.e. $s_i, u_i \ll 1$. If one moves from $\mathbf{x}^{\gamma}_{t_1}$ to $\mathbf{x}^{\gamma}_{t_1+\Delta t}$ along the orbit γ, this displacement vector changes to $\delta\vec{y}_{\Delta t}(\mathbf{x}^{\gamma}_{t_1}, t_{\rm loop}) = \delta\vec{y}(\mathbf{x}^{\gamma}_{t_1+\Delta t}, t_{\rm loop} - 2\Delta t)$. For a short enough time Δt all the components $s_i(\Delta t; \delta\vec{y}_0, \mathbf{x}_{t_1})$ and $u_i(\Delta t; \delta\vec{y}_0, \mathbf{x}_{t_1})$ remain small since it takes a certain time until the orbits γ and γ^i have deviated from each other again. This is a consequence of the deterministic dynamics of the system and makes clear that two orbits being close in phase space is not a local property. In analogy to the two-dimensional systems we therefore define the 'encounter region' as the set of all points $\mathbf{x}^{\gamma}_{t_1+\Delta t}$ such that each stable and unstable component of the displacement vector $\delta\vec{y}_{\Delta t}(\mathbf{x}^{\gamma}_{t_1}, t_{\rm loop})$ is smaller than a certain threshold value $c^s_i \lesssim 1$ and $c^u_i \lesssim 1$, respectively, see Fig. 5.1(b). These values $\{c^s_i, c^u_i\}$ are chosen in a way that the displacement vectors $\delta\vec{y}_{\Delta t}(\mathbf{x}^{\gamma}_{t_1}, t_{\rm loop})$ are given by the linearized equations of motion $\delta\vec{y}_{\Delta t}(\mathbf{x}^{\gamma}_{t_1}, t_{\rm loop}) \simeq M(\Delta t, \mathbf{x}^{\gamma}_{t_1})\, \delta\vec{y}(\mathbf{x}^{\gamma}_{t_1}, t_{\rm loop})$ as long as $\mathbf{x}^{\gamma}_{t_1+\Delta t}$ stays within the 'encounter region', while the linear approximation breaks down outside of it. Therefore, the numbers $\{c^s_i, c^u_i\}$ are purely classically defined quantities which characterize the breakdown of the linear approximation applied to the displacement vector $\delta\vec{y}$. As explained in Section 4.1 the values of $\{c^s_i, c^u_i\}$ can weakly depend on the position $\mathbf{x}$ in phase space or the displacement vector $\delta\vec{y}$ itself, but this dependence does not affect the final result for the spectral form factor in the semiclassical limit.

From the definition of the 'encounter region' one concludes that the range of values for Δt such that $\mathbf{x}^{\gamma}_{\Delta t}$ lies within an 'encounter region' is given by $-\Delta t^s \leq \Delta t \leq \Delta t^u$, where the times $\Delta t^{s,u}$ are defined by the implicit equations

$$\begin{aligned} \Delta t^s &= \min_{i=1,\ldots,(f-1)} \{\Delta t_i : |s_i(-\Delta t_i; \delta\vec{y}_0, \mathbf{x})| = c^s_i\} \quad \text{and} \\ \Delta t^u &= \min_{i=1,\ldots,(f-1)} \{\Delta t_i : |u_i(\Delta t_i; \delta\vec{y}_0, \mathbf{x})| = c^u_i\} \ . \end{aligned} \tag{5.3}$$

This means that $\Delta t^{s,u}$ are such that the displacement $\delta\vec{y}_{\Delta t^{s,u}}$ is just about to leave the hypercuboid

$$\mathcal{V} = \{(s_i, u_i) : |s_i| \leq c^s_i, |u_i| \leq c^u_i\} \tag{5.4}$$

that defines the 'encounter region'. The implicit Eqs. (5.3) replace the Eqs. (4.5) obtained in the case $f = 2$. They determine the times $\Delta t^s = \Delta t^s(\{s_i, u_i\}; \mathbf{x})$ and $\Delta t^u = \Delta t^u(\{s_i, u_i\}; \mathbf{x})$ as functions of all the components $\{s_i, u_i\}$ of the vector $\delta\vec{y}$ and the point $\mathbf{x}$ in phase space. The time duration of the encounter region

$$t_{\rm en}(\{s_i, u_i\}; \mathbf{x}) = \Delta t^u(\{s_i, u_i\}; \mathbf{x}) + \Delta t^s(\{s_i, u_i\}; \mathbf{x}) \tag{5.5}$$

is thus a classical object defined locally in phase space. It depends on the components $\{s_i, u_i\}$ of $\delta\vec{y}$ and is clearly invariant within a given 'encounter region'.

A partner orbit γ^p can be assigned to each 'encounter region' which arise if the time-reversed orbit γ^i comes close to γ itself. Equivalently to the $f = 2$ case its qualitative geometry is given by Eq. (4.7), see also Fig. 4.1(b). Quantitatively one can find the geometry of γ^p by solving the linearized equations of motion (4.8). The structure of these equations is formally independent of the dimensionality f. The partner orbit γ^p is then given by the $2f-2$ dimensional vectors $\delta\vec{x}$ that describe the deviations of γ^p from the orbits γ and γ^i. For a system with f degrees of freedom the matrices R, L^i and F are $2f-2$ dimensional. The general result (4.9) can be further simplified if the corresponding loop times $t_{\rm loop}$ and $T - t_{\rm loop}$ are large. For a system with f degrees of freedom one finds the solution

$$\begin{aligned}
\delta\vec{x}_{R,i} &= \delta\vec{y}^{\,s} = \sum_{i=1}^{f-1} s_i\, \vec{e}_i^{\,s}(\mathbf{x}^\gamma_{t_1}) & \delta\vec{x}_{R,e} &= \sum_{i=1}^{f-1} s_i\, \vec{e}_i^{\,u}(\mathbf{x}^\gamma_{t_2}) \\
\delta\vec{x}_{L^i,i} &= -\sum_{i=1}^{f-1} u_i\, \vec{e}_i^{\,s}(\mathbf{x}^\gamma_{t_2}) & \delta\vec{x}_{L^i,e} &= -\delta\vec{y}^{\,u} = -\sum_{i=1}^{f-1} u_i\, \vec{e}_i^{\,u}(\mathbf{x}^\gamma_{t_1})
\end{aligned} \tag{5.6}$$

in terms of the components of the displacement vector $\delta\vec{y} = \delta\vec{y}^{\,s} + \delta\vec{y}^{\,u}$. The Eqs. (5.6) provide the necessary extension of Eqs. (4.11) for an arbitrary number of degrees of freedom f. As we argued in some detail in Section 4.1 the solution (5.6) is not valid for vectors $\delta\vec{y}(\mathbf{x}^\gamma_{t_1}, t_{\rm loop})$ with $t_{\rm loop}$ being smaller than $2\Delta t^u(\{s_i, u_i\}; \mathbf{x})$ or $T - t_{\rm loop}$ being smaller than $2\Delta t^s(\{s_i, u_i\}; \mathbf{x})$, respectively. In this case of short loop times the solution (5.6) has to be replaced by $\delta\vec{x}_{R,i} = \delta\vec{y}$, $\delta\vec{x}_{R,e} = F\delta\vec{y}$, $\delta\vec{x}_{L^i,i} = 0$ and $\delta\vec{x}_{L^i,e} = 0$ yielding just the time-reversed orbit γ^i instead of a separate partner orbit γ^p.

For the evaluation of the semiclassical expression (2.38) for the form factor one needs the action difference S_{γ,γ^p} for the orbit pair (γ, γ^p) characterized by Eqs. (5.6). As we did not restrict the derivation of the action difference in Section 4.2 to two-dimensional systems the result (4.17) is also valid for $f > 2$. Together with Eqs. (5.6) we thus find

$$S_{\gamma,\gamma^p} \equiv S_\gamma - S_{\gamma^p} = S(\delta\vec{y}) = (\delta\vec{y}^{\,u})^T\, \Sigma\, \delta\vec{y}^{\,s} = \sum_{j=1}^{f-1} S_{\rm cl}\, s_j\, u_j \equiv \sum_{j=1}^{f-1} S_j \tag{5.7}$$

which is the necessary extension of Eq. (4.18). As in the special case $f = 2$ we again find that the result (5.7) is invariant under a small displacement of $\delta\vec{y}$ within a given 'encounter region' because of the conservation of the symplectic product under the dynamics. Since only small action differences $S_{\gamma,\gamma^p} \sim \hbar$ contribute significantly to the semiclassical form factor (2.38) the restriction of the considerations above to small components $|s_i|, |u_i| \sim \sqrt{\hbar/S_{\mathrm{cl}}} \ll 1$ is justified.

Besides the action difference S_{γ,γ^p} which enters the semiclassical form factor (2.38) there are also the weights w_γ and w_{γ^p} that include for example the MASLOV indices μ_γ and μ_{γ^p}, respectively. These weights are equal for an orbit pair (γ, γ^p) if small corrections of first order in u_i and s_i are neglected, i.e. $w_\gamma = w_{\gamma^p} + \mathcal{O}(\{s_i, u_i\})$. The proof follows the same lines as for two-dimensional systems, see Section 4.3. We apply relation (4.19) to the functions $f(\mathbf{x}) = 1$ and $f(\mathbf{x}) = \chi_i(\mathbf{x})$ yielding $T_\gamma \simeq T_{\gamma^p}$ and $\lambda_i^\gamma \simeq \lambda_i^{\gamma^p}$, respectively. Since the association of the MASLOV index with a winding number is independent of the number of degrees of freedom f [Rob91] one further finds $\mu_\gamma = \mu_{\gamma^p}$. As the weight w_γ is uniquely determined by the length of the orbit T_γ, its LYAPUNOV exponents $\{\lambda_i^\gamma\}$ and the MASLOV index μ_γ one can conclude that $w_\gamma \simeq w_{\gamma^p}$. In the spirit of a stationary-phase approximation we therefore keep only the action difference S_{γ,γ^p} in the phase while neglecting small differences in the pre-exponential factors in (2.38).

In the following we show how the described partner orbits γ^p determine the next-to-leading order result for the spectral form factor in systems with more than two degrees of freedom. We assume that the dominant terms beyond the diagonal approximation in Eq. (2.38) are due to the systematic action correlations of the orbit pairs (γ, γ^p) specified above. Thus the double sum over periodic orbits can be formulated as a single sum over orbits γ and a sum over all the partners γ^p for each orbit while all other terms are neglected. All partners γ^p of a given orbit γ are then characterized by the set of action differences $\{S_j\}$ defined in Eq. (5.7). These are the appropriate parameters to categorize the partner orbits as the $\{S_j\}$ depend only on the orbit pair (γ, γ^p) but not on the position within the 'encounter region' used to identify the orbit pair. Therefore, expression (2.38) can be rewritten as

$$K^{(2)}(\tau) = \tau \left\langle \int_{-S_{\max}^{(j)}(E)}^{S_{\max}^{(j)}(E)} \mathrm{d}S_1 \ldots \mathrm{d}S_{f-1} \left\langle \frac{\mathrm{d}^{f-1} N_\gamma(\{S_j\})}{\mathrm{d}S_1 \ldots \mathrm{d}S_{f-1}} \right\rangle_{\gamma, \tau T_H} \exp\left(\mathrm{i} \sum_{j=1}^{f-1} \frac{S_j}{\hbar} \right) \right\rangle_{\Delta E} \tag{5.8}$$

which yields Eq. (4.25) in the special case $f = 2$. The density of partners γ^p for a given orbit γ with respect to the set of action differences $\{S_j\}$ is denoted by $\mathrm{d}^{f-1} N_\gamma(\{S_j\})/\mathrm{d}S_1 \ldots \mathrm{d}S_{f-1}$. This quantity is the crucial ingredient and we will show how it can be calculated in systems with an arbitrary number of degrees of freedom. In contrast to the two-dimensional systems with $f = 2$ the derivation is significantly more involved because of the higher number of stable and unstable

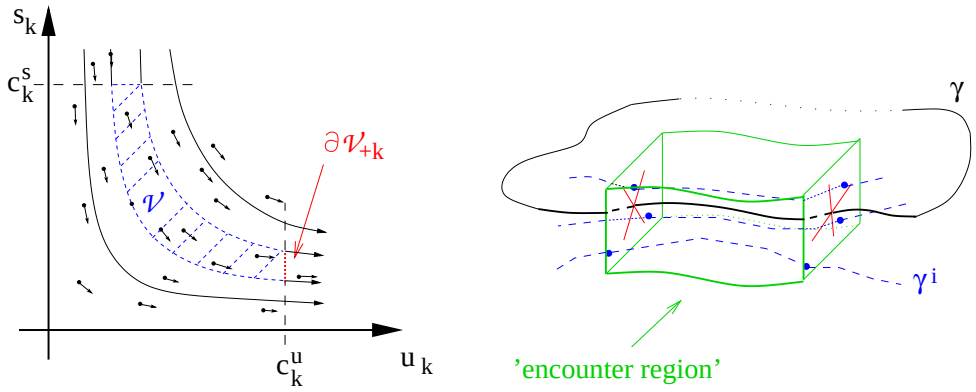

(a) 'Encounter region' in PSS (b) 'Encounter region' in phase space

Figure 5.1: (a) *Schematic drawing of a projection of the* Poincaré *surface of section (PSS). The flow of intersection points (black filled circles) is represented by the thin arrows. There are two ways to count the intersection points. Either the flux through the* $u_k = c_k^u$ *surface* $\partial\mathcal{V}_{+k}$ *(dotted line) is considered, as in Eq. (5.10), or one counts the number of points in the volume* $\mathcal{V}$ *of the 'encounter region' (dashed area) normalized by the time each point spends in it, as in Eq. (5.11). In subfigure* (b) *we show a sketch of the 'encounter region' in phase space corresponding to the lowest of the three pieces of* γ^i *(dashed lines).*

manifolds and Lyapunov exponents.

The basic idea is once more that one considers the dynamics within the Poincaré surface of section defined by the coordinates perpendicular to the flow, see Fig. 5.1(a), as its position is shifted following the phase space flow along the orbit γ, see Fig. 4.6. In order to count how many partner orbits exist with a given set of action differences $\{S_j\}$ one has to determine the flux of intersection points $\delta\vec{y}$ through the surface of the hypercuboid $\mathcal{V}$. According to Eq. (5.4) the k-th part of the total surface of the hypercuboid is defined by the set of points

$$\partial\mathcal{V}_{\pm k} = \{s_i, u_i : |s_i| < c_i^s; u_k = \pm c_k^u; |u_{i\neq k}| < c_i^u\} \quad \text{and} \quad \partial\mathcal{V} = \bigcup_{k=1}^{f-1} (\partial\mathcal{V}_{+k} \cup \partial\mathcal{V}_{-k}) \ . \tag{5.9}$$

This defines a $2f-3$ dimensional hypersurface $\partial\mathcal{V}$ in the $2f-2$ dimensional Poincaré surface of section. If the Poincaré surface of section is moved along $\mathbf{x}_t^\gamma$ with $0 < t < T_\gamma$ each intersection point of γ^i with this Poincaré surface of section is counted exactly once if one measures the flux through the hypersurface $\partial\mathcal{V}$ at the

end of the 'encounter region', see Fig. 5.1(a). This can be expressed as

$$\frac{\mathrm{d}^{f-1}N_\gamma(\{S_j\})}{\mathrm{d}S_1\ldots\mathrm{d}S_{f-1}} = 2\int_0^{T_\gamma}\mathrm{d}t\sum_{k=1}^{f-1}\int_{\{-c_i^{s,u}\}}^{\{c_i^{s,u}\}}\mathrm{d}^{f-1}s_i\,\mathrm{d}^{f-1}u_i\,\delta(u_k-c_k^u)\,\varrho(\{s_i,u_i\};\mathbf{x}_t^\gamma)\,\times \dot{u}_k(\{s_i,u_i\};\mathbf{x}_t^\gamma)\,\left(\prod_{j=1}^{f-1}\delta(S_{cl}s_ju_j-S_j)\right). \quad (5.10)$$

Here, the integration $\int \mathrm{d}u_k\delta(u_k-c_k^u)$ is just inserted for formal reasons to fix the kth component u_k as to integrate only over the kth part $\partial\mathcal{V}_{+k}$ of the hypersurface enclosing the 'encounter region'. The limits of the integrations over $\{s_i,u_i\}$ are given by the corresponding constants $\{c_i^s,c_i^u\}$ according to Eq. (5.9). The velocity of the flow perpendicular to the kth hypersurface is just given by Eq. (2.18), i.e. $\dot{u}_k(\{s_i,u_i\};\mathbf{x}_t^\gamma) = \chi_k(\mathbf{x}_t^\gamma)\,u_k$, and thus depends on u_k and on the position $\mathbf{x}_t^\gamma$ in phase space via the local growth rate $\chi_k(\mathbf{x})$ only. The density $\varrho(\{s_i,u_i\};\mathbf{x}_t^\gamma)$ entering Eq. (5.10) is the density of valid intersection points within the POINCARÉ surface of section, each corresponding to a partner orbit. The flux of intersection points $\delta\vec{y}(\mathbf{x}_{t_1}^\gamma,t_{\mathrm{loop}})$ through the surface $\partial\mathcal{V}_k$ of the hypercuboid $\mathcal{V}$ is therefore given by $\varrho(\{s_i,u_i\};\mathbf{x}_t^\gamma)\,\dot{u}_k(\{s_i,u_i\};\mathbf{x}_t^\gamma)$. In Eq. (5.10) only the $u_k=+c_k^u$ hypersurface $\partial\mathcal{V}_{+k}$ is considered while the $u_k=-c_k^u$ hypersurface $\partial\mathcal{V}_{-k}$ is accounted for by a factor of two. The multiple product of δ-functions restricts the actions to the values $\{S_j\}$. The expression (5.10) can be understood as a surface integral over $\partial\mathcal{V}$ and it reproduces Eq. (4.26) in the case $f=2$ where $\partial\mathcal{V}$ is just a line, see Fig. 5.1(a).

Before explicitly calculating the density of partners per action difference we first given an alternative version of Eq. (5.10). Using the fact that the number of points in phase space is conserved we transform the integrals over the hypersurface $\partial\mathcal{V}$ in Eq. (5.10) into an integration over the entire volume of the hypercuboid $\mathcal{V}$, see Fig. 5.1(a). This transformation actually links the approach outlined in Section 4.4 to the method used in [HMBH03]. The density of partners (5.10) with respect to the action differences $\{S_j\}$ can thus be rewritten as

$$\frac{\mathrm{d}^{f-1}N_\gamma(\{S_j\})}{\mathrm{d}S_1\ldots\mathrm{d}S_{f-1}} = \int_0^{T_\gamma}\mathrm{d}t\int_{\{-c_i^{s,u}\}}^{\{c_i^{s,u}\}}\mathrm{d}^{f-1}s_i\,\mathrm{d}^{f-1}u_i\,\frac{\varrho(\{s_i,u_i\};\mathbf{x}_t^\gamma)}{t_{en}(\{s_i,u_i\};\mathbf{x}_t^\gamma)}\left(\prod_{j=1}^{f-1}\delta(S_{cl}s_ju_j-S_j)\right). \quad (5.11)$$

Here, every intersection point is counted as long as it remains within the hypercuboid defined by the 'encounter region'. Therefore, one has to include the additional factor of $1/t_{en}$ which per definition (5.3) and (5.5) is the time each single intersection point spends within the 'encounter region'. Since all the intersection points that are in the 'encounter region' leave this region through the hypersurface $\partial\mathcal{V}$ used in Eq. (5.10) the volume integral in Eq. (5.11) does indeed give the number of intersection points

for given $\{S_j\}$. In contrast to Eq. (5.10) the second expression (5.11) is a volume integral over the total hypercuboid $\mathcal{V}$.

We prove the equality between (5.10) and (5.11) in more detail in Appendix A. The reason for introducing the two different expressions (5.10) and (5.11) is mainly a technical one. We apply either (5.10) or (5.11) depending on which one can be calculated easier. It turns out that this allows for a great simplification of the derivations to follow.

For the further evaluation of Eqs. (5.10) and (5.11) we first calculate the ergodic result for the density $\varrho(\{s_i, u_i\}; \mathbf{x})$ of intersection points in the POINCARÉ surface of section which represent the partner orbits. This density is defined for any point $\mathbf{x} = \mathbf{x}_0$ in phase space as

$$\varrho(\{s_i, u_i\}; \mathbf{x}) = \int_{2\Delta t^u}^{T_\gamma - 2\Delta t^s} \mathrm{d}t_{\mathrm{loop}} \prod_{i=1}^{f-1} \delta\left([\mathbf{x} - \mathcal{T}\mathbf{x}_{t_{\mathrm{loop}}}]_{u,i} - u_i\right) \delta\left([\mathbf{x} - \mathcal{T}\mathbf{x}_{t_{\mathrm{loop}}}]_{s,i} - s_i\right) \times \delta\left([\mathbf{x} - \mathcal{T}\mathbf{x}_{t_{\mathrm{loop}}}]_{\parallel}\right) \tag{5.12}$$

where the limits of the time integration are chosen such that the short loop lengths are excluded as they either do not occur at all or do not give partner orbits. As in the corresponding expression (4.27) the indices s, u in $[\mathbf{x}]_{s,u}$ denote the stable and unstable component of the perpendicular coordinates of $\mathbf{x}$, respectively.

To proceed we determine the weighted average over periodic orbits (2.41) of the number of partners (5.10) or (5.11) by applying the sum rule (2.42). This is the quantity which enters the spectral form factor (5.8). We find that the ergodic approximation to the density of intersection points (5.12) is determined by a leading contribution and a small correction. This ergodic approximation is justified for the following reasons. First, only small arguments $|s_i|, |u_i| \sim \sqrt{\hbar/S_{\mathrm{cl}}} \ll 1$ play a role in the semiclassical calculation of the form factor. Therefore, the cutoff-times $\Delta t^{u,s}$, Eq. (5.3), are large so that classical correlations between $\mathbf{x}_t$ and $\mathcal{T}\mathbf{x}_{t+t_{\mathrm{loop}}}$ can be neglected since $2\Delta t^u \leq t_{\mathrm{loop}} \leq T - 2\Delta t^s$. This means that the leading contribution to the density is uniform and can be expressed as $S_{\mathrm{cl}}^{f-1}/\Omega(E)$ times the length of the trajectory if long paths with $T \sim T_H \to \infty$ are considered. The factor S_{cl}^{f-1} comes from a coordinate transformation $(\{s_i, u_i\}) \to (\delta\mathbf{q}^\perp, \delta\mathbf{p}^\perp)$ in Eq. (5.12). As certain parts of the path are excluded in Eq. (5.12) the effective length entering the density yields a factor $T - 2t_{en}$. Hence, in the semiclassical limit $\varrho(\{s_i, u_i\}; \mathbf{x}_0)$ can be approximated by

$$\varrho(\{s_i, u_i\}; \mathbf{x}) = \varrho^{\mathrm{lead}} + \varrho^{\mathrm{corr}}(\{s_i, u_i\}; \mathbf{x}) \simeq S_{\mathrm{cl}}^{f-1} \left(\frac{T}{\Omega(E)} - \frac{2t_{en}(\{s_i, u_i\}; \mathbf{x})}{\Omega(E)} \right). \tag{5.13}$$

Except for the different prefactor S_{cl}^{f-1} this result has the same structure as the one obtained for $f = 2$, see Eq. (4.29).

If only the leading term of the density (5.13) is considered in the form factor (5.8) one finds that the result vanishes. This can be seen as follows. First we calculate the density of partners averaged over periodic orbits. In principle, one could either evaluate expression (5.10) or expression (5.11). However, as the leading term ϱ^{lead} does neither depend on the coordinates $\mathbf{x}$ nor on $\{s_i, u_i\}$ its contribution to the density of partners can be most easily calculated by means of (5.10). It yields

$$\left\langle \frac{\mathrm{d}^{f-1} N_\gamma^{\mathrm{lead}}(\{S_j\})}{\mathrm{d}S_1 \ldots \mathrm{d}S_{f-1}} \right\rangle_{\gamma, \tau T_H} \simeq 2^{f-1} \frac{\tau^2 T_H}{\Omega(E)} \sum_{k=1}^{f-1} \lambda_k T_H \prod_{j \neq k}^{f-1} \ln \frac{S_{cl} c_j^s c_j^u}{|S_j|} \,. \tag{5.14}$$

Here we used the fact that the time average of the local growth rate along an ergodic path can be obtained by the phase-space average $\langle \chi_k(\mathbf{x}) \rangle_{\mathbf{x}} = \lambda_k$. Setting $f = 2$ in Eq. (5.14) immediately reproduces the result (4.32) obtained in Section 4.4. If Eq. (5.14) is inserted in the form factor (5.8) one obtains $K^{(2,\mathrm{lead})}(\tau) = 0$ in the same manner as in Eq. (4.34). Therefore, one indeed has to include the small correction ϱ^{corr} given in Eq. (5.13) when evaluating the density of partners per action differences.

As we have shown, the leading term ϱ^{lead} does not contribute to the spectral form factor. Hence, we can restrict the following calculations to the contribution of ϱ^{corr}. However, it turns out that in this case it is technically favorable to use expression (5.11) instead of Eq. (5.10) for the density of partners. The reason is that the time $t_{\mathrm{en}}(\{s_i, u_i\}; \mathbf{x})$ depends in a subtle way on combinations of the $\{s_i, u_i\}$. This fact is a major difficulty when dealing with higher-dimensional systems ($f > 2$). Inserting ϱ^{corr} from Eq. (5.13) in Eq. (5.11) one finds

$$\left\langle \frac{\mathrm{d}^{f-1} N_\gamma^{\mathrm{corr}}(\{S_j\})}{\mathrm{d}S_1 \ldots \mathrm{d}S_{f-1}} \right\rangle_{\gamma, \tau T_H} \simeq -2^f \frac{\tau T_H}{\Omega(E)} \prod_{j=1}^{f-1} \ln \frac{S_{cl} c_j^s c_j^u}{|S_j|} \tag{5.15}$$

since the two appearances of t_{en} in Eqs. (5.11) and (5.13) mutually cancel. Again one can immediately check that the special case $f = 2$ as given in Eq. (4.33) is correctly reproduced.

The result (5.14) together with Eq. (5.15) gives the correct asymptotic form for the averaged density of partners, Eq. (5.10) or Eq. (5.11), in the semiclassical limit $\hbar \to 0$ where the relevant $\{S_j\}$ are small. In comparison to the leading part (5.14) the second contribution (5.15) is of the order of $\hbar^{f-1} \ln \hbar \ll 1$. Although only the sum of Eq. (5.14) and (5.15) enters in the calculation of the form factor (5.8) the smaller correction (5.15) must not be neglected. The reason for it lies in the fact that the ergodic part (5.14) gives a vanishing contribution to the form factor (5.8) because of the energy average. Therefore only the contribution Eq. (5.15) determines

the final result. It can be obtained by inserting Eq. (5.15) into (5.8) and yields

$$K^{(2)}(\tau) = -2\tau^2 \left\langle \frac{T_H}{\Omega(E)} \prod_{j=1}^{f-1} \left\{ -2 \int_{-S^{(j)}_{\max}(E)}^{S^{(j)}_{\max}(E)} \mathrm{d}S_j \, \exp\left(\mathrm{i}\frac{S_j}{\hbar}\right) \ln \frac{|S_j|}{S_{cl} c_j^s c_j^u} \right\} \right\rangle_{\Delta E} \simeq -2\tau^2 \,. \tag{5.16}$$

Hence we find for $f > 2$ the same contribution coming from the off-diagonal terms in the double sum over periodic orbits in Eq. (2.38) as for systems with two degrees of freedom.

In this section we have shown how to extend the approach presented in Chapter 4 to hyperbolic systems with an arbitrary number of degrees of freedom. We proved that the semiclassical evaluation of $K^{(2)}(\tau)$ gives the universal random-matrix theory result. Especially we demonstrated that no information about the set of LYAPUNOV exponents $\{\lambda_i\}$ or the constants $\{c_i^s, c_i^u\}$ defining the 'encounter region' enters the final result.

5.2 GOE – GUE transition

In this section we study the change in the energy level statistics if a small magnetic field $\mathbf{B}$ is applied so that the time-reversal symmetry is broken [TR03]. As we only want to outline the major mechanism we restrict the following considerations to the two-dimensional uniformly hyperbolic system. The intuitively most transparent derivation can be given within the framework of the configuration space approach summarized in Section 2.5. Let us furthermore assume that the applied magnetic field is weak, constant and perpendicular to the system. In this context, 'weak' has to be understood in a sense that the classical geometry of the orbits is only very slightly changed while the acquired additional phases due to the magnetic flux can be large compared to $\hbar$. Therefore we only consider the effect of the magnetic field with respect to a change in the exponential occurring in the spectral form factor (2.38) while the remaining pre-factors are treated as being unaffected by the $\mathbf{B}$-field. This again is in the spirit of a stationary phase approximation.

In the following paragraphs, we show that the semiclassical form factor can be written in the same manner as the result (2.30) of the parametric random-matrix theory. This allows for a physical interpretation of the transition parameter λ_{trans} in Eq. (2.30). The crossover between the universality classes as time-reversal symmetry is broken has been originally semiclassically obtained in [BGdAS95] within the diagonal approximation. Before we present a dynamical evaluation of this transition for the first off-diagonal correction we briefly summarize the necessary steps for the diagonal approximation. In this case only the orbit pairs (γ, γ) and (γ, γ^i) are included into the double sum over periodic orbits (2.38). The applied magnetic field induces no additional action difference for the pair (γ, γ) as these two orbits encircle

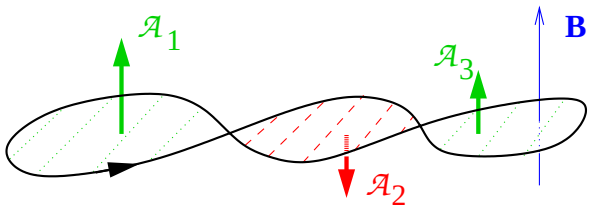

Figure 5.2: *Schematic drawing of a periodic orbit in configuration space that encloses three areas which are traversed with different orientations with respect to the direction of the magnetic field* $\mathbf{B}$*. Therefore, the total effective area is given by* $\mathcal{A}_\gamma = \mathcal{A}_1 - \mathcal{A}_2 + \mathcal{A}_3$*.*

the same area with the same orientation. However, for the other pair (γ, γ^i) an additional action difference S_{γ,γ^i} arises. Denoting the sum of oriented areas enclosed by γ as $\mathcal{A}_\gamma$, see Fig. 5.2, the action difference is given by

$$\frac{S_{\gamma,\gamma^i}}{\hbar} = \frac{S(\mathcal{A}_\gamma, \mathbf{B})}{\hbar} = \frac{2\pi\,\mathcal{A}_\gamma\,\mathbf{B}}{\varphi_0} \tag{5.17}$$

with the flux quantum $\varphi_0 = 2\pi\hbar/(2e)$. Hence, the diagonal approximation to the spectral form factor reads

$$K^{(1)}(\tau) = \tau \left\langle 1 + \exp\left[\mathrm{i}\frac{S_{\gamma,\gamma^i}}{\hbar}\right]\right\rangle_{\gamma,\tau T_H}, \tag{5.18}$$

where the first term in the sum corresponds to the pairs (γ, γ) and the second term to the pairs (γ, γ^i). The average over periodic orbits is calculated using the sum rule by replacing $\sum_\gamma \to \int \mathrm{d}T_\gamma \exp[\lambda T_\gamma]/T_\gamma$ and $|w_\gamma|^2 \to T_\gamma^2 \exp[-\lambda T_\gamma]$. As the action difference S_{γ,γ^i}, see Eq. (5.17), is proportional to the sum $\mathcal{A}$ of enclosed oriented areas the spectral form factor (5.18) depends on the distribution $P_A(\mathcal{A}, T)$ of these areas among all orbits of a given length $T = \tau T_H$. This distribution $P_A(\mathcal{A}, T)$ is approximately Gaussian [Ric00] and can thus be written as

$$P_A(\mathcal{A}, T) = (2\pi\beta T)^{-1/2} \exp\left[-\frac{\mathcal{A}^2}{2\beta T}\right] \tag{5.19}$$

with β being a system specific parameter.

In terms of this area distribution the relation (5.18) for the diagonal approximation can be reexpressed as

$$K^{(1)}(\tau) = \tau \left(1 + \frac{1}{\tau T_H} \int_0^{\tau T_H} \mathrm{d}T_\gamma\, T_\gamma\, \delta(\tau T_H - T_\gamma) \int_{-\infty}^{\infty} \mathrm{d}\mathcal{A}\, P_A(\mathcal{A}, T_\gamma) \exp\left[2\pi\mathrm{i}\frac{\mathcal{A}\mathbf{B}}{\varphi_0}\right]\right) \tag{5.20}$$

where we have included an additional integration over the oriented area $\mathcal{A}$. Evaluating this integral then directly leads to the result

$$K^{(1)}(\tau) = \tau \left(1 + \exp\left[-\frac{\tau T_H}{t_B}\right]\right) \tag{5.21}$$

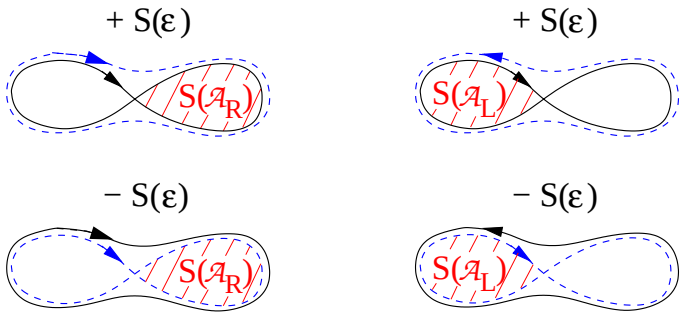

Figure 5.3: *The four different loop configurations that correspond to a single crossing are sketched. The orbit γ and its partner γ^p are represented by the solid and dashed line, respectively. The relative sign of the action difference $S(\varepsilon)$ is indicated for each configuration. As γ and γ^p traverse either loop $\mathcal{R}$ or loop $\mathcal{L}$ in opposite direction there is an additional phase determined by the enclosed areas $S(\mathcal{A}_R)$ or $S(\mathcal{A}_L)$.*

where $t_B \equiv \varphi_0^2/(2\pi^2\mathbf{B}^2\beta)$.

As a next step we apply the same procedure to the off-diagonal correction terms studied throughout this thesis. In the configuration space approach, see Section 2.5, these terms are associated with self-crossings that have a small crossing angle $\varepsilon \ll 1$. Therefore, the statistics of partner orbits γ^p is given by the statistics $P(\varepsilon, T)$ of crossing angles, see Eq. (2.55) and Eq. (3.1). The action difference due to the different geometries of γ and γ^p can also be related to the crossing angle ε, see Eq. (2.53). Additionally, we have to include the **B**-field induced action difference $S(\mathcal{A}_{(L,R)}, \mathbf{B}) = 2\pi\,\mathcal{A}_{(L,R)}\mathbf{B}/\varphi_0$ depending on which loop is traversed in what direction. The four possible cases are shown in Fig. 5.3. The off-diagonal contributions to the spectral form factor can then be written similarly to Eq. (2.54) as

$$K^{(2)}(\tau) = \frac{2|\mathbf{p}|^2}{\pi\, m^2 A}\,\tau\,\Re\int_0^\pi \mathrm{d}\varepsilon\,\sin\varepsilon\,\exp\left[\mathrm{i}\frac{S(\varepsilon)}{\hbar}\right]\int_{T_{\min}(\varepsilon)}^{T-T_{\min}(\varepsilon)} \mathrm{d}t_{\mathrm{loop}}\,(T - t_{\mathrm{loop}})\,\times$$
$$\left(\int_{-\infty}^{\infty}\mathrm{d}\mathcal{A}_R\,P_A\left(\mathcal{A}_R, t_{\mathrm{loop}} - T_{\min}(\varepsilon)\right)\exp\left[\mathrm{i}\frac{S(\mathcal{A}_R)}{\hbar}\right] + \right.$$
$$\left.\int_{-\infty}^{\infty}\mathrm{d}\mathcal{A}_L\,P_A\left(\mathcal{A}_L, T - t_{\mathrm{loop}} - T_{\min}(\varepsilon)\right)\exp\left[\mathrm{i}\frac{S(\mathcal{A}_L)}{\hbar}\right]\right) \tag{5.22}$$

where expression (3.1) for the crossing angle distribution $P(\varepsilon, T)$ has already been inserted and the sum rule (2.42) was applied. The minimal loop time is given by Eq. (3.2) as $T_{\min}(\varepsilon) = -2\lambda^{-1}\ln(c\varepsilon)$. The crossing angles ε categorize the partner orbits. The number of partners with given ε is then written as an integral over all

possible loop times t_{loop}. This integral starts at the minimal loop time $T_{\mathrm{min}}(\varepsilon)$ and extends to $T - T_{\mathrm{min}}(\varepsilon)$. For a given loop time t_{loop} one has also to integrate over the area distribution P_A. Since the two orbits γ and γ^p follow each other closely within the 'encounter region' that surrounds the crossing the magnetic flux does not cause an action difference until they leave this region. Hence, the loop times entering the area distribution P_A in Eq. (5.22) are reduced by $T_{\mathrm{min}}(\varepsilon)$. The integral over $\mathcal{A}_R$ thus yields the contribution of the upper left configuration in Fig. 5.3 while the integral over $\mathcal{A}_L$ corresponds to the upper right configuration in the same figure. The geometries shown in the second row of Fig. 5.3 are accounted for by taking twice the real part in Eq. (5.22). A straightforward evaluation of the integrals then gives the result for $K^{(2)}(\tau)$ which can be combined with result (5.21) for the diagonal approximation to give the semiclassical spectral form factor

$$K(\tau) \approx \tau \left(1 + (1 - 2\tau) \exp\left[-\frac{\tau T_H}{t_B} \right] \right) \quad \text{for} \quad \tau \ll 1 \,. \tag{5.23}$$

This result coincides with the form factor of the parametric random-matrix theory (2.30) in the short time limit. The transition parameter λ_{trans} can now be easily identified by comparing Eq. (2.30) with Eq. (5.23). It is given by $\lambda_{\mathrm{trans}}^2 = 4\beta T_H \mathbf{B}^2/\varphi_0^2$. Thus we find that the semiclassical treatment based on the inclusion of off-diagonal orbit pairs also shows the expected random-matrix theory behavior if time-reversal symmetry is broken, for example, by a magnetic field.

5.3 Matrix element fluctuations

As a further extension of the theory developed by Sieber and Richter we study the generalized form factor (2.27) with operators $\hat{a}, \hat{b} \neq \hat{1}$ for a system with strict time-reversal symmetry [TSMR04]. In this case, the additional quantities A_γ and B_γ as defined in Eq. (2.36) appear in the semiclassical expression (2.38) for $K_{ab}(\tau)$. In particular, we focus on the case where the phase-space average of the Wigner functions $a(\mathbf{x})$ and $b(\mathbf{x})$ vanishes. To this end we first present a quantum mechanically exact relation between $K_{ab}(\tau)$ and $K_{11}(\tau)$. Then we review the semiclassical evaluation of $K_{ab}(\tau)$ within the diagonal approximation for vanishing $\langle a(\mathbf{x})\rangle_{\mathbf{x}} = \langle b(\mathbf{x})\rangle_{\mathbf{x}} = 0$ and extend it to momentum dependent Wigner functions. Finally we calculate the contribution of the orbit pairs (γ, γ^p) and thus go beyond the diagonal approximation.

The generalized form factor is directly related to the spectral form factor which can be concluded from the definitions (2.23), (2.26) and (2.27). Consider an operator $\hat{\tilde{a}}$ that is obtained by shifting the original operator $\hat{a}$ by the mean value $\langle a(\mathbf{x})\rangle_{\mathbf{x}}$, i.e. $\hat{\tilde{a}} = \hat{a} - \langle a(\mathbf{x})\rangle_{\mathbf{x}}\hat{1}$, and similarly for $\hat{b}$. This implies that the phase-space averages of the Wigner functions of $\hat{\tilde{a}}$ and $\hat{\tilde{b}}$ are vanishing. In terms of these new operators

one then finds

$$K_{ab}(\tau) - \langle a(\mathbf{x})\rangle_{\mathbf{x}} \langle b(\mathbf{x})\rangle_{\mathbf{x}} K(\tau) = \langle a(\mathbf{x})\rangle_{\mathbf{x}} K_{1\tilde{b}}(\tau) + \langle b(\mathbf{x})\rangle_{\mathbf{x}} K_{\tilde{a}1}(\tau) + K_{\tilde{a}\tilde{b}}(\tau) \quad (5.24)$$

with $K(\tau) = K_{11}(\tau)$. This relation is quantum mechanically exact. The diagonal approximation (2.43) already suggests that the three terms on the right hand side of Eq. (5.24) must vanish to leading order in $\hbar$ in the semiclassical limit. Indeed, the application of SHNIRELMAN's theorem (2.44) yields

$$K_{ab}(\tau) \approx \langle a(\mathbf{x})\rangle_{\mathbf{x}} \langle b(\mathbf{x})\rangle_{\mathbf{x}} K(\tau) + \mathcal{O}(\hbar) . \quad (5.25)$$

This result relies on the fact that the set of eigenstates where SHNIRELMAN's theorem is not applicable is of measure zero in the semiclassical limit. Relation (5.24) implies that the leading term vanishes for $\langle a(\mathbf{x})\rangle_{\mathbf{x}} = 0$ or $\langle b(\mathbf{x})\rangle_{\mathbf{x}} = 0$. As we will show in this section, the correction is of the order of $1/T_H \sim \hbar^{f-1}$ in this case and involves the classical correlation function $\mathcal{C}_{ab}(t)$, see Eq. (2.46). The evaluation of this correction corresponds to the determination of $K_{\tilde{a}\tilde{b}}(\tau)$ in Eq. (5.24).

The semiclassical evaluation of Eq. (2.38) based on the diagonal approximation was already discussed in [EM95, EFK+95, Eck97, EFV00]. However, the results given there were restricted to operators $\hat{a}$ and $\hat{b}$ with associated WIGNER functions that are independent of the momentum $\mathbf{p}$. Here we review the derivation and include the case of $\mathbf{p}$-dependent operators as well. The contribution of the orbit pairs (γ, γ) and (γ, γ^i) in Eq. (2.38) is given by Eq. (2.40) and can be rewritten as

$$K_{ab}^{(1)}(\tau) = \frac{2}{T_H} \left\langle \frac{1}{T_\gamma} \int_0^{T_\gamma} \mathrm{d}t \int_0^{T_\gamma} \mathrm{d}t' \, a(\mathbf{x}_t^\gamma)\, b_s(\mathbf{x}_{t+t'}^\gamma) \right\rangle_{\gamma, \tau T_H} \quad (5.26)$$

where $b_s(\mathbf{x})$ is the symmetrized WIGNER function defined by

$$b_s(\mathbf{x}) \equiv \frac{b(\mathbf{x}) + b(\mathcal{T}\mathbf{x})}{2} . \quad (5.27)$$

The application of the sum rule (2.42) together with $\langle b_s(\mathbf{x})\rangle_{\mathbf{x}} = \langle b(\mathbf{x})\rangle_{\mathbf{x}}$ gives the result (2.43) in accordance with Eq. (5.25) derived on the basis of SHNIRELMAN's theorem. This can be seen most easily by rewriting Eq. (5.26) in terms of the classical correlation function (2.46) between $a(\mathbf{x}_0)$ and $b(\mathbf{x}_t)$. As the systems under consideration are strongly chaotic all classical correlation functions decay exponentially fast in the long-time limit [Gas98]. Hence, only the leading term proportional to $\langle a(\mathbf{x})\rangle_{\mathbf{x}} \langle b(\mathbf{x})\rangle_{\mathbf{x}}$ remains in the semiclassical limit while the contribution due to the classical correlations is of lower order, i.e. $\sim 1/T_H$.

Let us now consider the case where the operators $\hat{a}$ and $\hat{b}$ are chosen such that $\langle a(\mathbf{x})\rangle_{\mathbf{x}} = \langle b(\mathbf{x})\rangle_{\mathbf{x}} = 0$ meaning $\hat{\tilde{a}} = \hat{a}$ and $\hat{\tilde{b}} = \hat{b}$. In this case the leading semiclassical approximation vanishes and one has to study the next order corrections which are

now given by the third term on the right hand side in Eq. (5.24). To leading semiclassical order Eq. (5.26) can be written in terms of the classical correlation function $\mathcal{C}^s_{\tilde{a}\tilde{b}}(t) \equiv \mathcal{C}_{\tilde{a}\,\tilde{b}_s}(t)$ since $\langle a(\mathbf{x})\rangle_{\mathbf{x}}\langle b(\mathbf{x})\rangle_{\mathbf{x}} = 0$:

$$K^{(1)}_{\tilde{a}\tilde{b}}(\tau) \simeq \frac{2}{T_H}\int_0^{\tau T_H} \mathrm{d}t\, \mathcal{C}^s_{\tilde{a}\tilde{b}}(t) \simeq \frac{2}{T_H}\int_0^{\infty} \mathrm{d}t\, \mathcal{C}^s_{\tilde{a}\tilde{b}}(t)\,. \tag{5.28}$$

Due to the chaoticity of the system the classical correlation function $\mathcal{C}^s_{\tilde{a}\tilde{b}}(t)$ is rapidly, i.e. exponentially, decaying so that the integral in Eq. (5.28) can be extended to infinity. The result (5.28) is of order $1/T_H$. It is worth to note that Eq. (5.28) is completely symmetric with respect to the appearance of the operators $\hat{a}$ and $\hat{b}$ because $\mathcal{C}_{a\,b_s}(t) = \mathcal{C}_{a_s b}(t) = \mathcal{C}^s_{ab}(t)$. If $a(\mathbf{x})$ and $b(\mathbf{x})$ are functions of the position $\mathbf{q}$ only then Eq. (5.28) coincides with the result presented in [EM95, EFK$^+$95]. This can be seen by noting that $b_s(\mathbf{q}) = b(\mathbf{q})$ and thus $\mathcal{C}^s_{ab}(t) = \mathcal{C}_{ab}(t)$. Furthermore, our derivation does not rely on the fact that the quantities A_γ and B_γ defined in Eq. (2.36) follow a GAUSSian distribution, as assumed in [EM95, EFK$^+$95].

Since the main purpose of this section is to study the contribution of the off-diagonal orbit pairs to the form factor we now consider an extension of the theory for $K^{(2)}_{11}(\tau)$ developed in Chapter 4 and in Section 5.1 to $K^{(2)}_{ab}(\tau)$. The starting point is an expression similar to Eq. (5.8). When including the additional quantities A_γ for the orbit γ and B_{γ^p} for the partner orbit γ^p one can make use of the relation

$$B_{\gamma^p} + B_{\gamma^{p,i}} \simeq B_\gamma + B_{\gamma^i} = \frac{2}{T_\gamma}\int_0^{T_\gamma} \mathrm{d}t\, b_s(\mathbf{x}^\gamma_t)\,. \tag{5.29}$$

The validity of Eq. (5.29) can be seen by using relation (4.19) and noting that together with γ^p also its time-reversed version $\gamma^{p,i}$ is a partner orbit of γ. The difference between the two partner orbits γ^p and $\gamma^{p,i}$ is only that the role of the two parts $\mathcal{L}$ and $\mathcal{R}$ is interchanged. Therefore, the two partner orbits γ^p and $\gamma^{p,i}$ together pass almost exactly the same phase space points as the two original orbits γ and γ^i do. This property of the partner orbits leads to relation (5.29) which considerably simplifies the forthcoming calculations. Applying Eq. (5.29) to Eq. (2.38) one finds the generalization of Eq. (5.8) in the form

$$K^{(2)}_{ab}(\tau) = \tau \left\langle \int_{-S^{(j)}_{\max}(E)}^{S^{(j)}_{\max}(E)} \mathrm{d}S_1 \ldots \mathrm{d}S_{f-1}\, \exp\left(\mathrm{i}\sum_{j=1}^{f-1}\frac{S_j}{\hbar}\right)\times \right. \tag{5.30}$$
$$\left. \left\langle \frac{1}{T_\gamma}\frac{\mathrm{d}^{f-1}N_\gamma(\{S_j\})}{\mathrm{d}S_1\ldots\mathrm{d}S_{f-1}}\int_0^{T_\gamma}\mathrm{d}t' a(\mathbf{x}^\gamma_{t'})\frac{1}{T_\gamma}\int_0^{T_\gamma}\mathrm{d}t''\, b_s(\mathbf{x}^\gamma_{t'+t''})\right\rangle_{\gamma,\tau T_H}\right\rangle_{\Delta E}.$$

In analogy to the calculation presented in Section 5.1 we use Eq. (5.10) for the number of partners and shift the integration variable t' to $t'+t$ which is possible since the orbits γ are periodic. Then we apply the sum rule (2.42) to evaluate the leading contribution due to ϱ^{lead}, see Eq. (5.13), in Eq. (5.30) which yields

$$\left\langle \frac{1}{T_\gamma} \frac{\mathrm{d}^{f-1} N_\gamma^{\mathrm{lead}}(\{S_j\})}{\mathrm{d}S_1 \ldots \mathrm{d}S_{f-1}} \int_0^{T_\gamma} \mathrm{d}t' a(\mathbf{x}_{t'}^\gamma) \frac{1}{T_\gamma} \int_0^{T_\gamma} \mathrm{d}t'' \, b_s(\mathbf{x}_{t'+t''}^\gamma) \right\rangle_{\gamma,\tau T_H} \simeq \tag{5.31}$$

$$\frac{2^{f-1}}{\Omega(E)} \sum_{k=1}^{f-1} \left\langle \chi_k(\mathbf{x}) \int_0^{\tau T_H} \mathrm{d}t \, a(\mathbf{x}_t) \int_0^{\tau T_H} \mathrm{d}t' \, b_s(\mathbf{x}_{t+t'}) \right\rangle_{\mathbf{x}} \prod_{j\neq k}^{f-1} \ln \frac{S_{\mathrm{cl}} s_j^c u_j^c}{|S_j|} \, .$$

This result reproduces Eq. (5.14) for $a(\mathbf{x}) = b_s(\mathbf{x}) = 1$. For observables with $a(\mathbf{x}) \neq 0$ and $b(\mathbf{x}) \neq 0$ the leading term for $T_H \to \infty$ is given by replacing

$$\langle \chi_k(\mathbf{x}) a(\mathbf{x}_t) b_s(\mathbf{x}_{t+t'}) \rangle_{\mathbf{x}} \quad \to \quad \lambda_k \langle a(\mathbf{x}) \rangle_{\mathbf{x}} \langle b(\mathbf{x}) \rangle_{\mathbf{x}}$$

which is justified because of the rapid decay of all classical correlation functions in chaotic systems [Gas98]. Hence Eq. (5.31) inserted in Eq. (5.30) just gives $K_{ab}^{(2,\mathrm{lead})}(\tau) = 0$ as it was for $\hat{a} = \hat{b} = 1$, see Section 5.1.

In analogy to the procedure for the diagonal approximation we again study the case of vanishing mean values $\langle \tilde{a}(\mathbf{x}) \rangle_{\mathbf{x}} = \langle \tilde{b}(\mathbf{x}) \rangle_{\mathbf{x}} = 0$. In this case the leading term $\sim \lambda_k \langle \tilde{a}(\mathbf{x}) \rangle_{\mathbf{x}} \langle \tilde{b}(\mathbf{x}) \rangle_{\mathbf{x}}$ gives a vanishing contribution and the next order correction is obtained by substituting

$$\left\langle \chi_k(\mathbf{x}) \int_0^T \mathrm{d}t' \, \tilde{a}(\mathbf{x}_t) \tilde{b}_s(\mathbf{x}_{t+t'}) \right\rangle_{\mathbf{x}} \quad \to \quad \lambda_k \int_0^T \mathrm{d}t' \, \mathcal{C}_{\tilde{a}\tilde{b}}^s(t')$$

in result (5.31). Thus, also in this case we again find $K_{\tilde{a}\tilde{b}}^{(2,\mathrm{lead})}(\tau) = 0$ if Eq. (5.31) is inserted in Eq. (5.30).

As the contribution of ϱ^{lead} to $K_{ab}^{(2)}(\tau)$ vanishes we now derive the corresponding results for the small correction ϱ^{corr} given by Eq. (5.13). Following the lines in Section 5.1 we first evaluate the periodic orbit average $\langle \ldots \rangle_{\gamma,\tau T_H}$ in Eq. (5.30) by using Eq. (5.11). Since the encounter time t_{en} occurring in the density (5.13) exactly cancels with that in Eq. (5.11) we find

$$\left\langle \frac{1}{T_\gamma} \frac{\mathrm{d}^{f-1} N_\gamma^{\mathrm{corr}}(\{S_j\})}{\mathrm{d}S_1 \ldots \mathrm{d}S_{f-1}} \int_0^{T_\gamma} \mathrm{d}t' a(\mathbf{x}_{t'}^\gamma) \frac{1}{T_\gamma} \int_0^{T_\gamma} \mathrm{d}t'' \, b_s(\mathbf{x}_{t'+t''}^\gamma) \right\rangle_{\gamma,\tau T_H} \simeq \tag{5.32}$$

$$- \frac{2^f}{\Omega(E)} \frac{1}{\tau T_H} \int_0^{\tau T_H} \mathrm{d}t \, \langle a(\mathbf{x}) \, b_s(\mathbf{x}_t) \rangle_{\mathbf{x}} \prod_j^{f-1} \ln \frac{S_{\mathrm{cl}} s_j^c u_j^c}{|S_j|} \, .$$

Again we distinguish the two cases where the phase space averages of $a(\mathbf{x})$ and $b(\mathbf{x})$ are either non-vanishing or vanishing. In the first case the leading order term is given by substituting

$$\langle a(\mathbf{x})\, b_s(\mathbf{x}_t)\rangle_{\mathbf{x}} \to \langle a(\mathbf{x})\rangle_{\mathbf{x}} \langle b_s(\mathbf{x})\rangle_{\mathbf{x}} = \langle a(\mathbf{x})\rangle_{\mathbf{x}} \langle b(\mathbf{x})\rangle_{\mathbf{x}}$$

in Eq. (5.32) because the correction $T^{-1}\int_0^T \mathrm{d}t\, \mathcal{C}_{ab}^s(t)$ due to classical correlations is of order $\sim 1/T_H$ for rapidly decaying $\mathcal{C}_{ab}^s(t)$. Therefore, the first off-diagonal contribution to the form factor is then given by

$$K_{ab}^{(2)}(\tau) \simeq -2\, \langle a(\mathbf{x})\rangle_{\mathbf{x}} \langle b(\mathbf{x})\rangle_{\mathbf{x}}\, \tau^2$$

in accordance with the result (5.25) obtained by applying Shnirelman's theorem. On the other hand, in the case of vanishing mean values $\langle \tilde{a}(\mathbf{x})\rangle_{\mathbf{x}} = \langle \tilde{b}(\mathbf{x})\rangle_{\mathbf{x}} = 0$ the leading contribution is determined by the classical correlation function $\mathcal{C}_{ab}^s(t)$ via the substitution

$$\left\langle \tilde{a}(\mathbf{x})\, \tilde{b}_s(\mathbf{x}_t)\right\rangle_{\mathbf{x}} \to \mathcal{C}_{\tilde{a}\tilde{b}}^s(t)$$

in Eq. (5.32). Hence, inserting Eq. (5.32) in the expression (5.30) yields the following result for the form factor

$$K_{\tilde{a}\tilde{b}}^{(2)}(\tau) \simeq -2\tau \frac{1}{T_H} \int_0^\infty \mathrm{d}t\, \mathcal{C}_{\tilde{a}\tilde{b}}^s(t)\ . \tag{5.33}$$

Together with the diagonal approximation (5.28) we thus find

$$K_{\tilde{a}\tilde{b}}(\tau) \simeq \left(K(\tau) + \mathcal{O}(\tau^3)\right) \frac{1}{\tau T_H} \int_0^\infty \mathrm{d}t\, \mathcal{C}_{\tilde{a}\tilde{b}}^s(t) \quad \text{for} \quad \tau \ll 1 \tag{5.34}$$

in the semiclassical limit $T_H \sim \hbar^{1-f} \to \infty$. This is the central result of this section. It provides an extension of the earlier results in [EM95, EFK+95, Eck97, EFV00] in a compact form. In particular it includes the case of two different operators $\hat{a}$ and $\hat{b}$ whose Wigner functions can be momentum-dependent. It goes beyond the diagonal approximation and does not rely on the assumption of Gaussian fluctuations for the quantities A_γ and B_γ which enter the semiclassical expression of the form factor. If the result (5.34) could be shown to be correct for any value of τ, the variance of the diagonal matrix elements $\hat{a}_{nn}$ could be uniquely related to the classical correlation function $\mathcal{C}_{aa}(t)$ as described in Section 2.4. Our approach is a first step into this direction. It shows that the constant off-set (5.28) due to the diagonal approximation and the first correction due to off-diagonal orbit pairs depend in exactly the same way on the classical correlation function $\mathcal{C}_{ab}(t)$.

Repeating the same calculation as presented above for the other two contributions $K_{1\tilde{b}}(\tau)$ and $K_{\tilde{a}1}(\tau)$ one finds that the leading terms in $\hbar$ vanish. This is in accordance with (5.24) and Shnirelman's theorem. However, our method cannot be applied to determine the first non-vanishing corrections in these cases as they also depend on the higher-order corrections to the sum rule (2.42).

CHAPTER 6

Conclusions and outlook

6.1 Conclusions

In this thesis we have studied the statistical properties of the energy spectra of closed quantum systems with a chaotic classical counterpart. Following a conjecture by Bohigas, Giannoni and Schmit (BGS) the spectral statistics of chaotic systems is universal and can be described by the random-matrix theory predictions. This is similar to the situation when disordered systems are considered. The major difference between chaotic and disordered systems is that in the first case the classical motion is deterministic while it is a random walk in the second case. Although a great variety of experiments and numerical simulations supports the BGS-conjecture a formal proof is still lacking. Recently, a significant step towards such a proof was proposed by Sieber and Richter who analyzed a spectral two-point correlation function using semiclassical techniques. In particular they considered the spectral form factor $K(\tau)$ expressed by means of Gutzwiller's trace formula and showed how correlations in the actions of classical periodic orbits determine the next-to-leading order of $K(\tau)$. The central idea in their approach was to identify orbit pairs with a small action difference and to develop a statistical method for counting these pairs. The derivation was restricted to a very specific kind of system, namely the two-dimensional uniformly hyperbolic system. Furthermore, it was formulated in the framework of the configuration space. In this configuration-space approach each orbit pair is then associated to a crossing with small crossing angle. Hence, the number of orbit pairs is directly determined by the distribution of self-crossings. This approach together with the necessary methods concerning chaotic systems and

semiclassical approximations is briefly summarized in Chapter 2.

The purpose of this thesis is to present extensions and generalizations of the configuration-space approach by SIEBER and RICHTER into various directions. First of all, we investigated the crossing angle distribution for a *non-uniformly* hyperbolic billiard system. Our numerical analysis is based on the family of LIMAÇON billiards which includes the cardioid as a limiting case. Our results in Chapter 3 show that the qualitative form of the crossing angle distribution is the same as for the uniformly hyperbolic system. However, this is only the case if a very specific type of crossings (namely those corresponding to almost self-retracing loops with short loop lengths) is excluded. Furthermore we found that in a focusing billiard like the cardioid the crossings with small crossing angles always occur in families.

We then proceeded by developing a canonically invariant phase-space approach for *non*-uniformly hyperbolic two-dimensional systems which is presented in Chapter 4. In particular we showed that crossings in configuration space are not necessarily the relevant objects for the identification of correlated orbit pairs in the general case. Instead, we proposed the concept of 'encounter regions' that are defined as those parts in phase space where a periodic orbit comes close to its time-reversed version. Due to the deterministic dynamics of the system these 'encounter regions' are non-local objects in phase space with a finite length. This is in contrast to the approach based on the crossings as these are local in phase space. An important consequence is that an 'encounter region' may contain many crossings but nevertheless only one partner orbit is associated to the entire region. The crossing angle being the small parameter in the configuration space approach has to be replaced by a displacement vector in phase space. In terms of this displacement vector which points from the orbit to its time-reversed version we determine the geometry and the action of the partner orbit. This leads to the result that correlations in the classical actions in hyperbolic chaotic systems are caused by 'encounter regions' in phase space where an orbit and its time-reversed version come close together. These results are the foundations for an extension of the theory to non-uniformly hyperbolic systems. We presented arguments showing that the MASLOV indices that occur in these systems are equal for the periodic orbit and its partner. As a last step we developed a phase-space method to determine the number of partner orbits which effectively replaces the crossing angle distribution in the derivation of the form factor. All these results were then combined in order to determine the next-to-leading order contribution for the spectral form factor of a two-dimensional non-uniformly hyperbolic system. As a final result, we proved that also for these systems the next-to-leading order correction for the spectral form factor is universal and coincides with random-matrix theory.

The character of the different time scales involved in chaotic systems becomes clear in our derivation. The length of the involved orbits is on the order of the HEISENBERG time T_H. The dynamics of the systems introduces another important

time on the scale of the EHRENFEST time T_E. This time enters via the lengths of the 'encounter regions' t_{en} that are of the order of T_E. While the HEISENBERG time is proportional to some power of the parameter $S_{cl}/\hbar$ the EHRENFEST time depends logarithmically on it. Hence, the semiclassical limit $\hbar \to 0$ implies that these two time scales are much bigger than the time scales fixed by the classical system like the inverse LYAPUNOV exponent λ^{-1} or the mean free flight time. The hierarchy of time scales in the semiclassical limit is thus given by $\lambda T_H \gg \lambda T_E \gg 1$. However, it turns out that times of the scale T_E play a crucial role in our derivation although they are much smaller than the lengths of the periodic orbits which is $\sim T_H$. In fact, neglecting the finite size of the 'encounter region' leads to a vanishing contribution of the correlated orbit pairs to the form factor. This means that the deterministic character of the dynamics is reflected in a subtle way in the spectral statistics.

The extension of the configuration-space approach to the phase-space approach is essential if the theory is to be applied to systems with more than two degrees of freedom. In this case the occurrence of real crossings in configuration space is extremely unlikely. Such a generalization to higher-dimensional systems based on the phase space formulation is presented in Section 5.1. The most important result concerns the statistics of partner orbits as it is much more involved if the system has more than two degrees of freedom. By combining two different techniques — one associated with a volume integration while the other is based on a surface integral — we showed that the final result is once more given by the universal random-matrix theory prediction. In particular, we proved that all further time scales defined by the different LYAPUNOV exponents do not affect this result.

In order to provide another test for the method based on correlated orbit pairs we have investigated the effect of a weak magnetic field applied to the system. In the language of the random-matrix theory this mimics the transition from the GAUSSian orthogonal ensemble (GOE) valid for systems with time-reversal symmetry to the GAUSSian unitary ensemble (GUE) applicable to systems that lack this symmetry. In Section 5.2 we derived the contribution of the off-diagonal orbit pairs to the spectral form factor of a two-dimensional uniformly hyperbolic system. Our result provides a physical interpretation of the transition parameter introduced in the random-matrix theory. This transition parameter turned out to be proportional to the magnetic field and, furthermore, contains a system specific constant.

Finally we presented an application of our method to the fluctuations of quantum mechanical matrix elements. These fluctuations can be described by a classical correlation function. The way in which this classical correlation function enters the generalized form factor turns out to be exactly the same for the diagonal approximation and the contributions of the first off-diagonal orbit pairs. We showed that these classical correlations give rise to a contribution that is proportional to the inverse HEISENBERG time in either case.

6.2 Open questions and outlook

The most obvious open question is of course whether the approach based on orbit pairs with correlated actions can be developed further so that also higher-order corrections of $K(\tau)$ beyond the first off-diagonal contribution $\sim \tau^2$ can be calculated. In the intuitive picture of the configuration space approach that would mean to identify orbit pairs on the basis of not just one but multiple self-crossings. Several attempts into this direction were performed in the last few months, e.g. the calculation of the third order terms $\sim \tau^3$ for quantum graphs [BSW02a, Ber03] and, very recently, for chaotic HAMILTONian systems [MHB$^+$04]. These results indicate that a proof of the conjecture by BOHIGAS, GIANNONI and SCHMIT might be indeed found by means of semiclassical techniques. However, it is clear that a derivation of the spectral form factor $K(\tau)$ based on a series expansion in τ provides only one part of the entire picture because this expansion converges only for $0 \leq \tau \leq 1/2$. Therefore, it is also necessary to develop a theory that describes the large τ behavior of the spectral form factor.

Besides these more fundamental questions there is a wide field for the application of the semiclassical methods described in this thesis. The basic idea is the following. The spectral form factor is a product of two densities of states which in turn are given by traces over single particle GREEN's functions. In principle, it should be possible to transfer the techniques based on periodic orbits (which are associated with the spectral properties of closed systems in the semiclassical limit) to non-periodic orbits that determine various physical properties of open systems. Basically, the procedure of evaluating semiclassical expressions containing double sums over periodic orbits should be extensible to the evaluation of double or multiple sums over open paths. These double or multiple sums over open paths occur if the semiclassical expressions for products of GREEN's functions are considered. Therefore, one might be able to solve various open questions concerning the electronic transport through open ballistic systems for example on the basis of LANDAUER's theory which relates the conductance of a system to the scattering matrix. As many transport problems like shot noise or universal conductance fluctuations can be formulated in terms of products of single particle GREEN's functions a semiclassical treatment going beyond the diagonal approximation seems now in reach. A similar method might also be applicable to the semiclassical evaluation of linear response functions. First steps into this direction were performed in [RS02] where the weak localization corrections are studied and in [Las03, SPG03] where an analysis of relevant pairs of open paths to the problem of shot noise is given. Therefore, further research into this direction seems promising to overcome the limitations of the semiclassical methods to the diagonal approximation.

APPENDIX A

Conversion between volume and surface integral

In this appendix we prove the equality of the two different approaches for counting the partner orbits that we used in Section 5.1. In particular we show that Eq. (5.10) and Eq. (5.11) are equal. The general structure of this equality is of the type

$$\int_0^T \mathrm{d}t \int_{\mathcal{V}} \mathrm{d}^{2f-2}z \frac{\varrho(\vec{z},t)}{t_{\mathcal{V}}(\vec{z},t)} = \int_0^T \mathrm{d}t \int_{\partial\mathcal{V}_{\mathrm{out}}} \mathrm{d}\vec{A}\, \varrho(\vec{z},t)\, \vec{v}(\vec{z},t)\,. \tag{A.1}$$

Here, $\vec{z}$ is a vector in a $2f-2$ dimensional space. It abbreviates the coordinates $(\{s_i, u_i\})$ used in Section 5.1. The surface of any volume $\mathcal{V}$ in the vector space is denoted by $\partial\mathcal{V}$. In relation (A.1), $\partial\mathcal{V}_{\mathrm{out}}$ stands for that part of the total surface through which the flow leaves $\mathcal{V}$ in the long-time limit. More precisely speaking, the total flux between time 0 and T through any piece of $\partial\mathcal{V}_{\mathrm{out}}$ must be positive. Further, we assume periodicity so that $\varrho(\vec{z},t) = \varrho(\vec{z},t+T)$ and $\vec{v}(\vec{z},t) = \vec{v}(\vec{z},t+T)$ with $\varrho(\vec{z},t)$ being a density field made up of single points and $\vec{v}(\vec{z},t)$ being a velocity field. As the relation (A.1) is applied to the motion of points in phase space the current is conserved meaning that the total number of points is constant, i.e. $\dot{\varrho}(\vec{z}_t,t) = 0$. Hence the density is constant along the flow, i.e. $\varrho(\vec{z},0) = \varrho(\vec{z}_t,t)$. The time $t_{\mathcal{V}}(\vec{z},t)$ is defined as the total time a point spends in the volume $\mathcal{V}$ if it starts at time t at position $\vec{z}$ and moves until time $t+T$.

Let us first consider the case where the total density $\varrho(\vec{z},t)$ is given by a single

point starting at $\vec{z}_0$, i.e. $\varrho_{\vec{z}_0}(\vec{z},t) = \delta(\vec{z} - \vec{z}_t)$. Then the time $t_\mathcal{V}$ is given as

$$t_\mathcal{V}(\vec{z},t) = \int_t^{t+T} \mathrm{d}t' \; \Theta_\mathcal{V}(\vec{z}_{t'}) = \int_0^T \mathrm{d}t' \int_\mathcal{V} \mathrm{d}^{2f-2}z' \; \varrho_{\vec{z}_0}(\vec{z}',t') = t_\mathcal{V}(\vec{z}_0,0) \tag{A.2}$$

where $\Theta_\mathcal{V}(\vec{z})$ is one if $\vec{z} \in \mathcal{V}$ and zero otherwise. In Eq. (A.2) we made use of the periodicity of the motion. We then obtain for the left hand side of Eq. (A.1)

$$\begin{aligned}\int_0^T \mathrm{d}t \int_\mathcal{V} \mathrm{d}^{2f-2}z \; \frac{\varrho_{\vec{z}_0}(\vec{z},t)}{t_\mathcal{V}(\vec{z},t)} &= \int_0^T \mathrm{d}t \, \frac{1}{t_\mathcal{V}(\vec{z}_0,0)} \int_\mathcal{V} \mathrm{d}^{2f-2}z \; \delta(\vec{z} - \vec{z}_t) \\ &= \frac{1}{t_\mathcal{V}(\vec{z}_0,0)} \int_0^T \mathrm{d}t \int_\mathcal{V} \mathrm{d}^{2f-2}z \; \varrho_{\vec{z}_0}(\vec{z},t) = 1 \,.\end{aligned}$$

Thus we find that if the single point density is replaced by $\varrho(\vec{z},t) = \sum_{\{\vec{z}_0\}} \varrho_{\vec{z}_0}(\vec{z},t)$ which represents an arbitrary number n of points given by their initial conditions then the left hand side of Eq. (A.1) just gives the total number of particles n that pass $\mathcal{V}$ during one period. But this is exactly what the right hand side of Eq. (A.1) gives. It just measures the outgoing flux through the surface of $\mathcal{V}$ between time 0 and T which also yields the total number of particles n because the particle number in conserved. Finally we also note that the density $\varrho(\vec{z},t)$ is not restricted to a sum of δ-functions. Each of these δ-functions can also be multiplied with any function $g(\vec{z},t)$ that is constant when following the flow, i.e. $g(\vec{z}_0,0) = g(\vec{z}_t,t)$. In the context of Section 5.1, g could for example be any function of the action difference as in Eq. (5.10) and Eq. (5.11). If all local unstable growth rates $\chi_k(\mathbf{x})$ are non-negative one can directly identify $t_\mathcal{V} = t_{en}$ and thus the equality (A.1) means that Eq. (5.10) exactly equals Eq. (5.11). On the other hand, if these local unstable growth rates assume negative values in certain areas of the phase space then this implies that the unstable components of a displacement vector can also decrease on *short* time scales. This would lead to a multiple entry of the same point into the 'encounter region'. In this case the relation (A.1) means Eq. (5.11) is asymptotically equal to Eq. (5.10) as the length t_{en} becomes large so that $|t_\mathcal{V} - t_{en}| \ll t_{en}$ or similarly $t_\mathcal{V} \simeq t_{en}$.

Bibliography

[AA95] A.V. Andreev and B.L. Altshuler. Spectral statistics beyond random matrix theory. *Phys. Rev. Lett.* **75**, *902*, 1995.

[AAA95] O. Agam, B.L. Altshuler, and A.V. Andreev. Spectral statistics: From disordered to chaotic systems. *Phys. Rev. Lett.* **75**, *4389*, 1995.

[ADD+93] N. Argaman, F.-M. Dittes, E. Doron, J.P. Keating, A.Yu. Kitaev, M. Sieber, and U. Smilansky. Correlations in the actions of periodic orbits derived from quantum chaos. *Phys. Rev. Lett.* **71**, *4326*, 1993.

[AG93] D. Alonso and P. Gaspard. $\hbar$ expansion for the periodic orbit quantization of chaotic systems. *Chaos* **3**, *601*, 1993.

[AIS93] N. Argaman, Y. Imry, and U. Smilansky. Semiclassical analysis of spectral correlations in mesoscopic systems. *Phys. Rev. B* **47**, *4440*, 1993.

[AL97] Y. Alhassid and C.H. Lewenkopf. Signatures of chaos in the statistical distribution of conductance peaks in quantum dots. *Phys. Rev. B* **55**, *7749*, 1997.

[Arg95] N. Argaman. Semiclassical analysis of the conductance of mesoscopic systems. *Phys. Rev. Lett.* **75**, *2750*, 1995.

[Arg96] N. Argaman. Semiclassical analysis of the quantum interference corrections to the conductance of mesoscopic systems. *Phys. Rev. B* **53**, *7035*, 1996.

[Arn01] V.I. Arnol'd. *Mathematical methods of classical mechanics*. Springer New York, 2001.

[AS88] R. Aurich and F. Steiner. On the periodic orbits of a strongly chaotic system. *Physica D* **32**, *451*, 1988.

[ASY96] K.T. Alligood, T.D. Sauer, and J.A. Yorke. *Chaos: An introduction to dynamical systems*. Springer-Verlag New York Inc., 1996.

[AY81] V.M. Alekseev and M.V. Yakobson. Symbolic dynamics and hyperbolic dynamic systems. *Phys. Rep.* **75**, *287*, 1981.

[Bäc98] A. Bäcker. *Classical and Quantum Chaos in Billiards*. PhD thesis, Universität Ulm, 1998.

[BB97] M. Brack and R.K. Bhaduri. *Semiclassical Physics*. Addison-Wesley Publishing Company, Inc., 1997.

[BBR99] H. Bambi, L. Baowen, and D.C. Rouben. Numerical accuracy of bogomolny's semiclassical quantization scheme in quantum billiards. *J. Phys. A: Math. Gen.* **32**, *5419*, 1999.

[BD97] A. Bäcker and H.R. Dullin. Symbolic dynamics and periodic orbits for the cardioid billiard. *J. Phys. A: Math. Gen.* **30**, *1991*, 1997.

[Ber77] M.V. Berry. Regular and irregular semiclassical wave functions. *Jour. Phys. A* **10**, *2083*, 1977.

[Ber81] M.V. Berry. Semiclassical mechanics of regular and irregular motion. *Les Houches, Session XXXVI, 171*, 1981.

[Ber85] M.V. Berry. Semiclassical theory of spectral rigidity. *Proc. R. Soc. Lond. A* **400**, *229*, 1985.

[Ber87] M.V. Berry. Quantum chaology. *Proc. R. Soc. Lond. A* **413**, *183*, 1987.

[Ber89] M.V. Berry. Some quantum-to-classical asymptotics. In *Chaos and Quantum physics (Les Houches, Session* **LII***), 251*, 1989.

[Ber03] G. Berkolaiko. Form factor of large quantum graphs: evaluating orbits with time-reversal. *nlin.CD/0305009 v1 7 May*, 2003.

[BGdAS95] O. Bohigas, M.-J. Giannoni, A.M. Ozorio de Almeida, and C. Schmit. Chaotic dynamics and the goe-gue transition. *Nonlinearity* **8**, *203*, 1995.

[BGS84] O. Bohigas, M.J. Giannoni, and C. Schmit. Characterization of chaotic quantum spectra and universality of level fluctuation laws. *Phys. Rev. Lett.* **52**, *1*, 1984.

[BGS85] W. Ballmann, M. Gromov, and V. Schroeder. *Manifolds of Nonpositive Curvature*. Birkhäuser Boston Inc., 1985.

[BHH02] P.A. Braun, F. Haake, and S. Heusler. Action correlation of orbits through non-conventional time reversal. *J. Phys. A: Math. Gen.* **35** *1381*, 2002.

[BHMH02] P.A. Braun, S. Heusler, S. Müller, and F. Haake. Statistics of self-crossings and avoided crossings of periodic orbits in the hadamard-gutzwiller model. *Eur. Phys. J. B* **30**, *189*, 2002.

[BJS93] H.U. Baranger, R.A. Jalabert, and A.D. Stone. Quantum-chaotic scattering effects in semiconductor microstructures. *Chaos* **3**, *665*, 1993.

[BK96] E.B. Bogomolny and J.P. Keating. Gutzwiller's trace formula and spectral statistics: Beyond the diagonal approximation. *Phys. Rev. Lett.* **77**, *1472*, 1996.

[Bog88] E.B. Bogomolny. Smoothed wave functions of chaotic quantum systems. *Physica D* **31**, *169*, 1988.

[Bog00] E.B. Bogomolny. Spectral statistics and periodic orbits. *Proc. Intl. School Phys. E. Fermi: Course* **CXLIII***: New Directions in Quantum Chaos*, 2000.

[Boh89] O. Bohigas. Random matrix theories and chaotic dynamics. In *Chaos and Quantum physics (Les Houches, Session* **LII***), 87*, 1989.

[BR99] E.B. Bogomolny and D.C. Rouben. Semiclassical description of resonant tunneling. *Eur. Phys. J. B* **9**, *695*, 1999.

[BS94] H. Bruus and D. Stone. Quantum chaos in a deformable billiard: Applications to quantum dots. *Phys. Rev. B* **50**, *18275*, 1994.

[BS02] M. Barth and H.-J. Stöckmann. Current and vortex statistics in microwave billiards. *Phys. Rev. E* **65**, *066208/1*, 2002.

[BSS98] A. Bäcker, R. Schubert, and P. Stifter. Rate of quantum ergodicity in euclidean billiards. *Phys. Rev. E* **57**, *5425*, 1998.

[BSW02a] G. Berkolaiko, H. Schanz, and R.S. Whitney. Form factor for a family of quantum graphs: An expansion to third order. *nlin.CD/0205014 8 May*, 2002.

[BSW02b] G. Berkolaiko, H. Schanz, and R.S. Whitney. Leading off-diagonal correction to the form factor of large graphs. *Phys. Rev. Lett.* **88**, *104101-1*, 2002.

[BT77] M.V. Berry and M. Tabor. Level clustering in the regular spectrum. *Proc. R. Soc. Lond. A* **356**, *375*, 1977.

[Bun74] L.A. Bunimovich. On ergodic properties of certain billiards. *Funct. Anal. Appl.* **8**, *254*, 1974.

[Bun79] L.A. Bunimovich. On the ergodic properties of nowhere dispersing billiards. *Commun. Math. Phys.* **65**, *295*, 1979.

[BV86] N.L. Balazs and A. Voros. Chaos on the pseudosphere. *Phys. Rep.* **143**, *109*, 1986.

[Cas95] *Quantum chaos: between order and disorder*. Cambridge University Press, 1995.

[CRL90] S.C. Creagh, J.M. Robbins, and R.G. Littlejohn. Geometrical properties of maslov indices in the semiclassical trace formula for the density of states. *Phys. Rev. A* **42**, *1907*, 1990.

[CRR99] M. Combescure, J. Ralston, and D. Robert. A proof of the gutzwiller semiclassical trace formula using coherent states decomposition. *Commun. Math. Phys.* **202**, *463*, 1999.

[CVL02] G.G. Carlo, E.G. Vergini, and P. Lustemberg. Scar functions in the bunimovich stadium billiard. *J. Phys. A: Math. Gen.* **35**, *7965*, 2002.

[dV85] Y. Colin de Verdiére. Ergodicité et fonctions propres du laplacien. *Commun. Math. Phys.* **102**, *497*, 1985.

[Eck97] B. Eckhardt. Fluctuations and correlations in matrix elements. *Physica D* **109**, *53*, 1997.

[EFK+95] B. Eckhardt, S. Fishman, J. Keating, O. Agam, J. Main, and K. Müller. Approach to ergodicity in quantum wave functions. *Phys. Rev. E* **52**, *5893*, 1995.

[EFMW92] B. Eckhardt, S. Fishman, K. Müller, and D. Wintgen. Semiclassical matrix elements from periodic orbits. *Phys. Rev. B* **45**, *3531*, 1992.

[EFV00] B. Eckhardt, S. Fishman, and I. Varga. Semiclassical cross section correlations. *Phys. Rev. E* **62**, *7867*, 2000.

[Ein17] *Verh. Dtsch. Phys. Ges.* **19**, *82*, 1917.

[EM95] B. Eckhardt and J. Main. Semiclassical form factor of matrix element fluctuations. *Phys. Rev. Lett.* **75**, *2300*, 1995.

[EVP01] B. Eckhardt, I. Varga, and P. Pollmer. Correlations and fluctuations of matrix elements and cross sections. *Physica E* **9**, *535*, 2001.

[EW91] B. Eckhardt and D. Wintgen. Indices in classical mechanics. *J. Phys. A: Math. Gen.* **24**, *4335*, 1991.

[EY93] B. Eckhardt and D. Yao. Local Lyapunov exponents in chaotic systems. *Physica D* **65**, *100*, 1993.

[FH03] G.A. Fiete and E.J. Heller. Semiclassical theory of coherence and decoherence. *Phys. Rev. A* **68**, *22112*, 2003.

[FP86] M. Feingold and A. Peres. Distribution of matrix elements of chaotic systems. *Phys. Rev. A* **34**, *591*, 1986.

[FR97] J.A. Foxman and J.M. Robbins. Periodic orbit maslov indices for systems with time-reversal symmetry. *J. Phys. A: Math. Gen.* **30**, *8187*, 1997.

[FW89] H. Friedrich and D. Wintgen. *Phys. Rep.* **183**, *37*, 1989.

[GA93] P. Gaspard and D. Alonso. $\hbar$ expansion for the periodic-orbit quantization of hyperbolic systems. *Phys. Rev. A* **47**, *R3468*, 1993.

[GAB95] P. Gaspard, D. Alonso, and I. Burghardt. New ways of understanding semiclassical quantization. *Adv. Chem. Phys.* **90**, *105*, 1995.

[Gas98] P. Gaspard. *Chaos, scattering and statistical mechanics*. Cambridge University Press, 1998.

[GH02] J. Guckenheimer and P. Holmes. *Nonlinear Oscillations, Dynamical Systems, and Bifurcations of Vector Fields*. Springer-Verlag New York Inc., 2002.

[GM02a] I.V. Gornyi and A.D. Mirlin. From quantum disorder to quantum chaos. *J. Low Temp. Phys.* **126**, *1339*, 2002.

[GM02b] I.V. Gornyi and A.D. Mirlin. Wave function correlations on the ballistic scale: from quantum disorder to quantum chaos. *Physica E* **12**, *845*, 2002.

[GMGW98] Th. Guhr, A. Müller-Groeling, and H.A. Weidenmüller. Random-matrix theories in quantum physics: Common concepts. *Phys. Rep.* **299**, *189*, 1998.

[GR00] I.S. Gradshteyn and I.M. Rhyshik. *Table of Integrals, Series and Products, 6th ed.* Academic Press, 2000.

[Gut90] M.C. Gutzwiller. *Chaos in classical and quantum mechanics.* Springer-Verlag New York, Inc., 1990.

[HA84] J.H. Hannay and A.M. Ozorio De Almeida. Periodic orbits and a correlation function for the semiclassical density of states. *J. Phys. A: Math. Gen.* **17**, *3429*, 1984.

[Haa01] F. Haake. *Quantum signatures of chaos.* Springer-Verlag Berlin Heidelberg New York, 2001.

[Hel84] E. Heller. Bound state eigenfunctions of classically chaotic Hamiltonian systems: Scars of periodic orbits. *Phys. Rev. Lett.* **53**, *1515*, 1984.

[Hel89] E. Heller. Wavepacket dynamics and quantum chaology. In *Chaos and Quantum physics (Les Houches, Session* **LII***), 547*, 1989.

[Hel96] E.J. Heller. Quantum chaos for real. *Nature* **380**, *583*, 1996.

[Heu01] S. Heusler. The semiclassical origin of the logarithmic singularity in the symplectic form factor. *J. Phys. A: Math. Gen.* **34**, *L483*, 2001.

[HMBH03] S. Heusler, S. Müller, P. Braun, and F. Haake. Universal spectral form factor for chaotic dynamics. *nlin.CD/0309022*, 2003.

[Jen95] R.V. Jensen. The signature of chaos. *Nature* **373**, *16*, 1995.

[KS99] T. Kottos and U. Smilansky. Periodic orbit theory and spectral statistics for quantum graphs. *Ann. Phys.* **274**, *76*, 1999.

[KS01] T. Kottos and H. Schanz. Quantum graphs: a model for quantum chaos. *Physica E* **9**, *523*, 2001.

[KS03] T. Kottos and U. Smilansky. Quantum graphs: a simple model for chaotic scattering. *J. Phys. A: Math. Gen.* **36**, *3501*, 2003.

[Las03] A. Lassl. Semiklassik jenseits der Diagonalnäherung: Anwendung auf ballistische mesoskopische systeme. Master's thesis, Universität Regensburg, 2003.

[Ler03] I.V. Lerner. Nonlinear sigma model for normal and superconducting systems: a pedestrian approach. *cond-mat/0307471 v1 18 Jul*, 2003.

[Les89] *Chaos and Quantum physics (Les Houches, Session* **LII***)*, 1989.

[LL90] L.D. Landau and E.M. Lifschitz. *Mechanik*. Akademie-Verlag Berlin, 1990.

[LL92] A.J. Lichtenberg and M.A. Lieberman. *Regular and Chaotic Dynamics*. Springer-Verlag New York Inc., 1992.

[Mai90] P.C. Main. Chaos in quantum billiards. *Nature* **348**, *584*, 1990.

[Mar93] R. Markarian. New ergodic billiards: exact results. *Nonlinearity* **6**, *819*, 1993.

[Meh90] M.L. Mehta. *Random Matrices and the Statistical Theory of Energy Levels (new revised and enlarged edition)*. Academic Press, 1990.

[Mer98] E. Merzbacher. *Quantum Mechanics, 3rd ed.* John Wiley and Sons, Inc., 1998.

[MHB+04] S. Müller, S. Heusler, P. Braun, F. Haake, and A. Altland. Semiclassical foundation of universality in quantum chaos. *nlin.CD/0401021*, 2004.

[Mül03] S. Müller. Classical basis for quantum spectral fluctuations in hyperbolic systems. *Eur. Phys. J.* **B34**, *305*, 2003.

[NS03] T. Nagao and K. Saito. Form factor of a quantum graph in a weak magnetic field. *Phys. Lett. A* **311**, *353*, 2003.

[Ott93] E. Ott. *Chaos in Dynamical Systems*. Cambridge University Press, 1993.

[Pec83] P. Pechukas. Distribution of energy eigenvalues in the irregular spectrum. *Phys. Rev. Lett.* **51**, *943*, 1983.

[PM83] A. Pandey and M.L. Mehta. *Commun. Math. Phys.* **87**, *449*, 1983.

[Poi92] H. Poincaré. *Les Méthodes Nouvelles de la Mécanique Céleste*. Paris: Gauthier-Villars, 1892.

[Por65] C.E. Porter. *Statistical theories of spectra*. Academic Press, 1965.

[PP90] W. Parry and M. Pollicott. Zeta functions and the periodic orbit structure of hyperbolic dynamics. *Astérisque* **187**, *1*, 1990.

[PR93a] T. Prosen and M. Robnik. Energy level statistics in the transition region between integrability and chaos. *J. Phys. A: Math. Gen.* **26**, *2371*, 1993.

[PR93b] T. Prosen and M. Robnik. Survey of the eigenfunctions of a billiard system between integrability and chaos. *J. Phys. A: Math. Gen.* **26**, *5365*, 1993.

[Pra97] R.E. Prange. The spectral form factor is not self-averaging. *Phys. Rev. Lett.* **78**, *2280*, 1997.

[Pri95] H. Primack. Quantization of the three-dimensional Sinai billiard. *Phys. Rev. Lett.* **74**, *4831*, 1995.

[Pro97] T. Prosen. Quantization of a generic chaotic 3D billiard with smooth boundary. I. Energy level statistics. *Phys. Lett. A* **233**, *323*, 1997.

[PS98] H. Primack and U. Smilansky. On the accuracy of the semiclassical trace formula. *J. Phys. A: Math. Gen.* **31**, *6253*, 1998.

[PS00] H. Primack and U. Smilansky. The quantum three-dimensional sinai-billiard, a semiclassical analysis. *Phys. Rep.* **327**, *1*, 2000.

[Qua00] *Quantum Chaos Y2K*, 2000.

[Rei92] L.E. Reichl. *The Transition to Chaos*. Springer-Verlag New York, Inc., 1992.

[Rei96] V. Reitmann. *Reguläre und chaotische Dynamik*. B.G.Teubner Verlagsgesellschaft Leipzig, 1996.

[Ric00] K. Richter. *Semiclassical theory of Mesoscopic Quantum Systems*. Springer, Berlin, 2000.

[Ric01] A. Richter. Test of trace formulas for spectra of superconducting microwave billiards. *Found. Phys.* **31**, *327*, 2001.

[Rob83] M. Robnik. Classical dynamics of a family of billiards with analytic boundaries. *J. Phys. A: Math. Gen.* **16**, *3971*, 1983.

[Rob84] M. Robnik. Quantising a generic family of billiards with analytic boundaries. *J. Phys. A: Math. Gen.* **17**, *1049*, 1984.

[Rob91] J.M. Robbins. Maslov indices in the gutzwiller trace formula. *Nonlinearity* **4**, *343*, 1991.

[RS02] K. Richter and M. Sieber. Semiclassical theory of chaotic quantum transport. *Phys. Rev. Lett.* **89**, *206801-1*, 2002.

[Rue89] D. Ruelle. *Elements of differentiable dynamics and bifurcation theory*. Academic Press, Inc., 1989.

[SA93] B.D. Simons and B.L. Altshuler. Universalities in the spectra of disordered and chaotic systems. *Phys. Rev. B* **48**, *5422*, 1993.

[Sch84] H.G. Schuster. *Deterministic chaos: An introduction.* Physik Verlag Weinheim, 1984.

[Shn74] A.I. Shnirelman. Ergodic properties of eigenfunctions. *Ups. Math. Nauk* **29**, *181*, 1974.

[Sie] M. Sieber. Private communication.

[Sie02] M. Sieber. Leading off-diagonal approximation for the spectral form factor for uniformly hyperbolic systems. *J. Phys. A: Math. Gen.* **35**, *L613*, 2002.

[Sin63] Ya.G. Sinai. On the foundations of the ergodic hypothesis for a dynamical system of statistical mechanics. *Sov. Math. Dokl.* **4**, *1818*, 1963.

[Sin70] Ya.G. Sinai. Dynamical systems with elastic reflections. *Russ. Math. Surveys* **25**, *137*, 1970.

[Spe03] D. Spehner. Spectral form factor of hyperbolic systems: leading off-diagonal approximation. *J. Phys. A: Math. Gen.* **36**, *7269*, 2003.

[SPG03] H. Schanz, M. Puhlmann, and T. Geisel. Shot noise in chaotic cavities from action correlations. *Phys. Rev. Lett.* **91**, *134101*, 2003.

[SPS+95] M. Sieber, H. Primack, U. Smilansky, I. Ussishkin, and H. Schanz. Semiclassical quantization of billards with mixed boundary conditions. *J. Phys. A: Math. Gen.* **28**, *5041*, 1995.

[SR01] M. Sieber and K. Richter. Correlations between periodic orbits and their role in spectral statistics. *Physica Scripta* **T90**, *128*, 2001.

[SSA93] B.D. Simons, A. Szafer, and B.L. Altshuler. Universality in quantum chaotic spectra. *JETP Lett.* **57**, *276*, 1993.

[Stö99] H.-J. Stöckmann. *Quantum Chaos: An Introduction.* Cambridge University Press, 1999.

[SV03] U. Smilansky and B. Verdene. Action correlations and random matrix theory. *J. Phys. A: Math. Gen.* **36**, *3525*, 2003.

[Sza92] D. Szasz. On the k-property of some planar hyperbolic billiards. *Commun. Math. Phys.* **145**, *595*, 1992.

[Tan97] G. Tanner. How chaotic is the stadium billiard? A semiclasscial analysis. *J. Phys. A.: Math. Gen.* **30**, *2863*, 1997.

[Tan99] G. Tanner. Periodic orbit action correlations in the baker map. *J. Phys. A: Math. Gen.* **32**, *5071*, 1999.

[TR03] M. Turek and K. Richter. Leading off-diagonal contribution to the spectral form factor of chaotic quantum systems. *J. Phys. A: Math. Gen.* **36**, *L455*, 2003.

[TSMR04] M. Turek, D. Spehner, S. Müller, and K. Richter. Semiclassical form factor for spectral and matrix element fluctuations. *preprint*, 2004.

[Wig94] S. Wiggins. *Normally Hyperbolic Invariant Manifolds in Dynamical Systems*. Springer-Verlag New York Inc., 1994.

[Wil87] M. Wilkinson. A semiclassical sum rule for matrix elements of classically chaotic systems. *J. Phys. A* **20**, *2415*, 1987.

[Wil88] M. Wilkinson. Random matrix theory in semiclassical quantum mechanics of chaotic systems. *J. Phys. A* **21**, *1173*, 1988.

[WRT92] D. Wintgen, K. Richter, and G. Tanner. The semiclassical helium atom. *Chaos* **2**, *19*, 1992.

[Zel87] S. Zelditch. Uniform distribution of eigenfunctions on compact hyperbolic surfaces. *Duke Math. J.* **55**, *919*, 1987.

Acknowledgments

First of all I want to thank Klaus Richter for accepting me as a Ph.D. student. He gave me the opportunity to work on the fascinating subject of quantum chaos and introduced me to the rich field of modern semiclassical methods. In particular, I appreciate that he shared his enormous knowledge on many of the most recent research activities in the field. He has always been a good source of advice concerning both physical and non-physical issues. I am most grateful for his constant support from which I benefited a lot during my Ph.D. time.

I also want to thank Juan-Diego Urbina and Peter Schlagheck who are the 'semiclassical' backbone of our group. They were of great help whenever I struggled with smaller or bigger technical problems and often lead me to deeper insights into the more subtle questions of semiclassics. I also enjoyed a number of constructive discussions on other areas in physics and life in general. Furthermore I want to thank Juan-Diego Urbina for proof reading the most important parts of my thesis and commenting on it.

During my Ph.D. time I enjoyed many fruitful and sometimes controversial discussions and informal conversations with other scientists in this field. Here, I want in particular thank M. Sieber, D. Spehner, M. Brack, U. Smilansky, B. Eckhardt, S. Müller and Th. Dittrich for sharing their thoughts on a variety of issues regarding semiclassics.

Many thanks also go to Jens Siewert with whom I had the pleasure to share the office during my time in Regensburg. Being an 'outsider' with respect to quantum chaos and semiclassical methods he widened my view on a large number of modern physical topics. It was always great fun and extremely inspiring to have a discussion with him after numerous colloquia and seminar talks. Besides that I deeply appreciate his efforts to read very carefully through this thesis and to give me many

significant advices how to improve the presentation of my work.

A closely related field to my research on closed systems was investigated by Andreas Laßl who studied transport properties in open systems. Here I want to thank him for sharing all his insights and explaining his results to me in great detail. I also appreciate the comments he gave on my work after having proof-read it.

Further I would like to thank Andreas Jung, Josef Kainz and Christian Lechner for their continuous support concerning all my computer related questions and problems. I am thanking all the other members of our group and the 'Lehrstuhl' for the nice time I had — I liked being part of this 'Lehrstuhl' a lot. In particular I am grateful to our secretary Angela Reisser who was of much help whenever I had to deal with whatsoever administrative challenges.

Last but not least I am thanking my parents and my brother for all their support, encouragement and motivation during the last years.